

ICACT-TACT JOURNAL

Transactions on Advanced Communications Technology



Volume 2 Issue 5, Sep 2013, ISSN: 2288-0003

Editor-in-Chief

Prof. Thomas Byeongnam YOON, PhD.



**Global IT
Research Institute**

Journal Editorial Board

■ Editor-in-Chief

Prof. Thomas Byeongnam YOON, PhD.

Founding Editor-in-Chief

ICTACT Transactions on the Advanced Communications Technology (TACT)

■ Editors

Prof. Jun-Chul Chun, Kyonggi University, Korea

Dr. JongWon Kim, GIST (Gwangju Institute of Science & Technology), Korea

Dr. Xi Chen, State Grid Corporation of China, China

Prof. Arash Dana, Islamic Azad university , Central Tehran Branch, Iran

Dr. Pasquale Pace, University of Calabria - DEIS - Italy, Italy

Dr. Mitch Haspel, Stochastikos Solutions R&D, Israel

Prof. Shintaro Uno, Aichi University of Technology, Japan

Dr. Tony Tsang, Hong Kong Polytechnic University, Hong Kong

Prof. Kwang-Hoon Kim, Kyonggi University, Korea

Prof. Rosilah Hassan, Universiti Kebangsaan Malaysia(UKM), Malaysia

Dr. Sung Moon Shin, ETRI, Korea

Dr. Takahiro Matsumoto, Yamaguchi University, Japan

Dr. Christian Esteve Rothenberg, CPqD - R&D Center for. Telecommunications, Brazil

Prof. Lakshmi Prasad Saikia, Assam down town University, India

Prof. Moo Wan Kim, Tokyo University of Information Sciences, Japan

Prof. Yong-Hee Jeon, Catholic Univ. of Daegu, Korea

Dr. E.A.Mary Anita, Prathyusha Institute of Technology and Management, India

Dr. Chun-Hsin Wang, Chung Hua University, Taiwan

Prof. Wilaiporn Lee, King Mongkut's University of Technology North, Thailand

Dr. Zhi-Qiang Yao, XiangTan University, China

Prof. Bin Shen, Chongqing Univ. of Posts and Telecommunications (CQUPT), China

Prof. Vishal Bharti, Dronacharya College of Engineering, India

Dr. Marsono, Muhammad Nadzir , Universiti Teknologi Malaysia, Malaysia

Mr. Muhammad Yasir Malik, Samsung Electronics, Korea

Prof. Yeonseung Ryu, Myongji University, Korea

Dr. Kyuchang Kang, ETRI, Korea

Prof. Plamena Zlateva, BAS(Bulgarian Academy of Sciences), Bulgaria

Dr. Pasi Ojala, University of Oulu, Finland

Prof. CheonShik Kim, Sejong University, Korea

Dr. Anna bruno, University of Salento, Italy

Prof. Jesuk Ko, Gwangju University, Korea

Dr. Saba Mahmood, Air University Islamabad Pakistan, Pakistan

Prof. Zhiming Cai, Macao University of Science and Technology, Macau

Prof. Man Soo Han, Mokpo National Univ., Korea

Mr. Jose Gutierrez, Aalborg University, Denmark

Dr. Youssef SAID, Tunisie Telecom, Tunisia
Dr. Noor Zaman, King Faisal University, Al Ahsa Hofuf, Saudi Arabia
Dr. Srinivas Mantha, SASTRA University, Thanjavur, India
Dr. Shahriar Mohammadi, KNTU University, Iran
Prof. Beonsku An, Hongik University, Korea
Dr. Guanbo Zheng, University of Houston, USA
Prof. Sangho Choe, The Catholic University of Korea, Korea
Dr. Gyanendra Prasad Joshi, Yeungnam University, Korea
Dr. Tae-Gyu Lee, Korea Institute of Industrial Technology(KITECH), Korea
Prof. Ilkyeun Ra, University of Colorado Denver, USA
Dr. Yong Sun, Beijing University of Posts and Telecommunications, China
Dr. Yulei Wu, Chinese Academy of Sciences, China
Mr. Anup Thapa, Chosun University, Korea
Dr. Vo Nguyen Quoc Bao, Posts and Telecommunications Institute of Technology, Vietnam
Dr. Harish Kumar, Bhagwant Institute of Technology, India
Dr. Jin REN, North China University of Technology, China
Dr. Joseph Kandath, Electronics & Commn Engg, India
Dr. Mohamed M. A. Moustafa, Arab Information Union (AIU), Egypt
Dr. Mostafa Zaman Chowdhury, Kookmin University, Korea
Prof. Francis C.M. Lau, Hong Kong Polytechnic University, Hong Kong
Prof. Ju Bin Song, Kyung Hee University, Korea
Prof. KyungHi Chang, Inha University, Korea
Prof. Sherif Welsen Shaker, Kuang-Chi Institute of Advanced Technology, China
Prof. Seung-Hoon Hwang, Dongguk University, Korea
Prof. Dal-Hwan Yoon, Semyung University, Korea
Prof. Chongyang ZHANG, Shanghai Jiao Tong University, China
Dr. H K Lau, The Open University of Hong Kong, Hong Kong
Prof. Ying-Ren Chien, Department of Electrical Engineering, National Ilan University, Taiwan
Prof. Mai Yi-Ting, Hsiuping University of Science and Technology, Taiwan
Dr. Sang-Hwan Ryu, Korea Railroad Research Institute, Korea
Dr. Yung-Chien Shih, MediaTek Inc., Taiwan
Dr. Kuan Hoong Poo, Multimedia University, Malaysia
Dr. Michael Leung, CEng MIET SMIEEE, Hong Kong
Dr. Abu sahman Bin mohd Supa'at, Universiti Teknologi Malaysia, Malaysia
Prof. Amit Kumar Garg, Deenbandhu Chhotu Ram University of Science & Technology, India
Dr. Jens Myrup Pedersen, Aalborg University, Denmark
Dr. Augustine Ikechi Ukaegbu, KAIST, Korea
Dr. Jamshid Sangirov, KAIST, Korea
Prof. Ahmed Dooguy KORA, Ecole Sup. Multinationale des Telecommunications, Senegal
Dr. Se-Jin Oh, Korea Astronomy & Space Science Institute, Korea
Dr. Rajendra Prasad Mahajan, RGPV Bhopal, India
Dr. Woo-Jin Byun, ETRI, Korea
Dr. Mohammed M. Kadhum, School of Computing, Goodwin Hall, Queen's University, Canada
Prof. Seong Gon Choi, Chungbuk National University, Korea
Prof. Yao-Chung Chang, National Taitung University, Taiwan
Dr. Abdallah Handoura, Engineering school of Gabes - Tunisia, Tunisia
Dr. Gopal Chandra Manna, BSNL, India

Dr. Il Kwon Cho, National Information Society Agency, Korea
Prof. Jiann-Liang Chen, National Taiwan University of Science and Technology, Taiwan
Prof. Ruay-Shiung Chang, National Dong Hwa University, Taiwan
Dr. Vasaka Visoottiviseth, Mahidol University, Thailand
Prof. Dae-Ki Kang, Dongseo University, Korea
Dr. Yong-Sik Choi, Research Institute, IDLE co., Ltd, Korea
Dr. Xuena Peng, Northeastern University, China
Dr. Ming-Shen Jian, National Formosa University, Taiwan
Dr. Soobin Lee, KAIST Institute for IT Convergence, Korea
Prof. Yongpan Liu, Tsinghua University, China
Prof. Chih-Lin HU, National Central University, Taiwan
Prof. Chen-Shie Ho, Oriental Institute of Technology, Taiwan
Dr. Hyoung-Jun Kim, ETRI, Korea
Prof. Bernard Cousin, IRISA/Universite de Rennes 1, France
Prof. Eun-young Lee, Dongduk Woman s University, Korea
Dr. Porkumaran K, NGP institute of technology India, India
Dr. Feng CHENG, Hasso Plattner Institute at University of Potsdam, Germany
Prof. El-Sayed M. El-Alfy, King Fahd University of Petroleum and Minerals, Saudi Arabia
Prof. Lin You, Hangzhou Dianzi Univ, China
Mr. Nicolai Kuntze, Fraunhofer Institute for Secure Information Technology, Germany
Dr. Min-Hong Yun, ETRI, Korea
Dr. Seong Joon Lee, Korea Electrotechnology Research Institute, Korea
Dr. Kwihoon Kim, ETRI, Korea
Dr. Jin Woo HONG, Electronics and Telecommunications Research Inst., Korea
Dr. Heeseok Choi, KISTI(Korea Institute of Science and Technology Information), Korea
Dr. Somkiat Kitjongthawonkul, Australian Catholic University, St Patrick's Campus, Australia
Dr. Dae Won Kim, ETRI, Korea
Dr. Ho-Jin CHOI, KAIST(Univ), Korea
Dr. Su-Cheng HAW, Multimedia University, Faculty of Information Technology, Malaysia
Dr. Myoung-Jin Kim, Soongsil University, Korea
Dr. Gyu Myoung Lee, Institut Mines-Telecom, Telecom SudParis, France
Dr. Dongkyun Kim, KISTI(Korea Institute of Science and Technology Information), Korea
Prof. Yoonhee Kim, Sookmyung Women s University, Korea
Prof. Li-Der Chou, National Central University, Taiwan
Prof. Young Woong Ko, Hallym University, Korea
Prof. Dimiter G. Velev, UNWE(University of National and World Economy), Bulgaria
Dr. Tadasuke Minagawa, Meiji University, Japan
Prof. Jun-Kyun Choi, KAIST (Univ.), Korea
Dr. Brownson ObaridoaObele, Hyundai Mobis Multimedia R&D Lab , Korea
Prof. Anisha Lal, VIT university, India
Dr. kyeong kang, University of technology sydney, faculty of engineering and IT , Australia
Prof. Chwen-Yea Lin, Tatung Institute of Commerce and Technology, Taiwan
Dr. Ting Peng, Chang'an University, China
Prof. ChaeSoo Kim, Donga University in Korea, Korea
Prof. kirankumar M. joshi, m.s.uni.of baroda, India
Dr. Chin-Feng Lin, National Taiwan Ocean University, Taiwan
Dr. Chang-shin Chung, TTA(Telecommunications Technology Association), Korea

Dr. Che-Sheng Chiu, Chunghwa Telecom Laboratories, Taiwan
Dr. Chirawat Kotchasarn, RMUTT, Thailand
Dr. Fateme Khalili, K.N.Toosi. University of Technology, Iran
Dr. Izzeldin Ibrahim Mohamed Abdelaziz, Universiti Teknologi Malaysia , Malaysia
Dr. Kamrul Hasan Talukder, Khulna University, Bangladesh
Prof. HwaSung Kim, Kwangwoon University, Korea
Prof. Jongsub Moon, CIST, Korea University, Korea
Prof. Juinn-Horng Deng, Yuan Ze University, Taiwan
Dr. Yen-Wen Lin, National Taichung University, Taiwan
Prof. Junhui Zhao, Beijing Jiaotong University, China
Dr. JaeGwan Kim, SamsungThales co, Korea
Prof. Davar PISHVA, Ph.D., Asia Pacific University, Japan
Ms. Hela Mliki, National School of Engineers of Sfax, Tunisia
Prof. Amirmansour Nabavinejad, Ph.D., Sepahan Institute of Higher Education, Iran

Editor Guide

■ Introduction for Editor or Reviewer

All the editor group members are to be assigned as a evaluator(editor or reviewer) to submitted journal papers at the discretion of the Editor-in-Chief. It will be informed by eMail with a Member Login ID and Password.

Once logged the Website via the Member Login menu in left as a evaluator, you can find out the paper assigned to you. You can evaluate it there. All the results of the evaluation are supposed to be shown in the Author Homepage in the real time manner. You can also enter the Author Homepage assigned to you by the Paper ID and the author's eMail address shown in your Evaluation Webpage. In the Author Homepage, you can communicate each other efficiently under the peer review policy. Please don't miss it!

All the editor group members are supposed to be candidates of a part of the editorial board, depending on their contribution which comes from history of ICACT TACT as an active evaluator. Because the main contribution comes from sincere paper reviewing role.

■ Role of the Editor

The editor's primary responsibilities are to conduct the peer review process, and check the final camera-ready manuscripts for any technical, grammatical or typographical errors.

As a member of the editorial board of the publication, the editor is responsible for ensuring that the publication maintains the highest quality while adhering to the publication policies and procedures of the ICACT TACT(Transactions on the Advanced Communications Technology).

For each paper that the editor-in-chief gets assigned, the Secretariat of ICACT Journal will send the editor an eMail requesting the review process of the paper.

The editor is responsible to make a decision on an "accept", "reject", or "revision" to the Editor-in-Chief via the Evaluation Webpage that can be shown in the Author Homepage also.

■ Deadlines for Regular Review

Editor-in-Chief will assign a evaluation group(a Editor and 2 reviewers) in a week upon receiving a completed Journal paper submission. Evaluators are given 2 weeks to review the paper. Editors are given a week to submit a recommendation to the Editor-in-Chief via the evaluation Webpage, once all or enough of the reviews have come in. In revision case, authors have a maximum of a month to submit their revised manuscripts. The deadlines for the regular review process are as follows:

Evaluation Procedure	Deadline
Selection of Evaluation Group	1 week
Review processing	2 weeks
Editor's recommendation	1 week
Final Decision Noticing	1 week

■ Making Decisions on Manuscript

Editor will make a decision on the disposition of the manuscript, based on remarks of the reviewers. The editor's recommendation must be well justified and explained in detail. In cases where the revision is requested, these should be clearly indicated and explained. The editor must then promptly convey this decision to the author. The author may contact the editor if instructions regarding amendments to the manuscript are unclear. All these actions could be done via the evaluation system in this Website. The guidelines of decisions for publication are as follows:

Decision	Description
Accept	An accept decision means that an editor is accepting the paper with no further modifications. The paper will not be seen again by the editor or by the reviewers.
Reject	The manuscript is not suitable for the ICACT TACT publication.
Revision	The paper is conditionally accepted with some requirements. A revision means that the paper should go back to the original reviewers for a second round of reviews. We strongly discourage editors from making a decision based on their own review of the manuscript if a revision had been previously required.

■ Role of the Reviewer

Reviewer Webpage:

Once logged in the Member Login menu in left, you can find out papers assigned to you. You can also login the Author Homepage assigned to you with the paper ID and author's eMail address. In there you can communicate each other via a Communication Channel Box.

Quick Review Required:

You are given 2 weeks for the first round of review and 1 week for the second round of review. You must agree that time is so important for the rapidly changing IT technologies and applications trend. Please respect the deadline. Authors undoubtedly appreciate your quick review.

Anonymity:

Do not identify yourself or your organization within the review text.

Review:

Reviewer will perform the paper review based on the main criteria provided below. Please provide detailed public comments for each criterion, also available to the author.

- How this manuscript advances this field of research and/or contributes something new to the literature?
- Relevance of this manuscript to the readers of TACT?
- Is the manuscript technically sound?
- Is the paper clearly written and well organized?
- Are all figures and tables appropriately provided and are their resolution good quality?
- Does the introduction state the objectives of the manuscript encouraging the reader to read on?
- Are the references relevant and complete?

Supply missing references:

Please supply any information that you think will be useful to the author in revision for enhancing quality of the paper or for convincing him/her of the mistakes.

Review Comments:

If you find any already known results related to the manuscript, please give references to earlier papers which contain these or similar results. If the reasoning is incorrect or ambiguous, please indicate specifically where and why. If you would like to suggest that the paper be rewritten, give specific suggestions regarding which parts of the paper should be deleted, added or modified, and please indicate how.

Journal Procedure

Dear Author,

➤ **You can see all your paper information & progress.**

➤ **Step 1. Journal Full Paper Submission**

Using the Submit button, submit your journal paper through ICACT Website, then you will get new paper ID of your journal, and send your journal Paper ID to the Secretariat@icact.org for the review and editorial processing. Once you got your Journal paper ID, never submit again! Journal Paper/CRF Template

➤ **Step 2. Full Paper Review**

Using the evaluation system in the ICACT Website, the editor, reviewer and author can communicate each other for the good quality publication. It may take about 1 month.

➤ **Step 3. Acceptance Notification**

It officially informs acceptance, revision, or reject of submitted full paper after the full paper review process.

Status	Action
Acceptance	Go to next Step.
Revision	Re-submit Full Paper within 1 month after Revision Notification.
Reject	Drop everything.

➤ **Step 4. Payment Registration**

So far it's free of charge in case of the journal promotion paper from the registered ICACT conference paper! But you have to regist it, because you need your Journal Paper Registration ID for submission of the final CRF manuscripts in the next step's process. Once you get your Registration ID, send it to Secretariat@icact.org for further process.

➤ **Step 5. Camera Ready Form (CRF) Manuscripts Submission**

After you have received the confirmation notice from secretariat of ICACT, and then you are allowed to submit the final CRF manuscripts in PDF file form, the full paper and the Copyright Transfer Agreement. Journal Paper Template, Copyright Form Template, BioAbstract Template,

Journal Submission Guide

All the Out-Standing ICACT conference papers have been invited to this "ICACT Transactions on the Advanced Communications Technology" Journal, and also welcome all the authors whose conference paper has been accepted by the ICACT Technical Program Committee, if you could extend new contents at least 30% more than pure content of your conference paper. Journal paper must be followed to ensure full compliance with the IEEE Journal Template Form attached on this page.

➤ How to submit your Journal paper and check the progress?

Step 1. Submit	Using the Submit button, submit your journal paper through ICACT Website, then you will get new paper ID of your journal, and send your journal Paper ID to the Secretariat@icact.org for the review and editorial processing. Once you got your Journal paper ID, never submit again! Using the Update button, you can change any information of journal paper related or upload new full journal paper.
Step 2. Confirm	Secretariat is supposed to confirm all the necessary conditions of your journal paper to make it ready to review. In case of promotion from the conference paper to Journal paper, send us all the .DOC(or Latex) files of your ICACT conference paper and journal paper to evaluate the difference of the pure contents in between at least 30% more to avoid the self replication violation under scrutiny. The pure content does not include any reference list, acknowledgement, Appendix and author biography information.
Step 3. Review	Upon completing the confirmation, it gets started the review process thru the Editor & Reviewer Guideline. Whenever you visit the Author Homepage, you can check the progress status of your paper there from start to end like this, " Confirm OK! -> Gets started the review process -> ...", in the Review Status column. Please don't miss it!

Volume 2, Issue 5

- 1 On ICI Canceller for Mobile OFDM DTV Receivers 290
Hai Minh TRAN*, Tomohisa WADA**
** University of the Ryukyus, ** University of the Senbaru, Nishihara, Okinawa, Japan*
- 2 Simple and Feasible Dynamic Bandwidth and Polling Allocation for XGPON 298
Man-Soo HAN
Mokpo National Univ., Korea
- 3 Effective Use of Computational Resources in Multicore Distributed Systems 305
Hidehiro Kanemitsu*, Masaki Hanada**, Takashige Hoshiai***, Hidenori Nakazato*
** Waseda University, Japan, ** Tokyo University of Information Sciences, Japan, *** Sojo University, Japan*
- 4 A Stereo-Vision Approach for a Natural 3D Hand Interaction with an AR Object 315
Seonho Lee, Junchul Chun
Kyonggi University, Suwon, S. Korea
- 5 The Optimum Ring Ratio of 16-APSK in LTE Uplink over Nonlinear System 333
Pornpimon Chayratsami*, Sorapong Thuaykaew**
*King Mongkut Institute of Technology Ladkrabang, Bangkok, Thailand, **Celestica Inc., Leamchabang, Sriracha, Chon Buri, Thailand*

On ICI Canceller for Mobile OFDM DTV Receivers

Hai Minh TRAN*, Tomohisa WADA**

**Graduate School of Engineering and Science*

***Department of Information Engineering, University of the Ryukyus*

*&** *Senbaru 1, Nishihara, Okinawa 903-0213, Japan*

haitran@lsi.ie.u-ryukyu.ac.jp, wada@ie.u-ryukyu.ac.jp

Abstract— In mobile environment, the performance of OFDM mobile receivers is degraded severely because of Inter-Carrier-Interference (ICI) caused by Doppler Spread. So ICI canceller is an important task for designers of mobile OFDM receivers. [1] and [2] proposed an efficient method to reduce ICI. The main idea of this method is to linearly approximate time varying channel within one OFDM symbol. Then a large ICI matrix equation is given. However, in [1] and [2], the estimated values of the channel transfer function—the diagonal of the ICI matrix is corrupted by ICI. Consequently, the equalized signal still is distorted. In this paper, we propose an iterative method to improve performance of the conventional method in [1] and [2]. We implement Jacobi iteration method to solve the big ICI matrix equation. Thereby, we are able to implement ICI canceller by a simple FIR filter rather than finding the inverse of ICI matrix. Next, at second iteration of Jacobi method, we improve the accuracy the diagonal by removing ICI from pilot symbols and re-estimating the channel transfer function. Simulation results for ISDB-T mode 3 demonstrated that our method could double performance of the conventional method under TU-6 channel and Doppler Spread. The improvement is better for two paths and one path Doppler channel.

Keyword— Digital television (DTV), Inter-Carrier Interference (ICI), Jacobi Iteration, Orthogonal frequency-division multiplexing (OFDM).

I. INTRODUCTION

OFDM utilized a large number of orthogonal subcarrier to achieve high-spectral efficiency. The long duration symbol and guard interval protect useful part of OFDM symbols from inter-symbol-interference (ISI). Guard interval (GI) is implemented by cyclic prefix (CP). This scheme keeps OFDM symbols smoothly in time domain, and reduces out of band power of OFDM. Moreover, cyclic prefix keeps convolution of channel and OFDM symbol is circular

convolution. However, in mobile environment, GI or CP could not avoid Doppler-effect. Doppler-effect spreads energy of one sub-carriers to many other subcarriers. This is called ICI. In other word, in time-varying channel, the orthogonality among subcarriers is lost. Thus performance is degraded severely.

Many researches are conducted to deal with ICI caused by Doppler. In [1] and [2], an efficient approach is to linearly approximate time-varying channel within one OFDM symbol. Then we should solve a large ICI matrix equation. In [3], a method is proposed to solve the large ICI matrix equation. As most ICI power concentrates near the diagonal of ICI matrix, [3] considered D lines that are closest to the diagonal. Instead finding invert of $[N \times N]$ matrix, [3] find inverse of N matrix of order $[(2D + 1) \times (2D + 1)]$. This still requires heavy computation.

As pilot symbols suffer from ICI, the estimated values of the diagonal also is corrupted by ICI. In addition, the diagonal has the most important rule. Therefore, performance of [1], [2] is limited, even we solve the full ICI matrix equation. In this paper, we apply Jacobi iteration method to solve the large ICI equation, so we do not need calculate any inverse matrix. The simulation result shown that performance of Jacobi iteration at first iteration is the same as [3]. It is noted that Jacobi iteration method also is considered in [4]. However, in our method, we improve the diagonal of ICI matrix at second iteration of Jacobi method. By using output of the first iteration, we remove ICI from pilot symbols. Then, we re-estimate the diagonal of ICI matrix. As the diagonal is reliable, our method achieved a good improvement at second iteration.

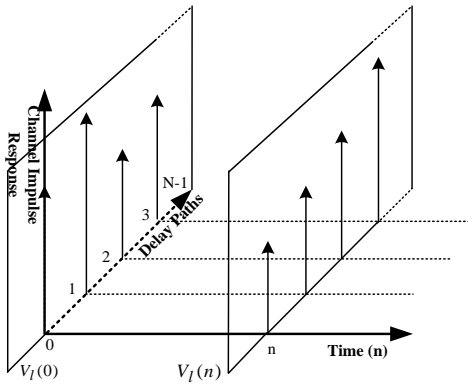
The rest of paper is organized as follows: Section II reviews the conventional method. Section III shows our proposed method. Section IV presents implementation of the proposed method. Simulation result is shown in section V. Finally, conclusion is presented in section VI.

II. REVIEW OF THE CONVENTIONAL METHOD

A. A Linear Approximation of Time Varying Channel

Time varying channel causes ICI. Therefore, we need characterizing time varying channel to define the ICI effect. By a linear approximation of time varying channel, the ICI is defined.

Manuscript received March 11, 2013. Hai Minh TRAN is with the Graduate School of Engineering and Science, University of the Ryukyus, Okinawa-ken, 903-013 Japan. (phone 080-427-6768; email: haitran@lsi.ie.u-ryukyu.ac.jp) Tomohisa WADA is with Department of Information Engineering, University of the Ryukyus. (email: wada@lsi.ie.u-ryukyu.ac.jp)


Figure 1. $V_l(n)$ in Time Domain

As in [1], the received signal in frequency domain can be written as follows:

$$Y(k) = X(k)H_{k,k} + \underbrace{\sum_{l=0, l \neq k}^{N-1} X(l) \cdot H_{k,l}}_{ICI} + W(k) \quad (1)$$

$X(k)$ and $Y(k)$ is transmitted and received signal respectively. l , and k are subcarrier indexes. N is number of subcarrier. W denotes random noise. The channel transfer function from l^{th} to k^{th} subcarrier is calculated as

$$H_{k,l} = \frac{1}{N} \sum_{n=0}^{N-1} \sum_{m=0}^{N-1} h(m,n) \cdot e^{-j\frac{2\pi lm}{N}} \cdot e^{-j\frac{2\pi}{N}n(k-l)} \quad (2)$$

$h(m,n)$ is channel impulse response, with m and n are delay path and time index, respectively. $H_{k,l}$ should be determined. However, we do not know $h(m,n)$ at all (m,n) . By assuming $h(m,n)$ changes linearly in time domain and within an OFDM symbol, $H_{k,l}$ can be determined.

$V_l(n)$ denotes Fourier Transform of channel impulse response $h(m,n)$ at n instant time.

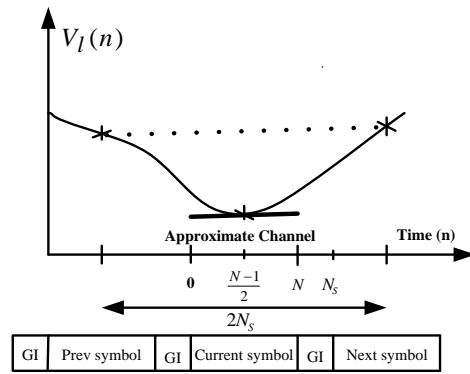
$$V_l(n) = \sum_{m=0}^{N-1} h(m,n) \cdot e^{-j\frac{2\pi}{N}lm} \quad (3)$$

$$H_{k,l} = \frac{1}{N} \sum_{n=0}^{N-1} V_l(n) \cdot e^{-j\frac{2\pi}{N}n(k-l)} \quad (4)$$

If $k = l$, we have

$$H_{k,k} = \frac{1}{N} \sum_{n=0}^{N-1} V_l(n) = \overline{V_l(n)} \quad (5)$$

$$\begin{bmatrix} Y(0) \\ Y(1) \\ \vdots \\ Y(N-2) \\ Y(N-1) \end{bmatrix} = \overbrace{\begin{bmatrix} H_{0,0} & \Phi_{-1}\overline{V_1} & \cdots & \Phi_{-N+2}\overline{V_{N-2}} & \Phi_{-N+1}\overline{V_{N-1}} \\ \Phi_1\overline{V_0} & H_{1,1} & \cdots & \Phi_{-N+3}\overline{V_{N-2}} & \Phi_{-N+2}\overline{V_{N-1}} \\ \vdots & \vdots & \ddots & \vdots & \vdots \\ \Phi_{N-2}\overline{V_0} & \Phi_{N-3}\overline{V_1} & \cdots & H_{N-2,N-2} & \Phi_{-1}\overline{V_{N-1}} \\ \Phi_{N-1}\overline{V_0} & \Phi_{N-2}\overline{V_1} & \cdots & \Phi_1\overline{V_{N-2}} & H_{N-1,N-1} \end{bmatrix}}^{ICI \text{ Matrix } [H]} \times \begin{bmatrix} X(0) \\ X(1) \\ \vdots \\ X(N-2) \\ X(N-1) \end{bmatrix} + \begin{bmatrix} W(0) \\ W(1) \\ \vdots \\ W(N-2) \\ W(N-1) \end{bmatrix} \quad (9)$$


Figure 2. Approximation of $V_l(n)$

If $h(m,n)$ is linear in time domain, then $V_l(n)$ also is linear in time domain. Instead of linear approximating $h(m,n)$, it is equivalent to linearly approximate $V_l(n)$. The two first terms of Taylor series for $V_l(n)$ is

$$V_l(n) \approx \overline{V}_l + \left(n - \frac{N-1}{2}\right) \cdot \overline{V}_l' \quad (5)$$

The first central difference at $\left(\frac{N-1}{2}\right)$ is approximated as

$$\overline{V}_l' \approx \frac{\overline{V}_l^{(next)} - \overline{V}_l^{(pre)}}{2N_s} \quad (6)$$

It is noted that error of the first central difference is $O(h^2)$, while the error of the first backward or forward difference is $O(h)$ [5]. Therefore, \overline{V}_l' is approximated by the first central difference. From (1), (4), and (5) we have the ICI equation:

$$Y(k) = X(k)H_{k,k} + \sum_{l=0, l \neq k}^{N-1} X(l)\overline{V}_l'\Phi_{\Delta_l} + W(k), \quad \Delta_l = l - k \quad (7)$$

$$\Phi_{\Delta_l} = \frac{1}{e^{j\frac{2\pi}{N}\Delta_l} - 1}, \quad l \neq k \quad (8)$$

For more detail about capability of linear approximating time varying channel, please refer to [1] and [2].

B. The Large ICI Matrix Equation

Equation (7) can be represented in matrix form as (9). In this paper, we assumed $[W] = [0]$.

In order to recover the transmitted signal, we should solve a very larger matrix equation. In ISDB-T mode 3, as number of subcarrier is ($N = 8192$), finding inverse of $[H]_{8192 \times 8192}$ is a heavy task. Therefore, it is necessary to reduce complexity of (9).

To solve the larger matrix equation, we investigate characteristics of matrix $[H]$. Firstly, we consider ICI power distribution. Absolute value of Φ_{Δ_l} indicates ICI power from l^{th} subcarrier to k^{th} subcarrier, $\Delta_l = (l - k)$ is distance between l^{th} and k^{th} subcarrier.

$$\Phi_{\Delta_l} = \frac{1}{2e^{j\frac{\pi\Delta_l}{N}} \sin\left(\frac{\pi\Delta_l}{N}\right)} \quad (10)$$

$$|\Phi_{\Delta_l}| = \frac{1}{\left|2 \sin\left(\frac{\pi\Delta_l}{N}\right)\right|} = \begin{cases} \frac{0.5N}{\pi\Delta_l} & \text{if } \Delta_l \rightarrow 0 \\ \frac{0.5N}{\pi(N + \Delta_l)} & \text{if } \Delta_l \rightarrow -N + 1 \end{cases} \quad (11)$$

$\Delta_l \rightarrow 0$ means that the subcarriers that are near l^{th} subcarrier causes a big ICI power on l^{th} subcarrier. $\Delta_l \rightarrow (-N + 1)$ means the subcarriers that are far l^{th} subcarrier may generate a big ICI power on l^{th} subcarrier. For example, Fig.1 shows ICI power from $(N - 1)$ subcarrier to 1^{st} subcarrier. In matrix form, ICI power concentrated on the elements that near the diagonal and the elements that at low-left corner or upper-right corner of $[H]$ matrix.

Because ICI power concentrates on near diagonal of $[H]$ matrix, in paper [1], [3] researchers considered D elements that closest the diagonal and solve $[(2D + 1) \times (2D + 1)]$ matrix size equation instead for $[N \times N]$ matrix equation. For example, $D = 1$, we have $[3 \times 3]$ matrix equation as

$$\begin{bmatrix} Y_0 \\ Y_1 \\ Y_2 \end{bmatrix} = \begin{bmatrix} H_{0,0} & \phi_1 \bar{V}_1 & \phi_2 \bar{V}_2 \\ \phi_{-1} \bar{V}_0 & H_{1,1} & \phi_1 \bar{V}_2 \\ \phi_{-2} \bar{V}_0 & \phi_{-1} \bar{V}_1 & H_{2,2} \end{bmatrix} \times \begin{bmatrix} X_0 \\ X_1 \\ X_2 \end{bmatrix} \quad (12)$$

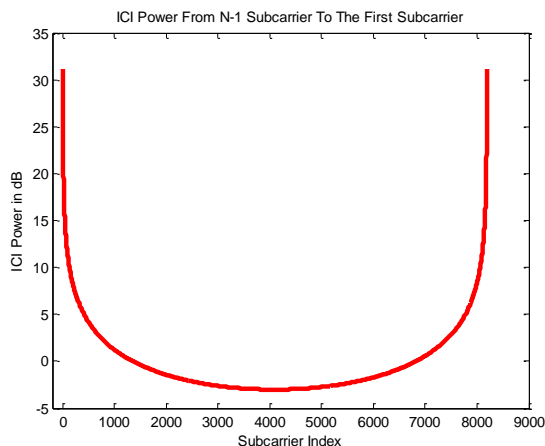


Figure 3. ICI Power From Other Subcarriers to First Subcarrier

By increasing D , we can achieve more improvement, but the computational complexity also is increased. Even ($D = 1$) we should find N invert matrix size of $[3 \times 3]$. In next section, by using Jacobi iteration we do not need calculate inverse of any matrix, while performance is remaining.

III. THE PROPOSAL METHOD

As section II, through linearly approximating time varying channel, the conventional method can define the ICI matrix equation. However, we face with two challenges. First, the given ICI matrix is very big such as $[H]_{8192 \times 8192}$ for ISDB-T mode 3. Second, the diagonal of the ICI matrix-the conventional channel transfer function is not accurate because of pilots were corrupted by ICI. To deal with the two challenges, we first apply Jacobi iteration method for solving the big ICI matrix. By this way, we do not need calculate any inverse matrix. Next, we re-estimate channel at 2^{nd} iteration to improve accuracy of the diagonal of the ICI matrix.

A. Jacobi Iteration Method for The Large ICI Matrix

In this section, we apply Jacobi iteration method for the large ICI matrix equation. First we separate the ICI matrix into two parts. The first part is the diagonal of ICI matrix as

$$[P] = \text{diag}[H_{0,0} \ H_{1,1} \ \dots \ H_{N-2,N-2} \ H_{N-1,N-1}] \quad (13)$$

The remained part of ICI matrix is

$$[T] = [H] - [P] \quad (14)$$

Equation (9) can be re-written as

$$[Y] = [P] \cdot [X] + [T] \cdot [X] \quad (15)$$

$$[P] \cdot [X] = [Y] - [T] \cdot [X] \quad (16)$$

According to Jacobi method, the approximate solution at $(k + 1)$ iteration is updated as:

$$[P] \cdot [X_{k+1}] = [Y] - [T] \cdot [X_k] \quad (17)$$

Because $[P]$ is diagonal matrix, it is easy to solve (17). The initial value X_0 is calculated from 1 tap equalizer. For example, k^{th} subcarrier is initiated as

$$X_0(k) = \frac{Y(k)}{H_{k,k}} \quad (18)$$

At each iteration, error is

$$e_{k+1} = [X]_{k+1} - [X] = ([I] - [P^{-1}][H])e_k = [M]e_k$$

$$e_{k+1} = [M]^k e_1 \leq |\lambda_M|^k e_1, \quad (19)$$

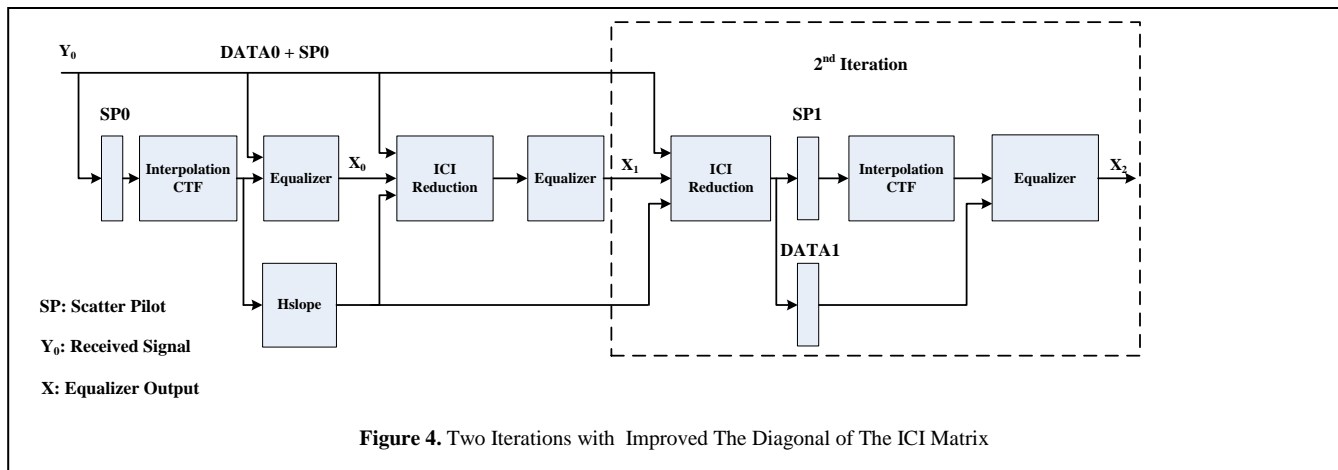


Figure 4. Two Iterations with Improved The Diagonal of The ICI Matrix

λ_M is the biggest engine value of $[M]$. In this case, as the diagonal is dominated, Jacobi iteration method is effective. For more detail about Jacobi iteration, please refer to [4], [5].

Since most ICI power concentrated near the diagonal, we can reduce size of $[T]$ to get the low complexity. We form $[T]$ by 30 elements that are nearest the diagonal. k^{th} subcarrier is updated at first iteration as

$$X_1(k) = \frac{Y_k - \sum_{\Delta=-15}^{15} X_0(\Delta + k) \cdot \overline{V_{\Delta+k}'} \cdot \Phi_{\Delta}}{H_{k,k}} \quad (20)$$

Φ_{Δ} , $\Delta = -15, -14, \dots, 15$ is fixed coefficient as (11). We can implement iteration equation by a FIR filter with 31 taps.

B. Two Iterations with Re-estimating Channel Transfer Function

Normally, the approximate solution at 2^{nd} iteration of Jacobi method is

$$X_2(k) = \frac{Y_k - \sum_{\Delta=-15}^{15} X_1(\Delta + k) \cdot \overline{V_{\Delta+k}'} \cdot \Phi_{\Delta}}{H_{k,k}} \quad (21)$$

We should remind that $H_{k,k}$ is estimated from pilots that were corrupted by ICI. Consequently, $X_k^{(2)}$ still is distorted. In order to improve performance, we re-estimate channel $H_{k,k}$ at 2^{nd} iteration.

Firstly, we remove ICI from pilot symbols by using output at 1^{st} iteration as

$$Y_1(m) = Y(m) - \sum_{\Delta=-15}^{15} X_1(\Delta + m) \cdot \overline{V_{\Delta+m}'} \cdot \Phi_{\Delta} \quad (22)$$

m is pilot symbol index. Secondly, the channel transfer function is re-estimated using $Y_1(m)$. Therefore, $H_{k,k}^{(re-estimate)}$ is more accurate. Finally, the recover signal at second iteration is updated as (23). The channel transfer

function -the diagonal of ICI matrix is the most important element of the ICI matrix. As the channel transfer function is refined at 2^{nd} iteration, we could achieve a significant improvement. The all above procedures are shown in Fig. 4.

$$X_k^{(2)} = \frac{Y_k - \sum_{\Delta_k=-15}^{15} X_{\Delta+k}^{(1)} \cdot \overline{V_{\Delta+k}'} \cdot \Phi_{\Delta}}{H_{k,k}^{(re-estimate)}} \quad (23)$$

IV. IMPLEMENTATION OF THE PROPOSAL METHOD

A. Implementation of ICI Canceller using FIR Filter

In this section, we present an implementation of ICI canceller using a FIR filter. By using linear approximating time varying channel, the ICI matrix is obtained. In addition, interestingly, the ICI coefficient Φ_{Δ} is constant. As Φ_{Δ} is constant, we can implement ICI canceller by using a FIR filter.

From (1) the transmitted signal can be recovered as

$$X(k) = \frac{Y(k) - \sum_{l=0, l \neq k}^{N-1} X(l) \cdot H_{k,l}}{H_{k,k}} \quad (24)$$

We separate (24) into two steps. At first step, ICI power is subtracted from the received signal, so the clean ICI signal is obtained. At second step, the clean ICI signal is equalized by dividing by conventional channel transfer function. At first step, we consider W nearest subcarrier to k^{th} subcarrier.

$$W = 2 \cdot Q + 1$$

The ICI term that impacts on k^{th} subcarrier is re-written as follow

$$ICI(k) = \sum_{\Delta=-Q}^Q X(k + \Delta) \cdot \overline{V_{\Delta+k}'} \cdot \Phi_{\Delta} \quad (25)$$

$$ICI(k) = conv(\Phi_{\Delta}, X(k) \cdot \overline{V_{\Delta+k}'} \quad (26)$$

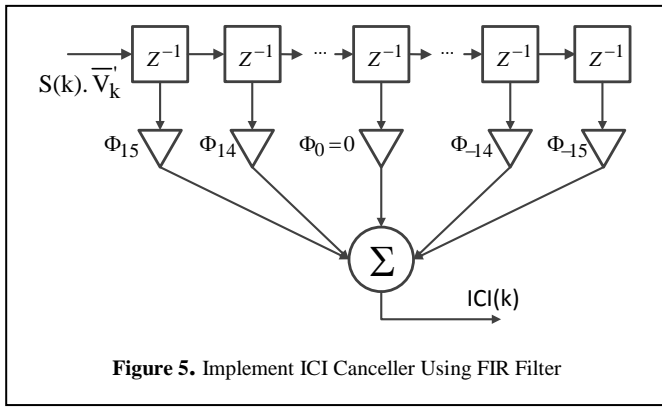


Figure 5. Implement ICI Canceller Using FIR Filter

As (26), $ICI(k)$ is output of a FIR filter with the coefficients are Φ_{Δ} , and input is $(X(k + \Delta) \cdot \overline{V_k})'$. The input $X(k + \Delta)$ is calculated by conventional 1 tap equalizer as (17). This value is called the initial value of ICI canceller. The FIR filter causes delay, so we have to locate and extract the ICI term from the FIR output. If the FIR filter has W taps, the extracted signal is within the range of

$$\left[\left(\frac{W-1}{2} + 1 \right) \left(N - \frac{W-1}{2} \right) \right]$$

For example $W = 31$, we have

$$ICI(k) = \sum_{\Delta=-15}^{\Delta=15} S(k + \Delta) \cdot \Phi_{\Delta} \cdot \overline{V_{\Delta+k}}' \quad (26)$$

Fig. (5) illustrates calculating $ICI(k)$ using a FIR with 31 taps Φ_{Δ} .

After the ICI term is calculated, we subtract the ICI term from the received signal. Thus, the clean ICI signal is obtained. Next, the clean ICI signal is equalized by only one tap equalizer as follow

$$X(k) = \frac{Y(k) - ICI(k)}{H_{k,k}} \quad (27)$$

The number of FIR coefficients is W , it means we consider ICI from the W closest subcarriers to the interest subcarrier k . Therefore, the value W determines how much ICI is removed from the received signal. The bigger W , the more ICI is removed. However, the big W increases FIR implementation cost. In next section, we show how to find a reasonable W .

B. Finding a Reasonable ICI Window Size

In this section, we explain how to choose a reasonable W , the number taps of FIR filter. We can choose a maximum ($W = N$) to ensure the best ICI canceller performance. However, that is not necessary, even a big W increases FIR implementation cost.

Φ_{Δ} quantifies ICI from l^{th} subcarrier to k^{th} subcarrier. We exam $|\Phi_{\Delta}|$ to know how strong the ICI from l^{th} subcarrier to k^{th} subcarrier is.

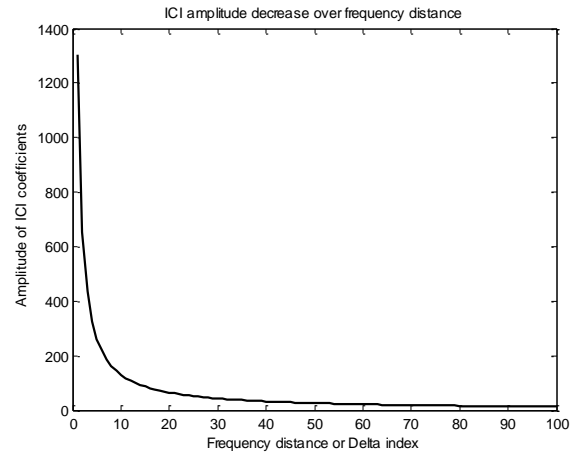


Figure 6. ICI Amplitude Decays over Frequency Distance

$$\Phi_{\Delta} = \frac{1}{2je^{j\frac{\pi}{N}\Delta} \cdot \sin\left(\frac{\pi\Delta}{N}\right)} \quad (28)$$

$$|\Phi_{\Delta}| = \frac{0.5}{\left| \sin\left(\frac{\pi\Delta}{N}\right) \right|} \quad (29)$$

From (29), the ICI amplitude decays over the distance from l^{th} subcarrier to k^{th} subcarrier. It decays quickly with the rate of $\left| \sin\left(\frac{\pi\Delta}{N}\right) \right|$. Fig. (6) shows the ICI amplitude $|\Phi_{\Delta}|$ decreases over frequency distance Δ .

More specifically, we compare the ICI power is removed by W coefficients with the total ICI. The removed ICI power is numerator of (30), and the total ICI is the denominator.

$$ICI_{considered} = \frac{\sum_{n=1}^{\frac{W-1}{2}} \left(\frac{0.5}{\sin\left(\frac{\pi\Delta}{N}\right)} \right)^2}{\sum_{n=1}^{\frac{N}{2}} \left(\frac{0.5}{\sin\left(\frac{\pi\Delta}{N}\right)} \right)^2} \quad (30)$$

If $W = 31$ and $N = 8192$, we have

$$ICI_{considered} = \frac{\sum_{\Delta=1}^{15} \left(\frac{0.5}{\sin\left(\frac{\pi\Delta}{N}\right)} \right)^2}{\sum_{\Delta=1}^{4096} \left(\frac{0.5}{\sin\left(\frac{\pi\Delta}{N}\right)} \right)^2} = 96.0793\% \quad (31)$$

If $W = 63$, $N = 8192$

$$ICI_{considered} = 98.0071\% \quad (32)$$

From (31), we conclude that, $W = 31$ results in 96.0793%

ICI is removed. If we increase W to 63, the removed ICI is 98.0703%. Obviously we can ($W = 31$) to keep implementation at low cost. In section IV, we will compare bit error rate with different values of W .

V. SIMULATION RESULT

In this section, firstly, we compare Jacobi iteration method and direct solving the ICI matrix in [3]. Secondly, we evaluate and compare our proposed method with the conventional method. Finally, we investigate our proposal method with different value of ICI window size W . We apply our proposal method for ISDB-T mode 3. The parameter of OFDM system is shown in table I. We evaluate our proposal method under three different channel conditions. These are the TU-6 channel, two path Doppler channel, and one path Doppler channel. The detail channel parameters are shown in table II, III, IV.

A. Comparison of Jacobi Iteration Method and Direct Solving ICI Matrix

As section I, [3] proposed a method to solve the large ICI matrix equation. Instead finding inverse of $[N \times N]$ matrix, [3] find inverse of N matrix order of $[(2D + 1) \times (2D + 1)]$. We set $D = 2, 7, 15$ and solve matrix order of $[5 \times 5]$, $[15 \times 15]$, $[31 \times 31]$, respectively. As shown in Fig. 5, under TU-6 channel condition, as D increases, the performance is improved. Because most ICI energy concentrated near the diagonal, improvement by increasing ($D = 2$) to ($D = 7$) or ($D = 15$) is small.

TABLE I. ISDB-T MODE 3 PARAMETERS

Parameters	Values
FFT size	8192
Number of sub-carrier	5617
Carrier interval	992.06 (Hz)
Effective Sym. Duration	1008 μ s
Guard interval	126 μ s
Modulation	64QAM

TABLE II. TU-6 CHANNEL

Tap number	Delay (μ s)	Power (dB)	Doppler Spread (Hz)
1	0.0	-3.0	[0 200]
2	0.2	0.0	[0 200]
3	0.5	-2.0	[0 200]
4	1.6	-6.0	[0 200]
5	2.3	-8.0	[0 200]
6	5.0	-10.0	[0 200]

TABLE III. TWO PATHS DOPPLER CHANNEL

Tap number	Delay (μ s)	Power (dB)	Doppler Spread (Hz)
1	0.0	0.0	[0 200]
2	12.3	-3.0	[0 200]

TABLE IV. ONE PATH DOPPLER CHANNEL

Tap number	Delay (μ s)	Power (dB)	Doppler Spread (Hz)
1	12.3	-3.0	[0 200]

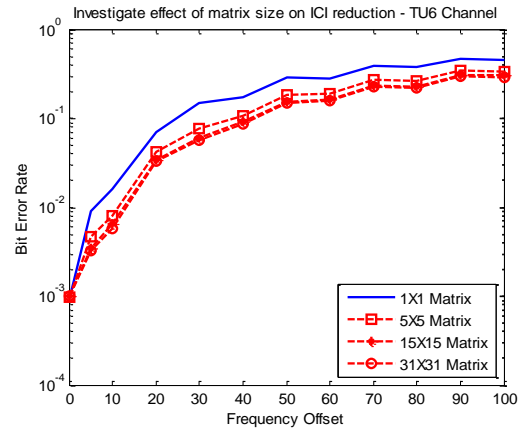


Figure 5. The Original Method with different value of D under TU-6 Channel

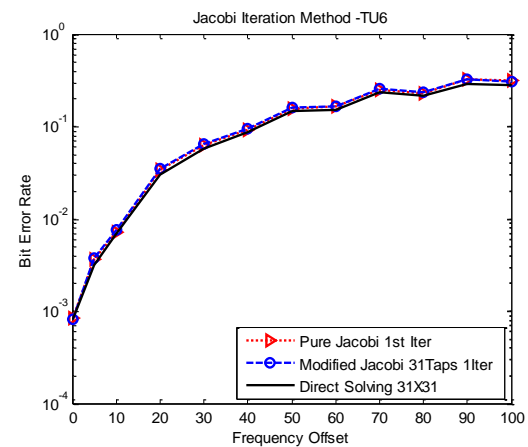


Figure 6. Jacobi Iteration Method with TU-6 Channel

Next, we compared Jacobi iteration method and method in [3] with ($D = 15$). In Fig 6, pure Jacobi means $[T] = [H] - [P]$, and $[P]$ is the diagonal of $[H]$. Modified Jacobi 31 taps used 30 lines that closest the diagonal of ICI matrix for $[T]$. In Fig. 6, under TU-6 channel, the modified Jacobi with 31 taps achieved a performance as ($D = 15$) or pure Jacobi iteration.

B. Comparison of Our Proposed Method and the Conventional Method

In this section, we compare our proposal method with the conventional method under three different channel conditions. We investigate improvement of our proposal method with re-estimating channel at 2nd and 3rd iteration.

By removing ICI from pilot symbols and re-estimating channel at 2nd iteration, the re-estimate channel is more accurate. Thereby, our proposal method improved performance significantly. In Fig. 7, under TU-6 channel, the proposed method doubles performance of 1st iteration-the conventional method over a wide range of frequency offset. Moreover, the proposed method achieved more improvement for two paths and one path Doppler channel. This is because the residual ICI in two paths and one path Doppler channel is less than that in TU-6 channel.

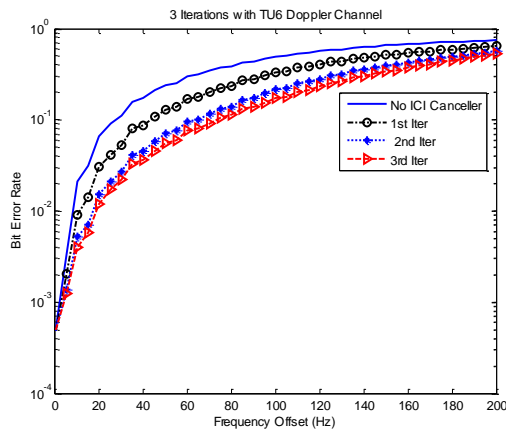


Figure 7. The Proposed Method with TU-6 Channel

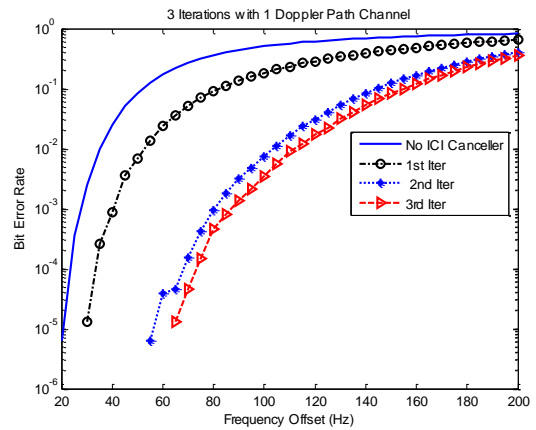


Figure 9. The Proposed Method with One Path Doppler Channel

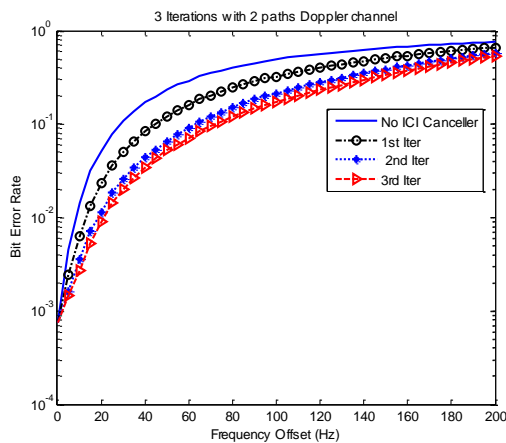


Figure 8. The Proposed Method with Two Paths Doppler Channel

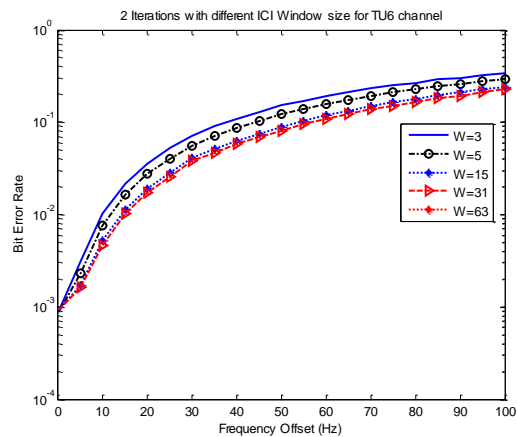


Figure 10. The Proposed Method with Different ICI Window Size

In more detail, at 2nd iteration, by reducing ICI effect in pilot symbols, the diagonal is improved. However, the residual ICI in pilot symbols still degrade reliability of the diagonal. As number of paths channel decreases, the residual ICI becomes smaller and the diagonal suffer less effect of the ICI residual. Therefore, the proposed method got more improvement for one and two paths channel.

In order to get more improvement, we extend our proposed method to 3 iterations. The signal is derived from 2nd iteration is clearer and closer to real transmitted signal. The output at 2nd iteration is utilized to remove ICI from pilot symbols. Then, the channel transfer function $H(k, k)$ is re-estimated. As a result $H(k, k)$ is more accurate, and output at 3rd iteration is better. In Fig. 7, 8, 9, simulation results show 3rd iteration achieved better performance than 2nd iteration.

C. ICI Canceller with Different ICI Window Size W

As our above analysis, the bigger W the more ICI is removed. In addition, ($W = 31$) and ($W = 63$) provide similar performance, and almost ICI is considered. We evaluate bit error rate with different W at 1st iteration, and 2nd iteration. In Fig. 10 and Fig. 11, $W = 3, 5, 15, 31, 63$. The bit error rate confirmed the bigger W , the better performance. In addition, it is a slightly different between $W = 31$ and $W = 63$. Therefore, $W = 31$ is a reasonable choice for ICI window size.

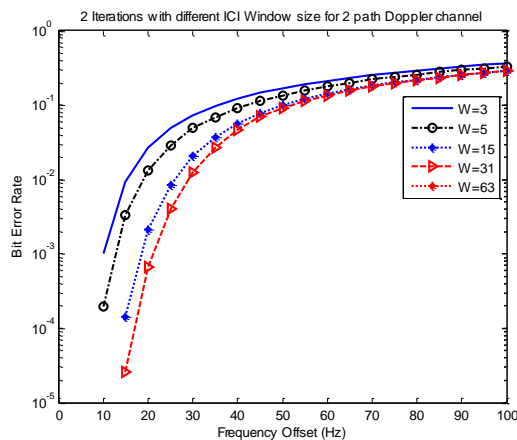


Figure 11. The Proposed Method with Different ICI Window Size

VI. CONCLUSION

In this paper, we achieved a good improvement by removing ICI from pilots and re-estimating channel transfer function-the diagonal of ICI matrix at 2nd, and 3rd iteration. The performance of our method is evaluated and compare with original method. As simulation result, our method doubled performance of

original method for TU-6 channel. The improvement is better for two paths and one path Doppler channel.

In addition, instead of direct solving ICI matrix, we applied Jacobi iteration with low complexity. We also present a simple and beautiful implementation of ICI canceller using FIR filter. This method is easy for hard-ware implementation. Moreover, we prove that 96% the ICI is considered by only 31 FIR taps. It is not necessary to choose a big number FIR taps such as maximum N taps. Therefore, we can keep the FIR at low cost. The simulation with different W also is consistent with our numerical analysis.

REFERENCES

- [1] Fischer, V. and Kupsiers, A. and Karsunke, D., "ICI reduction method for ofdm systems", *Hamburg: 8th International OFDM-Workshop*, pp. 1-5, 2003.
- [2] Mostofi, Y. and Cox, D.C., "ICI mitigation for pilot-aided OFDM mobile systems", *Wireless Communication, IEEE Transactions on, IEEE*, vol. 4, no. 2, pp. 765-774, 2005.
- [3] Jeon, W.G. and Chang, K.H. and Cho, Y.S., "An equalization technique for orthogonal frequency-division multiplexing systems in time-variant multipath channels", *Communications, IEEE Transactions on, IEEE*, vol. 47, no. 1, pp. 27-32, 1999.
- [4] Molisch, A.F. and Toeltsch, M. and Vermani, S., "Iterative methods for cancellation of intercarrier interference in OFDM systems", *Vehicular Technology, IEEE Transactions on, IEEE*, vol. 56, no. 4, pp. 2158—2167, 2007
- [5] Strang, G. and Massachusetts Institute of Technology, "Computational science and engineering", Wellesley-Cambridge Press Wellesley, MA, 2007.



Hai Minh Tran was born in Hanam, Vietnam, on June 09, 1988. He received the B.S. degree from Hanoi University of Technology, Vietnam in 2011.

He is currently a Master student in Graduate School of Engineering and Science, University of the Ryukyus. His research interests are channel estimation with its application to digital television mobile receiver and LTE system.



Tomohisa Wada received the BS degree in electronic engineering from Osaka Univ., Osaka, Japan, in 1983, M.S.E.E degree from Stanford Univ., Stanford CA, in 1992, and Ph.D. in electronic engineering from Osaka Univ. in 1994.

He joined the ULSI Laboratory Mitsubishi Electric Corp., Itami, Japan, in 1983. From 1983 to 1999, he has been engaged in the development of CMOS/BiCMOS static RAMs, 3-D graphics controller ASIC, flash memory, low-voltage static RAM, and synchronous burst static RAMs. In 1998, he joined Mitsubishi Electric Corp., Semiconductor Group, Memory ICI Division, Itami, where he has been working on the development of application specific synchronous burst static RAMs. In 1999, he became an Associate Professor with the Department of Information Engineering, Univ. of the Ryukyus, Okinawa, Japan. Since 2001, he has been a Professor at the Department of Information Engineering, Univ. Of the Ryukyus, Okinawa, Japan. In 2001, He was the founding member of Magna Design Net, Inc., which is a fab-less LSI design Company for communication related digital signal processing such as OFDM. Currently, he is also the chief scientist of Magna Design Net, Inc. From 1999 up to now, he has been engaged in the research and development of high bandwidth communication systems such as terrestrial video broadcasting receivers and wireless LAN. Currently, his research includes system-level large-scale VLSI design, digital signal processing for high-bandwidth communication, error correction algorithm and circuit, networking software and protocols.

Simple and Feasible Dynamic Bandwidth and Polling Allocation for XGPON

Man-Soo HAN

Dept. of Information and Communications, Mokpo National Univ., Korea
 mshan@mokpo.ac.kr

Abstract—In this paper, we propose a simple and feasible dynamic bandwidth allocation (SFDBA) algorithm in order to utilize the unallocated bandwidth and to achieve the implementation feasibility. SFDBA is based on an immediate allocation with colorless grant (IACG) algorithm but SFDBA uses only a single available byte counter and a single down counter for multiple queues of a same service class. Since multiple queues share the same available byte counter, the unallocated bandwidth of a queue can be utilized by another queues. For better service fairness, SFDBA changes the starting queue of scheduling in a round-robin manner. Using simulations, we show that SFDBA is superior to existing methods in mean delay, frame delay variance and frame loss rate.

Keywords—Keywords: Passive Optical Network, Dynamic Bandwidth Allocation, Polling, XGPON

I. INTRODUCTION

XGPON (10-gigabit-capable Passive Optical Network) consists of an optical line termination (OLT) and multiple optical network units (ONUs) [1]. In order to allocate non-collision transmission slots to ONUs, the OLT receives requests from ONUs and performs dynamic bandwidth allocation (DBA).

In the XGPON technology, the OLT has to produce DBA result in every frame duration which has a fixed to 125 μ s [1], [2]. Therefore, it is crucial that a DBA algorithm can be run within the frame duration in XGPON. Many algorithms have been proposed for GPON DBA [5]–[11]. To the best of our knowledge, however, only a GigaPON access network (GIANT), an immediate allocation with colorless grant (IACG), and efficient bandwidth utilization (EBU) have been physically implemented. These algorithms are simple and compliant to the GPON standards.

The GIANT algorithm is the first DBA algorithm that is physically implemented [6], [7]. In GIANT, each queue has a down counter for bandwidth allocation. The OLT can allocate bandwidth to a queue only when the down counter of the queue has expired. The simplicity of GIANT provides the implementation feasibility. Although GIANT provides good performance, it degrades performance since a request of a queue can not be granted until the down counter has expired.

In [8], IACG algorithm had been introduced. In IACG, each queue has an available byte counter and a down counter

in order for the fast bandwidth allocation. The OLT can immediately allocate a bandwidth to a queue if its available byte counter has a positive value. The available byte counter is decreased by the grant amount. The available byte counter is recharged when its down counter has expired. It was shown that IACG outperforms GIANT in [8]. Although IACG provides good performance, it does not effectively utilize the unused bandwidth of queues. The unused bandwidth of a queue cannot be used by another queues. It is desirable that the unused bandwidth is utilized by queues whose request sizes are larger than their reserved service bandwidth.

In [9], EBU algorithm had been introduced. EBU improves the unallocated bandwidth problem of IACG. In EBU, each queue has an available byte counter and a down counter like IACG. To utilize the unused bandwidth, the available byte counter can be negative. In addition, at the end of scheduling, the unused remainder of the available byte counter is added to the negative available byte counters. It was shown that EBU increases the utilization of the unused bandwidth compared to IACG in [9]. However, the operation of the available byte counter is complex and an extra stage is required for the update of the available byte counters. Therefore, the implementation complexity of EBU is higher than that of IACG.

In this paper, we propose a simple and feasible dynamic bandwidth allocation (SFDBA) algorithm in order to utilize the unused bandwidth and to achieve the implementation feasibility. SFDBA is based on IACG but it uses only a single available byte counter and a single down counter for a group of queues of a same service class. Since multiple queues share the common available byte counter, the unused bandwidth of a queue can be utilized by another queues. For better service fairness, SFDBA changes the starting queue of scheduling in a round-robin manner. Since only a common counter is used for a group of queues, SFDBA is simpler than IACG. Hence SFDBA is more feasible than IACG. Using simulations, we show that SFDBA is superior to IACG in mean delay, frame delay variance and frame loss rate. In addition, we illustrate that SFDBA is better than EBU in mean delay and frame delay variance despite that SFDBA is simpler than EBU.

In this paper, in the section II, we explain the bandwidth utilization problem of IACG algorithm and describe the proposed SFDBA algorithm. Then, we explain the polling mechanism of the proposed SFDBA algorithm in the section III. In the section IV, we evaluate performance of each algorithm and show that SFDBA algorithm outperforms IACG algorithm using simulations. Also we compare performance of SFDBA

Manuscript received June 6, 2013.

M.-S. Han is with the Dept. of Information and Communication, Mokpo National Univ., Jeonnam, Korea (phone: +82-61-450-2744; fax: +81-61-450-6470; e-mail: mshan@mokpo.ac.kr).

algorithm to that of EBU algorithm using simulations. The conclusions are given in the section V.

II. SIMPLE AND FEASIBLE DYNAMIC BANDWIDTH ALLOCATION

Fig. 1 shows the XGPON system. The XGPON system consists of an OLT and N ONUs. To support multiple service classes, ONU i maintains a queue q_{ij} for a service class j . A service class is known as a transmission container (T-CONT) type in XGPON technology. In this paper, we consider three service classes: T-CONT types 2, 3 and 4. Since a static bandwidth allocation is used for T-CONT type 1 in XGPON, we do not consider the T-CONT type 1. An incoming frame from users to ONU i is saved in q_{ij} if its T-CONT type is j . A queue has its unique Allocation Identifier (AllocID).

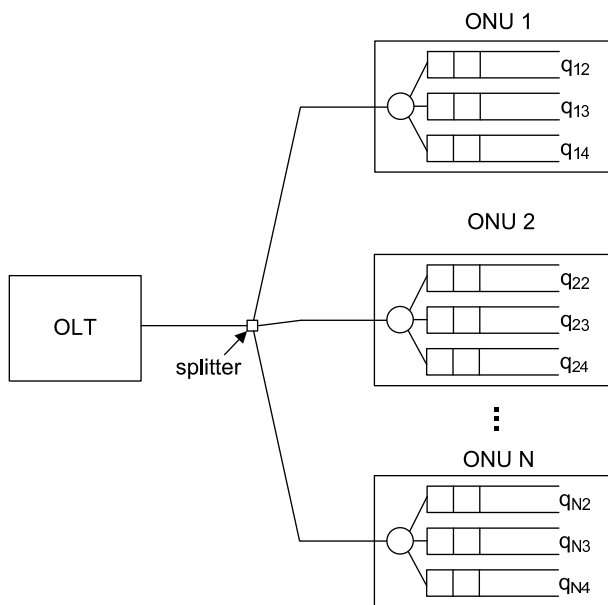


Fig. 1. XGPON system

In the downstream direction, the OLT broadcasts frames to each ONU. When a frame arrives from the OLT, each ONU accepts only if the destination of the frame is matched. In the upstream direction, ONUs transmit frames to the OLT in a time division multiple access manner. To assign a non-overlapping transmission time-slot to each ONU, the OLT performs dynamic bandwidth allocation (DBA).

In XGPON, every operation of OLT and ONU is synchronized with a fixed frame duration (FD) which is $125 \mu s$ long. The OLT collects the requests from ONUs, performs the DBA and produces the DBA result in every FD. The DBA result has the transmission slot information for an upcoming single FD. To receive the requests from ONUs, the OLT assigns a dynamic bandwidth report upstream (DBRu) transmission slot to a queue of an ONU. Using the DBRu slot, the queue sends its queue length to the OLT.

In IACG algorithm, a queue q_{ij} has two service parameters: a service interval S_{ij} with unit of FD and a maximum

allocation byte A_{ij} that can be maximally allocated to q_{ij} during its service interval S_{ij} . The queue q_{ij} has a down counter T_{ij} which is decreased by 1 for each FD. In addition, the queue q_{ij} maintains an available byte counter V_{ij} which denotes the remaining service bytes during its S_{ij} .

When the down counter T_{ij} has expired, T_{ij} is recharged to S_{ij} and the available byte counter V_{ij} is reset to A_{ij} . Let r_{ij} be the request of queue q_{ij} . In IACG, the OLT grants the minimum of the request r_{ij} and the value of V_{ij} . The OLT immediately decreases each the request r_{ij} and the value of V_{ij} by the grant amount. The maximum grant size of q_{ij} is limited by A_{ij} .

We now explain the bandwidth utilization problem of IACG. In IACG, a queue cannot use an unused bandwidth of another queue. For example, consider two queues of T-CONT type j , q_{1j} and q_{2j} . Suppose that $r_{1j} = 100$, $V_{1j} = 0$, $r_{2j} = 0$, and $V_{2j} = 100$. Then IACG will not grant any bandwidth for queue q_{1j} despite V_{2j} remains unused. This inefficiency of IACG degrades the DBA performance.

In order to solve the utilization problem of IACG, we propose SFDBA algorithm. In SFDBA, a queue does not have the individual counters T_{ij} and V_{ij} . Instead, all queues of the same T-CONT type share a single down counter and a single available byte counter. Let T_j and V_j be the common down counter and the common available byte counter of T-CONT type j , respectively. Also let S_j and A_j be the common service interval and the common maximum allocation byte of T-CONT type j , respectively.

The common down counter T_j is decreased by 1 for each FD. When the down counter T_j has expired, T_j is recharged to S_j and the common available byte counter V_j is reset to A_j . The common maximum allocation byte A_j is calculated by

$$\frac{A_j}{S_j} = \sum_{i=1}^N \frac{A_{ij}}{S_{ij}}. \quad (1)$$

In SFDBA, the OLT grants the minimum of the request r_{ij} and the value of V_j . The OLT immediately decreases each of the value of V_j and the request r_{ij} by the grant amount.

Since the single available byte counter is used for multiple queues, the upstream channel can be monopolized by a queue. To prevent the monopolization, the maximum grant size of a queue can be limited. In this case, the OLT grants the minimum of the request r_{ij} , the maximum grant size and the value of V_j . Another method to prevent the monopolization is traffic policing using the leaky bucket method [13] to control the traffic arrival rate of a queue. Since traffic policing is required in XGPON, we assume that the leaky bucket method is used in this paper for simplicity.

Fig. 2 shows the pseudo code of SFDBA for T-CONT type j where $j = 2, 3, 4$. Scheduling is performed in the order of T-CONT types 2, 3, and 4. In Fig. 2, the round robin pointer P_j denotes the ONU number at which scheduling starts. To provide the service fairness, the starting ONU number in the scheduling is changed in the round robin fashion. The variable F is the remaining bytes of FD and its initial value is 38,880 bytes when the upstream channel speed is 2.5 Gbps. The variable g_{kj} is the grant amount of queue q_{kj} . The

```

// k = ONU number
// j = T-CONT type
k = stop = Pj;
while(1){
    if (Vj > 0 and F > 0){
        gkj = min(Vj, rkj, F);
        Vj = Vj - gkj;
        rkj = rkj - gkj;
        F = F - gkj;
    } else if (alloc_end = 0 and F = 0){
        Pj = k;
        alloc_end = 1;
    }
    Tj = Tj - 1;
    if (Tj = 0){
        Tj = Sj;
        Vj = Aj;
        PFkj = 0;
    }
    k++;
    k = k mod N;
    if (k = stop) break;
}
    
```

Fig. 2. Pseudo code of SFDBA for T-CONT type 2, 3 and 4

variable *alloc_end* means the end of the allocation. When *alloc_end* = 1, the allocation has ended. The initial values of *g_{kj}* and *alloc_end* are zero. The variable *PF_{kj}* denotes the polling flag of *q_{kj}*. The polling flag *PF_{kj}* is used in the polling operation of SFDBA and will be explained in Section III.

For the previous utilization example of IACG, we apply SFDBA by assuming $V_j = V_{1j} + V_{2j} = 100$. Then SFDBA will grant 100 byte for queue *q_{1j}*. Unlike IACG, the unused bandwidth of *q_{2j}* is used by *q_{1j}* in SFDBA.

If the total sum of requests is less than the size of FD, then the upstream channel cannot be fully allocated. To utilize the unallocated remainder of FD, the remainder is evenly distributed to each ONU in IACG [8]. To distinguish the remainder from normal grants, the remainder has T-CONT type 5 and is called as the colorless grant. An ONU can send packets arrived after the ONU sent its request using the colorless grant. Note that ONU does not has a queue with T-CONT type 5. Using the colorless grant, ONU transmits packets from queues in the order of T-CONT types 2, 3 and 4. We use the colorless grant scheme of IACG in SFDBA. At the end of DBA, the colorless grant of ONU *k* is given by F/N where *F* is the remaining bytes of FD.

III. POLLING OPERATION OF SFDBA

Now we describe the polling method of SFDBA. Fig. 3 describes the transmission timing diagram of XGPON. In Fig. 3, the maximum distance between an OLT and ONU is 20 Km. Also, *U_i* means the *i*-th upstream FD and *D_i* denotes the *i*-th downstream FD. RTT is the round trip time between an ONU and an OLT. If the distance between the OLT and the ONU is 20 Km, RTT is 200 μ s. The variable *T_O* is the ONU response time to receive the grant result from the OLT and to prepare an upstream response. In this paper, *T_O* = 35 μ s as in [1].

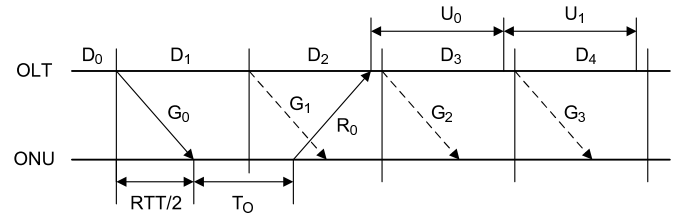


Fig. 3. Transmission timing diagram

In this paper, we modify the polling mechanism of IACG [8]. In Fig. 3, *G_i* is the *i*-th grant result and *R₀* is the first request of the ONU. The DBRu field is used by the ONU to transmit its request. The *i*-th grant result is produced by the DBA operation in *D_i* and is transmitted to the ONU at the beginning of the downstream FD, *D_{i+1}*. When the ONU receives the grant result, it waits for *T_O*, then sends its request *R₀* and data packets during the upstream FD, *U₀*. The request *R₀* is the total length of packets in a queue. Since the request *R₀* is sent before data packets, it does not reflect the grant result *G₀*. The requests received during *U₀* are used in the DBA at the downstream FD, *D₄*. Since SFDBA may produce grant results for the ONU during *D₁*, *D₂*, and *D₃*, the grant results must be reflected in *R₀*. Thus, in order to obtain the correct request, the OLT has to subtract the grant results *G₀*, \dots , *G₃* from *R₀* at the beginning of *D₄*. Therefore, the OLT needs to remember the four most recent grant results for obtaining the correct request.

We now explain the DBRu field allocation mechanism of SFDBA. Queue *q_{kj}* has a polling flag *PF_{kj}*. The OLT can allocate the DBRu field to queue *q_{kj}* when *PF_{kj}* = 0. If the OLT allocate the DBRu field to *q_{kj}*, the flag *PF_{kj}* is set to 1. The flag *PF_{kj}* is reset to 0 when the down counter *T_j* has expired. Therefore, queue *q_{kj}* has a chance to receive the DBRu field once per the service interval *S_j*.

Fig. 4 describes the pseudo code of the SFDBA polling operation. In Fig. 4, *L_j* is the ONU number at which the polling operation starts for T-CONT type *j*. The variable *DBR_{kj}* means whether or not the DBRu field is assigned to *q_{kj}*. The variable *DS* is the size of the DBRu field. In the XGPON standard, the size *DS* is 4 bytes. The variable *poll_end* represents the end of polling operation. The polling flag *PF_{kj}* is set to 0 when the down counter *T_j* has expired as shown in Fig. 2.

```

// k = ONU number
// j = T-CONT type
k = stop = Lj;
while(1){
    DBRkj = 0;
    if (PFkj = 0 and F > 0){
        PFkj = 1;
        DBRkj = 1;
        F = F - DS;
    } else if (poll_end = 0 and F = 0){
        Lj = k;
        poll_end = 1;
    }
    k++;
    k = k mod N;
    if (k = stop) break;
}
    
```

Fig. 4. Pseudo code of SFDBA polling operation

IV. PERFORMANCE EVALUATION

A. Comparison to IACG

Now we compare performance of SFDBA, IACG and predictive-colorless-grant offset-based scheduling with flexible intervals (PCG-OSFI) [10] using simulations. We consider an XGPON system with $N = 16$, the maximum ONU line rate of 200 Mbps, the upstream channel rate of 2.5 Gbps. Also suppose that the maximum round trip time between the OLT and ONUs is 200 μ s, and the ONU response time is 35 μ s. The size of a queue q_{ij} is 1 Mbytes.

For the T-CONT type 2 of IACG, we set $A_{i2} = 7812$, $S_{i2} = 5$, which is equivalent to 100 Mbps. For the T-CONT type 3 of IACG, we set $A_{i3} = 15624$, $S_{i3} = 10$. That is, 100 Mbps is given to the T-CONT type 3. For the T-CONT type 4 of IACG, $A_{i4} = 15624$, and $S_{i4} = 10$, which is equivalent to 100 Mbps. For the T-CONT type 2 of SFDBA, we set $S_2 = 5$ and we obtain $V_2 = 7812 \times N$ from Eq. (1). For the T-CONT types 3 and 4, we set $S_3 = S_4 = 10$. Then we have $V_3 = V_4 = 15624 \times N$. The reserved bandwidth for each T-CONT type of PCG-OSFI is equal to that of IACG.

We use the self-similar traffic model of [12] where each ONU is fed by a number of Pareto distributed on-off processes. The shape parameters for the on and off intervals are set to 1.4 and 1.2, respectively. Hence, the Hurst parameter is 0.8. The frame size follows the tri-modal distribution [12], where the frame sizes are 64, 500, and 1500 bytes and their load fractions are 60%, 20% and 20%, respectively as in [6]. Each simulation is performed until the total number of frames transmitted by ONUs exceeds 10^9 for each algorithm.

Traffic is balanced so that each ONU and each queue has an identical traffic load fraction. The traffic load of each ONU

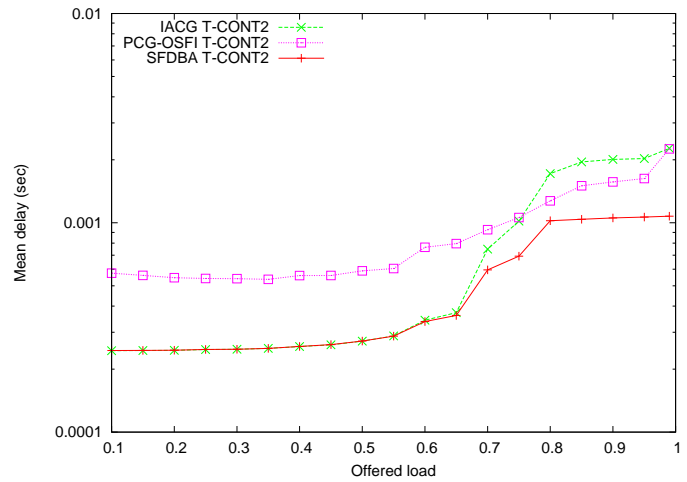


Fig. 5. Mean delay of T-CONT type 2

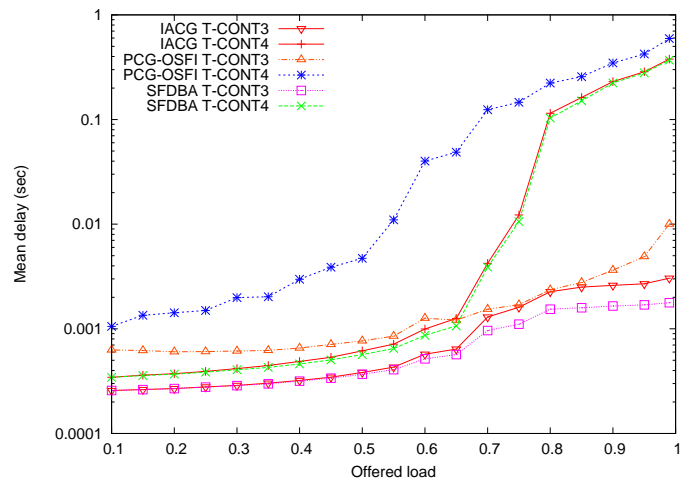


Fig. 6. Mean delay of T-CONT types 3 and 4

varies from 0.1 to 0.99. Figs. 5 and 6 show the mean delay of each algorithm. Note that the offered load means the input traffic load of a single ONU in the Figs. As we can see from Figs. 5 and 6, the proposed method outperforms other methods in mean delay.

Figs. 7 and 8 depict the frame delay variance of each algorithm. Figs. 7 and 8 show that the proposed method outperforms other methods in frame delay variance. Fig. 9 illustrates the frame loss rate of each algorithm for T-CONT types 2 and 3. Thanks to the utilization of unused bandwidth, the loss rate of SFDBA is better than those of other methods.

B. Comparison to EBU

To increase the DBA efficiency, EBU can allocate an additional DBRu field to a queue [9]. In EBU, the OLT allocates the DBRu field once per its service interval like IACG. Also the OLT can allocate an additional DBRu field to a queue. If the grant $g_{ij} > 0$ and the DBRu field is not allocated to the

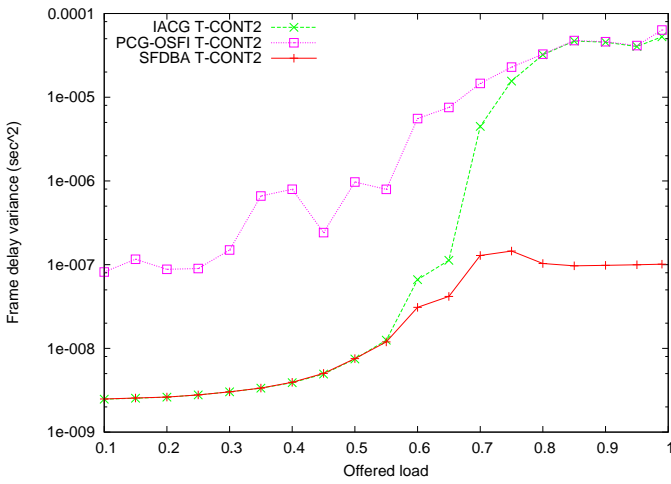


Fig. 7. Frame delay variance of T-CONT type 2

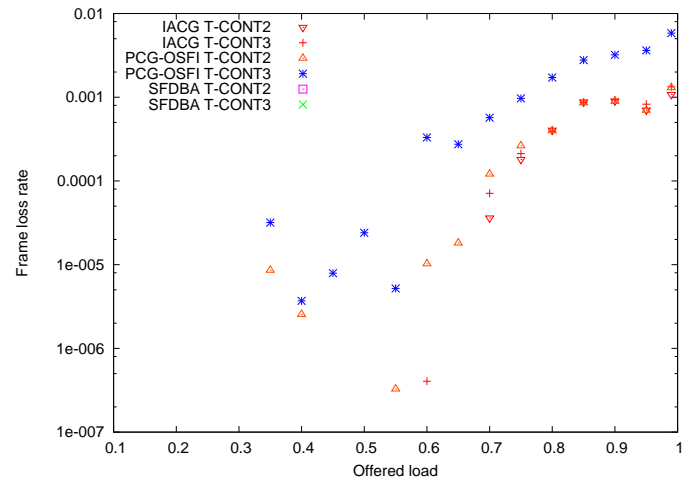


Fig. 9. Frame loss rates of T-CONT types 2 and 3

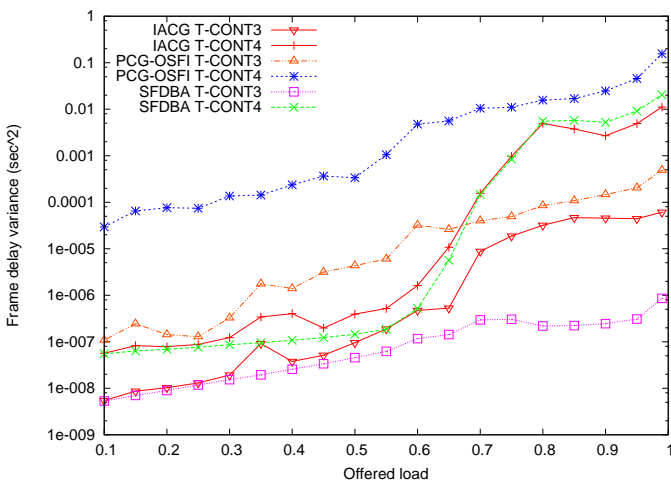


Fig. 8. Frame delay variance of T-CONT types 3 and 4

queue q_{ij} then the OLT allocates the additional DBRu field to the queue q_{ij} . It was shown that the additional DBRu is very effective in [9]. To compare performance of EBU with that of SFDBA, we apply the additional DBRu mechanism to the polling operation of SFDBA in this subsection.

We use the same system, the same parameters, and the same traffic of the subsection IV-A. For the T-CONT type 2 of EBU, we set $A_{i2} = 7812$, $S_{i2} = 5$, which is equivalent to 100 Mbps. For the T-CONT type 3 of EBU, we set $A_{i3} = 15624$, $S_{i3} = 10$. That is, 100 Mbps is given to the T-CONT type 3. For the T-CONT type 4 of EBU, $A_{i4} = 15624$, and $S_{i4} = 10$, which is equivalent to 100 Mbps. We do not use the non-assured T-CONT type 3 of EBU.

Figs. 10 and 11 show the mean delay of each algorithm. As we can see from Figs. 10 and 11, the proposed SFDBA outperforms the EBU algorithm in mean delay. In EBU, an unused bandwidth of a queue q_{ij} is added to the available byte counter of another queue only when the down counter T_{ij} has

expired. It means that the unused bandwidth of the queue q_{ij} cannot be utilized until its down counter T_{ij} has expired. In contrast, since SFDBA uses a common available byte counter, an unused bandwidth of a queue can be immediately used by another queues. This difference makes the proposed SFDBA algorithm works better than the EBU algorithm.

Figs. 12 and 13 depict the frame delay variance of each algorithm. Figs. 12 and 13 show that the proposed SFDBA is better than the EBU method in frame delay variance. Fig. 14 illustrates the frame loss rate of each algorithm for T-CONT type 4. The frame loss rates of T-CONT types 2 and 3 are zero in both algorithm thanks to the utilization of the unused bandwidth and the additional polling mechanism. The frame loss rates of both algorithms are comparable to each other for T-CONT type 4 as we can see in Fig. 14.

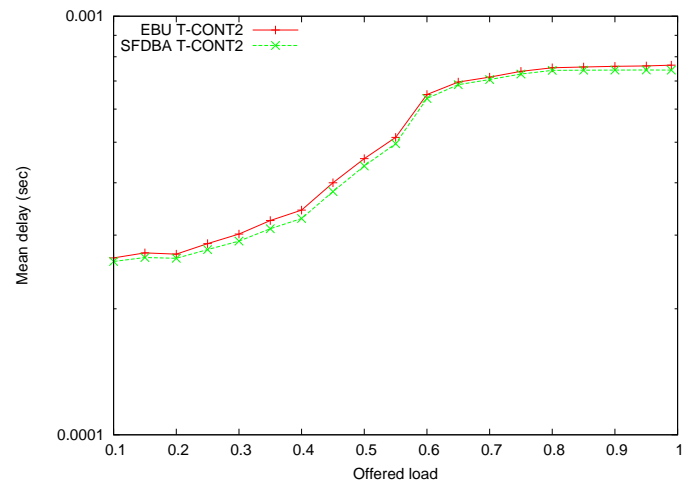


Fig. 10. Mean delay of T-CONT type 2

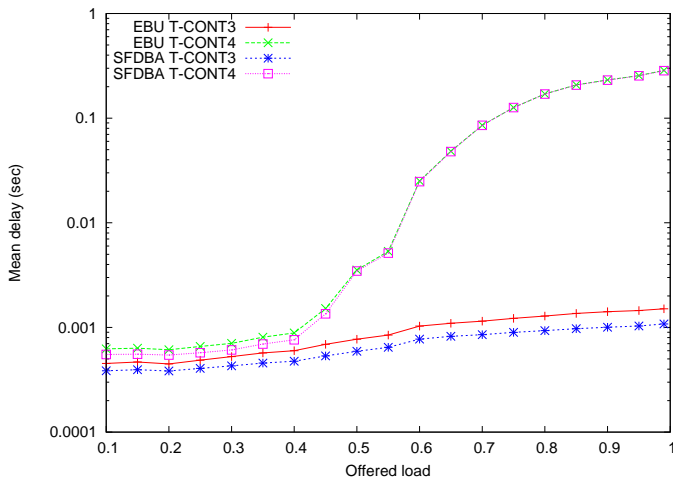


Fig. 11. Mean delay of T-CONT types 3 and 4

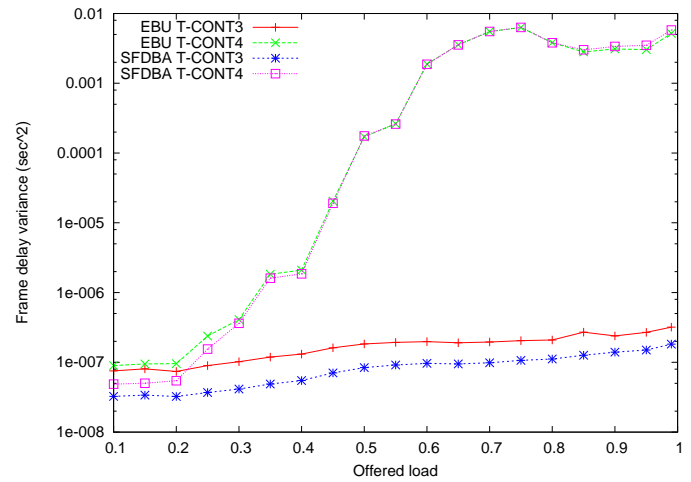


Fig. 13. Frame delay variance of T-CONT types 3 and 4

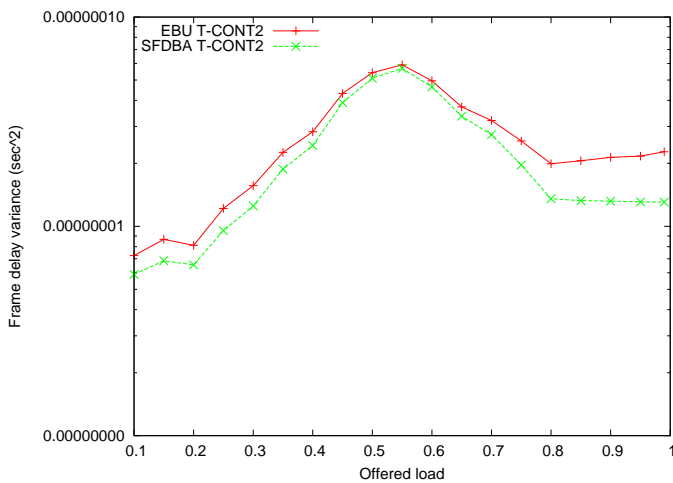


Fig. 12. Frame delay variance of T-CONT type 2

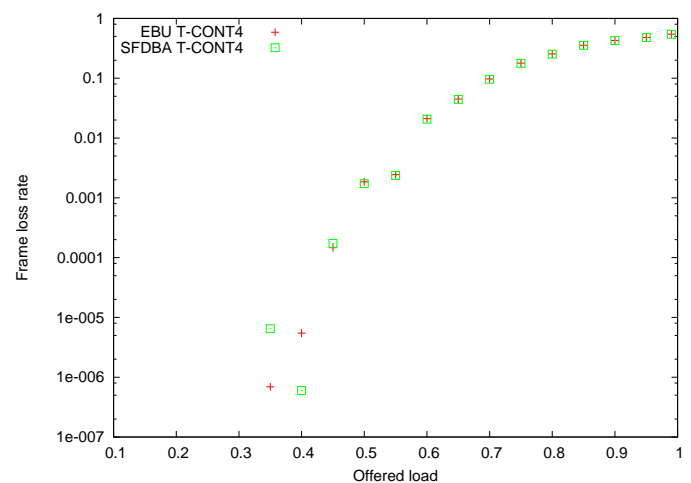


Fig. 14. Frame loss rate of T-CONT type 4

V. CONCLUSIONS

We have proposed the SFDBA algorithm for the dynamic bandwidth allocation of XGPON by modifying the IACG algorithm. In IACG, a queue has a down counter to count its service interval and has an available byte counter to control its service amount. Because of the individual counters, a queue can not utilize the unused bandwidth of another queues in IACG. In order to solve the utilization problem of IACG, in SFDBA, all queues of a same T-CONT type use a common down counter and a common available byte counter. Thanks to the common counters, a queue can utilize the unused bandwidth of another queues. Using simulations, we have shown SFDBA outperforms existing algorithms in mean delay, frame delay variance and frame loss rate.

REFERENCES

[1] ITU-T Rec. G.987.3 Rev.2, "10-Gigabit-capable passive optical networks (XG-PON): Transmission convergence (TC) specifications,"

2010.
 [2] ITU-T Rec. G.987.1, "10 Gigabit-capable passive optical network (XG-PON): General requirements," 2010.
 [3] ITU-T Rec. G.984.3, "Gigabit-capable passive optical networks (G-PON): Transmission convergence layer specification," 2008.
 [4] ITU-T Rec. G.984.1, "Gigabit-capable passive optical networks (G-PON): General characteristics," 2008.
 [5] J. D. Angelopoulos, H. C. Leligou, and T. Argyriou, "Prioritized multiplexing of traffic accessing an FSAN-compliant GPON," Third IFIP-TC6 Networking Conference, Arthens, Greece, 2004.
 [6] H. C. Leligou, Ch. Linardakis, K. Kanonakis, J. D. Angelopoulos, and Th. Orphanoudakis, "Efficient medium arbitration of FSAN-compliant GPONs," *Int. J. Comm. Syst.*, vol. 19, no. 5, pp. 603-617, June 2006.
 [7] J. D. Angelopoulos, T. Argyriou, S. Zontos, and T. Van Caenegem, "Efficient transport of packets with QoS in an FSAN-aligned GPON," *IEEE Comm. Mag.*, vol. 42, no. 2, pp. 92-98, Feb. 2004.
 [8] M.-S. Han, H. Yoo, B.-Y. Yoon, B. Kim, and J.-S. Koh, "Efficient dynamic bandwidth allocation for FSAN-Compliant GPON," *OSA J. Opt. Netw.*, vol. 7, no. 8, pp. 783-795, Jul. 2008.
 [9] M.-S. Han, H. Yoo, and D.-S. Lee, "Development of Efficient Dynamic

- Bandwidth Allocation Algorithm for XGPON,” ETRI Journal, vol. 35, no. 1, pp. 18-26. 2013.
- [10] K. Kanonakis and I. Tomkos, “Offset-Based Scheduling With Flexible Intervals for Evolving GPON Networks,” Journal of Lightwave Technology, vol. 27, no. 15, pp. 3259-3268, Aug. 2009.
- [11] C. H. Chang, N. M. Alvarez, P. Kourtessis, R. M. Lorenzo, and J. M. Senior, “Full-Service MAC Protocol for Metro-Reach GPONs,” Journal of Lightwave Technology, vol. 28, no. 7, pp. 1016-1022, April 2010.
- [12] G. Kramer, Ethernet passive optical networks, McGraw-Hill, 2005.
- [13] A. S. Tanenbaum, “Computer Networks, Fourth Edition,” Prentice Hall PTR, 2003.



Man Soo Han received the B.S., M.S. and Ph.D. degrees in electrical engineering from Korea Advanced Institute of Science and Technology (KAIST), Korea in 1992, 1994 and 1999 respectively. He was a senior researcher of the Electronics and Telecommunications Research Institute (ETRI) Daejeon, Korea from 1999 to 2003. He is an associate professor in the Department of Information and Communications Engineering at Mokpo National University, Korea. His research interest includes scheduling in high speed networks, passive optical networks and wireless networks. He is a member of IEEE, OSA, IEICE, and KICS.

Effective Use of Computational Resources in Multicore Distributed Systems

Hidehiro Kanemitsu*, Masaki Hanada**, Takashige Hoshiai***, Hidenori Nakazato****

*Media Network Center, Waseda University, Japan

**Department of Information Systems, Tokyo University of Information Sciences, Japan

***Department of Computer and Information Science, Sojo University, Japan

****Global Information and Telecommunication Institute, Waseda University, Japan.

kanemih@ruri.waseda.jp, mhanada@rsch.tuis.ac.jp, hoshiai@cis.sojo-u.ac.jp, nakazato@waseda.jp

Abstract—In the last decades, many kinds of task execution models such as grid and cloud computing have been developed. In such distributed systems, each task is processed by respective processor in multicore computers e.g., household PCs which we can easily harness in recent years. If there is one policy to automatically decide the “best” combination and the number of processors (and computers), we effectively utilize those computational resources, thereby large number of jobs can be executed in parallel. In this paper, we propose a method for mapping of execution units for such environments. The method adopts a remapping technology after processor-execution unit mapping[11] is finished. Experimental comparisons by a simulation show the advantages of the proposed method.

Index Terms—Task Clustering, Multicore, Distributed Systems, Parallel Computing

I. INTRODUCTION

RECENTLY, task execution models are becoming diverse, e.g., grid computing[1], cloud computing. Such computational models often require parallel execution models such as parametric job execution, background data analysis for data mining, and searching for a target value in a key-value store[2]. Irrespective of dedicated computers or household computers, they should be effectively used when a parallel execution model is applied. Moreover, requirements for job execution tends to become diverse due to multiple demands from the job submitter. To handle with such diversity, multi-objective approaches for task scheduling and resource allocation model have been proposed and being under development[3], [4], [5]. Those approaches assume that requirements (e.g., QoS, deadline for the job execution, total costs, and so on) are decided by a job submitter, i.e., an user. Thus, those multi-objective approaches focus on how to satisfy every objective specified by an user. If multiple objective should be satisfied

at the same time in a distributed environment, dynamic natures such as every computer’s load and CPU status and so on must be taken into account. To do this, provisioning is needed for preparing calculate every problems provided by those objectives. For example, how to propagate each computer’s resource information and how to aggregate “peers” to construct peer groups in the overlay network based on specific criteria in advance are indispensable[3], [6], [7].

We proposed a method for effective use of computational resources each of which has a single processor in a heterogeneous distributed system [11]. The method automatically derives set of mapping between each processor and each assignment unit (i.e., the set of tasks in a “ DAG (Directed Acyclic Graph) ” program such as a workflow type job), by which the degree of contribution for each processor toward the response time minimization is maximized. However, the method does not assume more realistic situations, e.g., each computer may have a parallel execution scheme such as multicore and multi OS by virtualization. Thus, our previously proposed method can not be applied to those environments. If a model which accommodates them, the response time can be minimized with a smaller number of computers. In this paper, we propose a theoretical method for deciding the set of mapping between each computer and each assignment unit for effective use of computational resources, where each computer can have parallel execution scheme. The proposed method assumes that a computer with two or more processors as “ two or more processors are completely connected over the network with infinite network bandwidth ”. Then a lower bound of assignment unit size is mathematically decided for each processor for limiting the number of processors. Actual assignment units are generated by a task clustering algorithm until each size exceeds the lower bound. Among processors which belong to the same computer, every task in assignment units is locally scheduled without degrading task parallelism. Consequently, the required number of computer can be smaller than that of the method proposed in [11]. Experimental comparison is conducted by a simulation program. In the simulation, we evaluate the degree of contribution for each computer and show advantages of the proposed method over related works and the method we proposed in [11].

The remainder of this paper is organized as follows. Sec. II presents our assumed model. Then problem definitions and the objective of the proposal are presented in sec. III. The detailed

Manuscript received June 25, 2013.

Hidehiro Kanemitsu is with Media Network Center, Waseda University, 1-104, Totsuka, Shinjuku, Tokyo, Japan (phone: +81-3-3204-8223; e-mail: kanemih@ruri.waseda.jp).

Masaki Hanada is with Department of Information Systems, Tokyo University of Information Sciences, 4-1, Onaridai, Wakaba, Chiba, Japan (phone:+81-43-236-1101;e-mail: mhanada@rsch.tuis.ac.jp).

Takashige Hoshiai is with Department of Computer and Information Science, Sojo University, 4-22-1, Ikeda, Nishi, Kumamoto, Japan (phone: +81-96-326-3111;e-mail: hoshiai@cis.sojo-u.ac.jp).

Hidenori Nakazato is with Global Information and Telecommunication Institute, Waseda University, Bldg. 29-7, 1-3-10 Nishi-Waseda Shinjuku-ku, Tokyo, Japan (phone: +81-3-3203-4151; e-mail: nakazato@waseda.jp) .

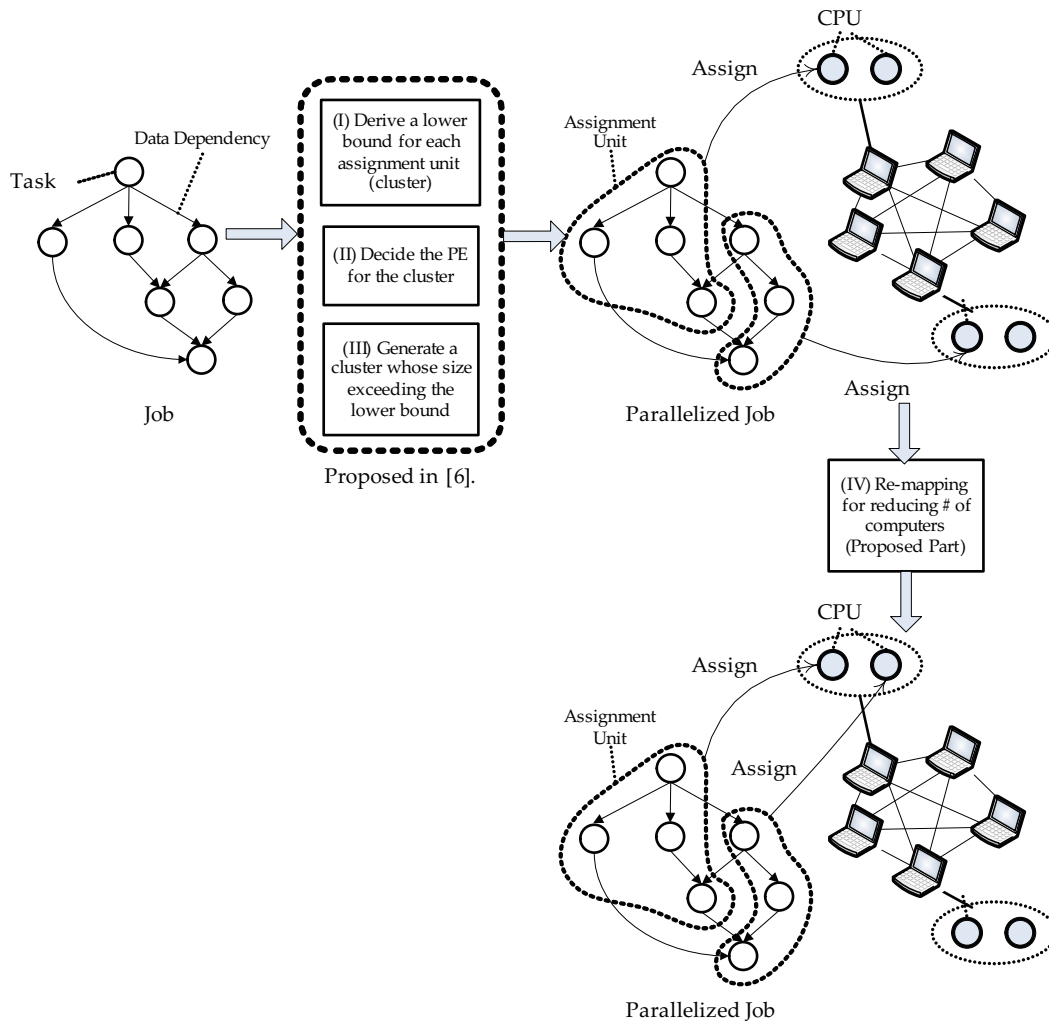


Fig. 1. Proposed part

content of the proposal is presented in sec. IV, and theoretical analysis in terms of effect of the proposal is presented in sec. V. Advantages of the proposal is shown by the experimental comparisons in sec. VI. Finally, a conclusion and a future work are presented in sec. VII.

II. ASSUMED MODEL

A. Job Model

An assumed job is expressed as a Directed Acyclic Graph (DAG), which is known as one of task graph representations. Let $G_{cls}^s = (V_s, E_s, V_{cls}^s)$ be the DAG, where s is the number of task merging steps (described in the latter half part in this subsection), V_s is the set of tasks after s task merging steps, E_s is the set of edges (data communications among tasks) after s task merging steps, and V_{cls}^s is the set of clusters which consists of one or more tasks after s task merging steps. An i -th task is denoted as n_i^s . Let $w(n_i^s)$ be a size of n_i^s , i.e., $w(n_i^s)$ is the sum of unit times taken for being processed by the reference processor element. We define data dependency and direction of data transfer from n_i^s to n_j^s as $e_{i,j}^s$. And $c(e_{i,j}^s)$ is the sum of unit times taken for transferring data from n_i^s to n_j^s over the reference communication link.

One constraint imposed by a DAG is that a task can not be started execution until all data from its predecessor tasks arrive. For instance, $e_{i,j}^s$ means that n_j^s can not be started until data from n_i^s arrives at the processor which will execute n_j^s . And let $pred(n_i^s)$ be the set of immediate predecessors of n_i^s , and $suc(n_i^s)$ be the set of immediate successors of n_i^s . If $pred(n_i^s) = \emptyset$, n_i^s is called START task, and if $suc(n_i^s) = \emptyset$, n_i^s is called END task. If there are one or more paths from n_i^s to n_j^s , we denote such a relation as $n_i^s \prec n_j^s$.

B. Task Clustering

We denote the i -th cluster in V_{cls}^s as $cls_s(i)$. If n_k^s is included in $cls_s(i)$ by “the $s + 1$ th task merging”, we formulate one task merging as $cls_{s+1}(i) \leftarrow cls_s(i) \cup \{n_k^s\}$. If any two tasks, i.e., n_i^s and n_j^s , are included in the same cluster, they are assigned to the same processor. Then the communication between n_i^s and n_j^s is localized, so that we define $c(e_{i,j}^s)$ becomes zero. Task clustering[8], [9], [10] is a set of task merging steps, that is finished when certain criteria have been satisfied.

C. System Model

We assume that each computer is completely connected to others, with not identical processing speeds and communication bandwidths. Each computer has one or more processing elements (PE). The set of computers is expressed as $M = \{M_1, M_2, \dots, M_m\}$. The set of PEs in M_i is expressed as $P_i = \{P_{i,1}, P_{i,2}, \dots, P_{i,|P_i|}\}$, and let the set of processing speeds in P_i as α_i , i.e., $\alpha_i = \{\alpha_{i,1}, \alpha_{i,2}, \dots, \alpha_{i,|P_i|}\}$, where $|P_i| = |\alpha_i|$.

As for data communication among computers, let the set of communication bandwidths be β , i.e.,

$$\beta = \begin{pmatrix} \infty & \beta_{1,2} & \beta_{1,3} & \dots & \beta_{1,m} \\ \beta_{2,1} & \infty & \beta_{2,3} & \dots & \beta_{2,m} \\ \beta_{3,1} & \beta_{3,2} & \infty & \dots & \beta_{3,m} \\ \vdots & \vdots & \vdots & \ddots & \vdots \\ \beta_{m,1} & \beta_{m,2} & \beta_{m,3} & \dots & \infty \end{pmatrix} \quad (1)$$

$\beta_{i,j}$ means the bandwidth from M_i to M_j . We assume that a communication bandwidth between two computers, e.g., M_i and M_j is the same between any one of P_i and any one of P_j . The processing time in the case that n_k^s is processed on $P_{i,p}$ is expressed as $t_p(n_k^s, \alpha_{i,p}) = w(n_k^s)/\alpha_{i,p}$. The data transfer time of $e_{k,l}^s$ over $\beta_{i,j}$ is $t_c(e_{i,j}^s, \beta_{k,l}) = c(e_{i,j}^s)/\beta_{k,l}$. This means that both processing time and data transfer time are not changed with time, and suppose that data transfer time within one computer is negligible.

III. PROBLEM DEFINITION

A. Processor Utilization in Singlecore Distributed systems

In this paper, we propose a method for processor utilization in a distributed system, where each computer has one or more PEs. The difference between the method proposed in [11] and a method in this paper is whether such multicore computers are considered or not. According to [11], ‘‘processor utilization’’, in other words, ‘‘effective use of computational resources’’, means to maximize the degree of contribution for reducing the schedule length for each PE. Fig. 1 shows a process flow we are assuming. A job is processed by three steps, i.e., (I) a lower bound for each cluster (set of tasks) execution time is derived, (II) mapping procedure to assign a PE to a cluster, (III) task clustering algorithm to generate actual clusters. Since these procedures were proposed in [11], we describe only the abstract.

1) *Lower Bound Derivation for each Cluster Execution Time:* According to fig. 1, the method proposed in [11] derives a lower bound for each cluster execution time (total task execution time in a cluster on a PE). To impose a lower bound, the number of required PEs is limited to some extent. At the same time, the response time should be minimized for achieving processor utilization.

Since the schedule length can not be derived until every task is scheduled, each lower bound should be decided with estimating the schedule length. This is because these three procedures in fig. 1 are performed before a task scheduling[14]. Thus, the method in [11] defines an indicative value for the schedule length as WSL (Worst Schedule Length) [11]. Let

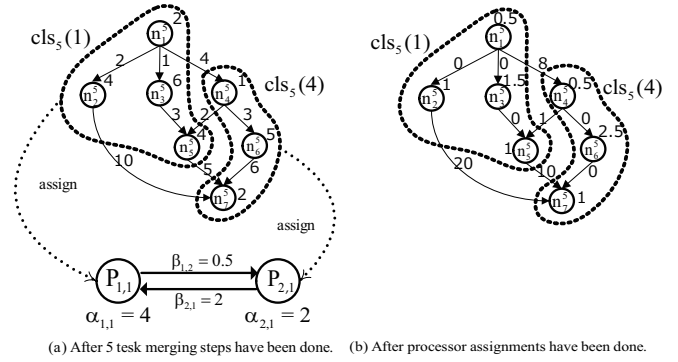


Fig. 2. Example of WSL

define ‘‘WSL after s -th task merging step’’ as $sl_w(G_{cls}^s, \phi_s)$, which means the largest value that the response time can take when every task is executed as late as possible after s task merging steps and the mapping state ϕ_s has been decided.

Fig. 2 shows one example of how WSL is decided. In this figure, (a) is the state after 4 task merging steps have been finished, and (b) is the state that each generated cluster is assigned to one actual PE. In (b), note that data communication time in the same PE is set to 0. Then we WSL is derived by tracing $n_1^5 \rightarrow n_3^5 \rightarrow n_5^5 \rightarrow n_2^5 \rightarrow n_7^5$, i.e., $sl_w(G_{cls}^6, \phi_6) = 25$.

In [11], it is proved that minimizing WSL has good effect on the schedule length, i.e., it is necessary that WSL should be minimized to minimize the schedule length. Since actual WSL after s -th task merging step can not be decided until s task merging steps have been finished, we must estimate the upper bound of WSL after $s - 1$ task merging steps have been finished(i.e., before s -th task merging step). If we define an upper bound of the difference between WSL after s -th task merging step and the initial WSL(i.e., 0-th task merging step) as $\Delta sl_w^{s-1}(\delta)$, we have

$$\Delta sl_w^{s-1}(\delta) = \left(\frac{\max_{n_k^0 \in V_0} \{w(n_k^0)\}}{\alpha_p} + \frac{\max_{e_{k,l}^0 \in E_0} \{c(e_{k,l}^0)\}}{\beta(p)} \right) \frac{\sum_{n_k^0 \in seq_{s-1}^<} w(n_k^0)}{\delta \alpha_p} + \delta - \frac{\max_{e_{k,l}^0 \in E_0} \{c(e_{k,l}^0)\}}{\max_{\beta_{p,q} \in \beta} \{\beta_{p,q}\}}, \quad (2)$$

where ϕ_0 is the initial mapping state that each task is assigned to a ‘‘virtual PE’’ having the maximum processing speed and the maximum communication bandwidth. At the mapping state ϕ_0 , the critical path length equals to the WSL at the initial state ϕ_0 (for more details, see [11]). At eq. (2), δ is the lower bound of each cluster execution time. δ is derived by temporarily assuming identical network, where we derive the lower bound for every cluster execution time on tasks dominating the WSL. $seq_{s-1}^<$ is a set of tasks on a path dominating $sl_w(G_{cls}^{s-1}, \phi_{s-1})$ (e.g., at (b) in fig. 2, $seq_5^<$ is $\{n_1^5, n_3^5, n_5^5, n_7^5\}$ or $\{n_1^5, n_2^5, n_7^5\}$).

Fig. 3 shows one example how δ is derived. In this figure, (a) is the state after 4 task merging steps have been finished. In (a) there are unmerged tasks each of which is assigned to the

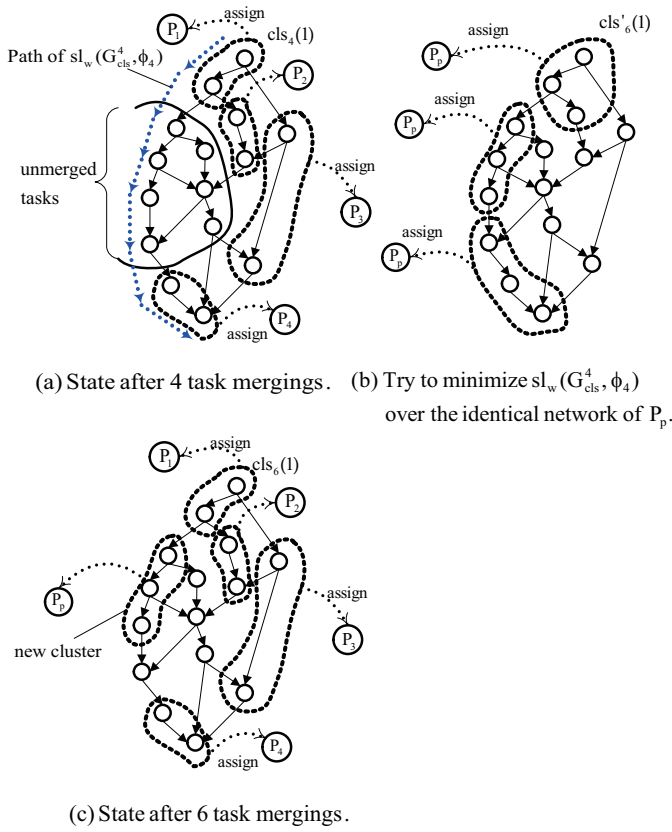


Fig. 3. Assumed model for WSL derivation

“virtual PE” having the maximum processing speed and communication bandwidth, respectively. On the other hand, other tasks are assigned to an actual PE. In this state, the dashed line corresponds to the path of WSL, i.e., $sl_w(G^4_{cls}, \phi_4)$. Then we temporarily assume these tasks will be clustered and each cluster is assigned to an identical PE (in (b), the PE is P_p). We have $\Delta sl_{w,up}^4(\delta)$, which is a function with respect to δ . From (b) we obtain the optimal value of δ (let call “ δ_{opt} ”) by which $\Delta sl_{w,up}^4(\delta)$ is minimized. Once δ_{opt} is obtained, every cluster in (b) is restored to clusters in (a) and then unmerged tasks in (a) are merged into one new cluster until its execution time exceeds δ_{opt} (see (c)). It is assumed that the cluster execution time of the new cluster in (c) exceeds δ_{opt} after 6 task merging steps (it was not enough after 5 task merging steps).

We obtain the minimum value of $sl_{w,up}^{s-1}$ by differentiating eq. (2) with respect to δ . If we define the value of δ when $sl_{w,up}^{s-1}$ takes the minimum as $\delta_{opt}^s(P_p)$, we have

$$\delta_{opt}^s(P_p) = \sqrt{\frac{\sum_{n_k^0 \in seq_{s-1}} w(n_k^0)}{\alpha_p} \left(\frac{\max_{n_k^0 \in V_0} \{w(n_k^0)\}}{\alpha_p} + \frac{\max_{e_{k,l}^0 \in E_0} \{c(e_{k,l}^0)\}}{\beta(p)} \right)},$$

where $\beta(p)$ is the minimum communication bandwidth of P_p . $\delta_{opt}^s(P_p)$ is the lower bound of the cluster execution time to be generated after s -th task merging step. If $\delta_{opt}^s(P_p)$ is applied to $\Delta sl_{w,up}^{s-1}(\delta)$, we have

$$\Delta sl_{w,up}^{s-1}(\delta_{opt}^s(\alpha_p, \beta(p))) = \frac{2}{\alpha_p} \times \sqrt{\sum_{n_k^0 \in seq_{s-1}} w(n_k^0) \left(\frac{\alpha_p \max_{e_{k,l}^0 \in E_0} \{c(e_{k,l}^0)\}}{\beta(p)} + \max_{n_k^0 \in V_0} \{w(n_k^0)\} \right)} - \frac{\max_{e_{k,l}^0 \in E_0} \{c(e_{k,l}^0)\}}{\max_{\beta_{p,q} \in \beta} \{\beta_{p,q}\}}. \quad (3)$$

2) *Processor Selection*: At this phase, a PE to be assigned to a new cluster (e.g., “new cluster” at fig. 3) is decided. If $\Delta sl_{w,up}^{s-1}(\delta_{opt}^s(\alpha_p, \beta(p)))$ is minimized by applying actual values of α_p and $\beta(p)$, the PE having these values should be selected for processor assignment. Then the minimized $\Delta sl_{w,up}^{s-1}(\delta_{opt}^s(\alpha_p, \beta(p)))$ is obtained, by which the upper bound of WSL can be minimized.

3) *Task clustering*: Since the PE to be assigned has been decided, both values of $\delta_{opt}^s(P_p)$ and $\Delta sl_{w,up}^{s-1}(\delta_{opt}^s(\alpha_p, \beta(p)))$ are decided. The objective of the task clustering is to generate the cluster whose execution time exceeds $\delta_{opt}^s(P_p)$ and to minimize WSL, i.e., $sl_w(G^s_{cls}, \phi_s)$. One policy of the task clustering is to select *pivot* (a cluster in which at least one task belongs to $sl_w(G^{s-1}_{cls}, \phi_{s-1})$) and *target* (a cluster in which at least one task has data dependency with one of task in *pivot*). These two clusters are merged into a new cluster, and then if the cluster execution time of the cluster does not exceed $\delta_{opt}^s(P_p)$, the cluster becomes the “new *pivot*”. Then the new *target* is selected for more merging steps.

By repeating (1) - (3), every cluster execution time becomes larger than each decided lower bound. In such an obtained output DAG, it was found that the degree of contribution for speed up can be maximized[11].

B. Objective of the Proposal

The method for processor utilization described above has good effect on a “single core distributed system”, where each PE is completely connected over the network. However, the method does not take into account the locality among PEs. In fig. 1, a multicore distributed system is assumed. If the method proposed in [11] is applied in such an environment, each cluster (assignment unit) is assigned to different computers (see fig. 1). Thus, we propose a processor mapping policy taking into account the locality among PEs. In the top part of fig. 1, two clusters are assigned to different computers. This is because that the method proposed in [11] tries to find the PE to be assigned to a cluster by only applying its performance information to eq. (3). On the other hand, the bottom part of fig. 1 corresponds to the result by applying the proposal. In this case, both clusters are assigned to the same computer. The process of our proposal is performed after three steps ((I)-(III) in fig. 1).

IV. PROPOSAL

As stated in the previous section, the proposed method is performed after three steps proposed in [11] have finished. In

INPUT: $\langle G_{cls}^R, \phi_R \rangle$, where R is # of task merging step required to obtain the output DAG of [11].

OUTPUT: $\langle G_{cls}^{R'}, \phi_{R'} \rangle$, where R' is R plus “# of the remapping required to obtain the output DAG of the proposal”.

Define $P(cls_R(k), \phi_R) = P_{i,p}$, where $cls_R(k)$ is assigned to $P_{i,p}$ at ϕ_R .

Define $M(cls_R(k), \phi_R) = M_i$, where $P(cls_R(k), \phi_R) = P_{i,p}$ is included in M_i .

Define $com_R(k)$ as the set of tasks in $cls_R(k)$ s.t., they have outgoing or incoming communication with other clusters.

Define CHK is the set of clusters dominating $sl_w(G_{cls}^R, \phi_R)$ obtained by the method of [11].

1. **WHILE** $CHK \neq \emptyset$ **DO**
2. Find $cls_R(k)$ s.t.,

$$\varphi(cls_R(k)) = \max_{cls_R(i) \in CHK} \{\varphi(cls_R(i))\};$$
3. Set an immediate predecessor or successor task of $in_R(k)$ or $out_R(k)$ as n_u^R , s.t., $n_u^R \in cls_R(l)$;
4. **FOR EACH** $cls_R(l)$ **DO**
5. $\Delta(k, \alpha_{i,p}, \alpha_{j,q}) \leftarrow \varepsilon(k, \alpha_{i,p}, \alpha_{j,q}) - \omega(k, \alpha_{j,q})$;
6. **END FOR**
7. Find max of $\Delta(k, \alpha_{i,p}, \alpha_{j,q})$ and move $cls_R(k)$ to $P_{j,q}$;
8. Remove $cls_R(k)$ from CHK ;
9. **END WHILE**

Fig. 4. Procedures for cluster remapping.

this section, we present details in the proposal.

A. Algorithm Overview

As stated above, it was proved that minimizing WSL can lead to reduction of the schedule length. Thus, at first clusters dominating WSL must be specified for “remapping”. This is because such a remapping can make WSL smaller than that obtained after three steps ((I)-(III) at fig. 1), thereby it is conceivable that the schedule length is also made smaller by the localization of the data communication.

Fig. 4 shows the cluster remapping algorithm, and fig. 5 shows one example of the algorithm with using the same notations as fig. 4. The algorithm firstly tries to find a cluster to be moved by tracing tasks in seq_R^{\leftarrow} (line 1 - 9 at fig. 4). In fig. 5, (a) means the state after procedures proposed in [11] have been finished. In this state, suppose that colored tasks belong to seq_R^{\leftarrow} . At first, one cluster in which at least one task belongs to seq_R^{\leftarrow} is selected for the remapping algorithm. The selection criterion is based on calculating the evaluation value (i.e., Δ function at line 7 in fig. 4). This evaluation value means how long the response time can be reduced by moving the cluster to another PE. For each cluster dominating WSL, the algorithm derive Δ function as an evaluation value and then select the cluster as a moving target by which the response time can effectively reduced.

B. Cluster Selection

The proposed cluster remapping is to move each cluster dominating $sl_w(G_{cls}^R, \phi_R)$ to one of unassigned PEs. Thus, as first the algorithm finds one of those clusters for each moving procedure. Intuitively, the cluster to be selected for the remapping is the one which has the greatest effect on the WSL, i.e., that has the most execution time and communication time in $sl_w(G_{cls}^R, \phi_R)$. This is because that WSL can be largely reduced by moving such a cluster to the faster PE. Moreover, localization of large amount of communication can contribute to the reduction of WSL. Thus, the criterion for selecting the

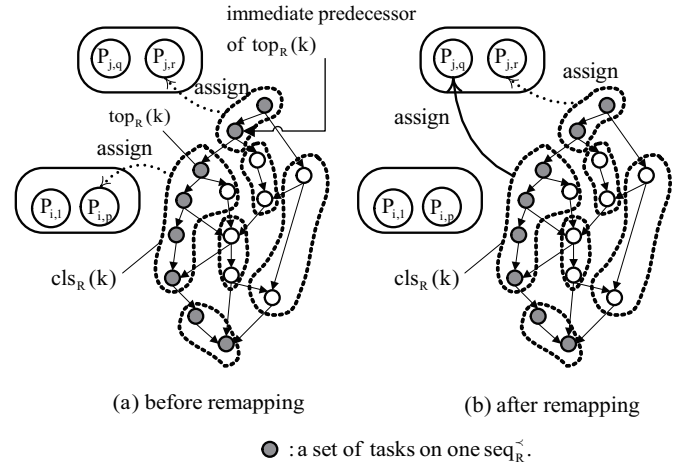


Fig. 5. Example of the cluster remapping algorithm

cluster to be moved is the one having the maximum sum of communication time and task execution time in WSL.

Next, we describe the details of the criterion for cluster selection. Let us return to the definition of $sl_w(G_{cls}^R, \phi_R)$, whose details of the derivation are defined in table. I (for more details, see [12]). As can be seen in table. I, $sl_w(G_{cls}^R, \phi_R)$ is derived by taking the maximum of $LV_R(i)$, which is derived by applying $TL_R(i)$ and $BL_R(i)$. $TL_R(i)$ means the maximum start time of a task in $cls_R(i)$, while $BL_R(i)$ means the maximum elapsed time from start time of a task to the finish time of the END task including communication time (i.e., the path length from a task to the END task). In the table, $in_R(i)$ and $out_R(i)$ are sets of tasks having incoming communications and outgoing communications, respectively (In fig. 2, $in_5(1) = \{n_5^5\}$, and $out_5(1) = \{n_1^5, n_2^5, n_5^5\}$). Communication time taken by a cluster in WSL is derived by an incoming communications(edge) and an outgoing communications(edge). On the other hand, task execution time taken by a cluster (let define as $cls_R(i)$ in WSL is derived by calculating the maximum of $S(n_k^R, i)$ for each $n_k^R \in cls_R(i)$ defined in table. I. $S(n_k^R, i)$ means the start time of n_k^R in $cls_R(i)$ when n_k^R is scheduled as late as possible. For example, in fig. 2(b), we have

$$\begin{aligned} S(n_3^5) &= \frac{1}{4} \sum_{n_k^5 \in cls_5(1)} w(n_k^5) - \frac{1}{4}(w(n_3^5) + w(n_5^5)) \\ &= \frac{1}{4}(w(n_1^5) + w(n_2^5)) = 1.5. \end{aligned} \quad (4)$$

After the time of $S(n_k^R, i)$ has been elapsed, n_k^R can be processed. Then n_k^R sends data to other tasks in other clusters as outgoing communications. Thus, the total time taken by data communication and task execution of one cluster in WSL can be defined as follow.

$$\begin{aligned} \varphi(cls_R(i)) &= com_{in}(cls_R(i)) + S(n_k^R, i) + t_p(n_k^R, \alpha_{p,q}) \\ &\quad + com_{out}(cls_R(i)), \end{aligned} \quad (5)$$

where $com_{in}(cls_R(i))$ is the incoming communication time as a part of $TL_R(i)$, $com_{out}(cls_R(i))$ is the outgoing communication time as a part of $BL_R(i)$. That is, $\varphi(cls_R(i))$ is

TABLE I
PARAMETER DEFINITION RELATED TO $sl_w(G_{cls}^R)$ (HERE $n_k^R \in cls_R(i)$).

Parameter	Definition
$top_R(i)$	$\{n_k^R \forall n_l^R \in pred(n_k^R) s.t., n_l^R \notin cls_R(i)\} \cup \{START\ Tasks \in cls_R(i)\}$.
$in_R(i)$	$\{n_k^R \exists n_l^R \in pred(n_k^R) s.t., n_l^R \notin cls_R(i)\} \cup \{START\ Tasks \in cls_R(i)\}$.
$out_R(i)$	$\{n_k^R \exists n_l^R \in suc(n_k^R) s.t., n_l^R \notin cls_R(i)\} \cup \{END\ Tasks \in cls_R(i)\}$.
$desc(n_k^R, i)$	$\{n_l^R n_k^R < n_l^R, n_l^R \in cls_R(i)\} \cup \{n_k^R\}$
$S(n_k^R, i)$	$\sum_{n_l^R \in cls_R(i)} t_p(n_l^R, \alpha_p) - \sum_{n_l^R \in desc(n_k^R, i)} t_p(n_l^R, \alpha_p)$.
$tlevel(n_k^R)$	$\begin{cases} \max_{n_l^R \in pred(n_k^R)} \{tlevel(n_l^R) + t_p(n_l^R, \alpha_p) + t_c(e_{l,k}, \beta_{q,p})\}, & \text{if } n_k^R \in top_R(i). \\ TL_R(i) + S(n_k^R, i), & \text{otherwise.} \end{cases}$
$TL_R(i)$	$\max_{n_k^R \in top_R(i)} \{tlevel(n_k^R)\}..$
$blevel(n_k^R)$	$\max_{n_l^R \in suc(n_k^R), n_l^R \notin cls_R(i)} \{t_p(n_k^R, \alpha_p) + t_c(e_{k,l}, \beta_{p,q}) + blevel(n_l^R)\}$.
$level(n_k^R)$	$tlevel(n_k^R) + blevel(n_k^R)$.
$BL_R(i)$	$\max_{n_k^R \in out_R(i)} \{S(n_k^R, i) + blevel(n_k^R)\}$.
$LV_R(i)$	$TL_R(i) + BL_R(i) = \max_{n_k^R \in cls_R(i)} \{level(n_k^R)\}$.
$sl_w(G_{cls}^R, \phi_R)$	$\max_{cls_R(i) \in V_{cls}^R} \{LV_R(i)\}$.

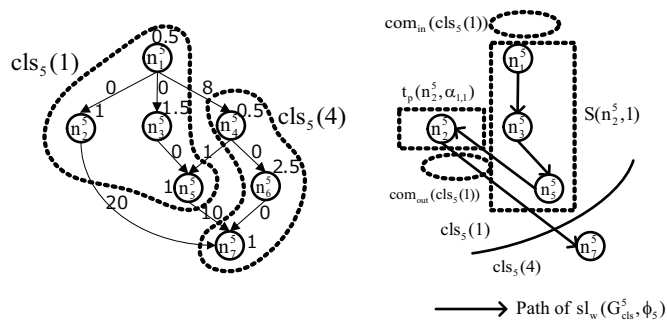


Fig. 6. Example of the cluster selection criteria

total time involved by $cls_R(i)$.

Fig. 6 shows one example of how $\varphi(cls_R(i))$ is decided. In this figure, the path of WSL is the same as fig. 2. At the left side, $cls_5(1)$ and $cls_5(4)$ have been assigned to individual PEs, and the right side shows elements of $\varphi(cls_5(1))$. A dashed circle corresponds to the area for communications, while a dashed rectangle corresponds to the area for task executions. In this example, $com_{in}(cls_5(1))$ is 0 because there is no incoming communication at $cls_5(1)$. Since the path of $sl_5(G_{cls}^5)$ is $n_1^5, n_3^5, n_5^5, n_2^5$ as fig. 2, we have

$$\begin{aligned}
 com_{in}(cls_5(1)) &= 0, \\
 com_{out}(cls_5(1)) &= t_c(e_{2,7}^5, \beta_{1,2}) = 10, \\
 \varphi(cls_5(1)) &= com_{in}(cls_5(1)) + S(n_2^5, 1) \\
 &\quad + t_p(n_2^5, \alpha_{1,1}) + com_{out}(cls_5(1)) \\
 &= 0 + 3 + 1 + 20 = 24. \tag{6}
 \end{aligned}$$

In fig. 4, at line 2 the algorithm finds a cluster $cls_R(k)$ having the maximum φ value in CHK for cluster remapping.

C. Cluster Remapping

Suppose that a cluster which will be checked is $cls_R(k)$, and $cls_R(k)$ was assigned to $P_{i,p} \in M_i$ by the method[11]. Then the algorithm calculates the difference between $\varepsilon(k, \alpha_{i,p}, \alpha_{j,r})$ and $\omega(k, \alpha_{j,q})$. They are defined as follows.

$$\begin{aligned}
 \varepsilon(k, \alpha_{i,p}, \alpha_{j,r}) &= \frac{1}{\alpha_{i,p}} \sum_{n_u^R \in cls_R(k)} w(n_u^R) + \frac{1}{\beta_{q,p}} \sum_{\substack{n_x^R \in cls_R(k), \\ n_y^R \in cls_R(l)}} c(e_{y,x}) \\
 &\quad + \frac{1}{\beta_{q,p}} \sum_{\substack{n_x^R \in cls_R(k), \\ n_y^R \in cls_R(l)}} c(e_{x,y}), \tag{7}
 \end{aligned}$$

$$\omega(k, \alpha_{j,q}) = \frac{1}{\alpha_{j,q}} \sum_{n_u^R \in cls_R(k)} w(n_u^R). \tag{8}$$

$\varepsilon(k, \alpha_{i,p}, \alpha_{j,r})$ is the sum of cluster execution time and data communication time (incoming communication and outgoing communication with a specific cluster (let define as $cls_R(l)$ and $cls_R(l)$ is assigned to $P_{j,r}$)). That is, $\varepsilon(k, \alpha_{i,p}, \alpha_{j,r})$ means the total time taken to process $cls_R(k)$ and to communicate with $cls_R(l)$. On the other hand, $\omega(k, \alpha_{j,q})$ does not require data communication time with $cls_R(l)$ because it is included in the same computer (let assume no cluster is assigned to $P_{j,q}$). Then we define the evaluation value as follow.

$$\Delta(k, \alpha_{i,p}, \alpha_{j,q}) = \varepsilon(k, \alpha_{i,p}, \alpha_{j,q}) - \omega(k, \alpha_{j,q}). \tag{9}$$

For each cluster $cls_R(k)$, the algorithm finds the maximum value of $\Delta(k, \alpha_{i,p}, \alpha_{j,q})$ with varying j and q . This is the same meaning as varying l in $cls_R(l)$ (at line 5 in fig. 4). When the cluster $cls_R(l)$ or $P_{j,q}$ is found at line 7 in fig. 4, the cluster is removed from the set of clusters CHK . When CHK becomes

empty, the algorithm is finished.

Selection of the target for moving the cluster $cls_R(k)$ by maximizing $\Delta(k, \alpha_{i,p}, \alpha_{j,q})$ means that the algorithm tries to find the PE by which the time taken for processing and data communication is minimized.

V. THEORETICAL ANALYSIS

Since an objective of the proposed cluster remapping is to reduce WSL in order to minimize the schedule length, with maintaining the number of required PEs. Thus, in this section we analyze the possibility for WSL reduction by each cluster remapping procedure. Assume that an cluster $cls_R(k)$ is assigned to $P_{i,p}$ and $cls_R(k)$ dominates WSL, i.e., $sl_W(G_{cls}^R)$. Then suppose that $cls_R(k)$ is moved to $P_{j,q}$ by a cluster remapping procedure. We define $\varphi(cls_R(k))$ after the remapping as $\varphi'(cls_R(k))$ and the difference of $\varphi(cls_R(k))$ as $\Delta\varphi(cls_R(k))$. Similarly, let differences of $com_{in}(cls_R(k))$, $S(n_m^R)$, and $com_{out}(cls_R(k))$ be $\Delta com_{in}(cls_R(k))$, $\Delta S(n_m^R)$, and $\Delta com_{out}(cls_R(k))$, respectively. Then we have

$$\begin{aligned} \Delta\varphi(cls_R(k)) &= \varphi(cls_R(k)) - \varphi'(cls_R(k)) \\ &= \Delta com_{in}(cls_R(k)) + \Delta S(n_m^R) \\ &\quad + t_p(n_m^R, \alpha_{i,p}) - t_p(n_m^R, \alpha_{j,q}) \\ &\quad + \Delta com_{out}(cls_R(k)) \\ &= \left(\frac{1}{\beta_{u,i}} - \frac{1}{\beta_{u,j}} \right) c(e_{r,s}^R) \\ &\quad + \left(\frac{1}{\alpha_{i,p}} - \frac{1}{\alpha_{j,q}} \right) \sum_{n_l^R \in cls_R(k)} w(n_l^R) \\ &\quad + \left(\frac{1}{\beta_{i,v}} - \frac{1}{\beta_{j,v}} \right) c(e_{y,z}^R), \end{aligned} \quad (10)$$

where $cls_R(k)$ is moved from $P_{i,p}$ to $P_{j,q}$, while $e_{r,s}^R$ is a communication part of $TL_R(k)$ ($n_r^R \notin cls_R(k), n_s^R \in cls_R(k)$), and $e_{y,z}^R$ is a communication part of $BL(k)$ ($n_y^R \in cls_R(k), n_z^R \notin cls_R(k)$). If $\varphi(cls_R(k)) > 0$, WSL can be reduced by this cluster remapping procedure. Otherwise, WSL may not be reduced. In this analysis we present the lower bound of $\varphi(cls_R(k))$ in several cases.

At line 5 in fig. 4, the target PE for cluster remapping is selected by computing every incoming and outgoing communication of the cluster selected at line 2 in fig. 4. Thus, we have 2 cases for analyzing the effect on the WSL reduction by cluster remapping, i.e., (i) $com_{in}(cls_R(k))$ or $com_{out}(cls_R(k))$ is localized and the WSL path is not changed, and (ii) both $com_{in}(cls_R(k))$ and $com_{out}(cls_R(k))$ are not localized (other communications are localized).

- (i) $com_{in}(cls_R(k))$ or $com_{out}(cls_R(k))$ is localized and the WSL is not changed:

This case means that $u = j$ or $j = v$ obtained by cluster remapping. Consequently, $\frac{1}{\beta_{u,j}} = 0$ or $\frac{1}{\beta_{j,v}} = 0$. Without loss of generality, suppose that $\frac{1}{\beta_{u,j}} = 0$, while $com_{out}(cls_R(k))$ remains unlocalized, i.e., $\frac{1}{\beta_{j,v}} \neq 0$.

From eq. (10), we have

$$\begin{aligned} \Delta\varphi(cls_R(k)) &= \frac{1}{\beta_{u,i}} c(e_{r,s}^R) \\ &\quad + \left(\frac{1}{\alpha_{i,p}} - \frac{1}{\alpha_{j,q}} \right) \sum_{n_l^R \in cls_R(k)} w(n_l^R) \\ &\quad + \left(\frac{1}{\beta_{i,v}} - \frac{1}{\beta_{j,v}} \right) c(e_{y,z}^R). \end{aligned} \quad (11)$$

From eq. (11), there are 4 cases for satisfying $\varphi(cls_R(k)) \geq 0$ depending on magnitude relationships of $\alpha_{i,p}$ to $\alpha_{j,q}$, and $\beta_{i,v}$ to $\beta_{j,v}$.

- (i-I) The case of $\alpha_{i,p} \leq \alpha_{j,q}$, $\beta_{i,v} \leq \beta_{j,v}$:

In this case, the target PE to which $cls_R(k)$ has faster processing speed and wider communication bandwidth. Let the maximum of processing speed, communication bandwidth, and data size be $\alpha_{max}, \beta_{max}, c_{max}$, respectively. Let the minimum of processing speed, communication bandwidth, and data size be $\alpha_{min}, \beta_{min}, c_{min}$, respectively. Then we have

$$\begin{aligned} \Delta\varphi(cls_R(k)) &\geq \frac{1}{\beta_{max}} c_{min} \\ &\quad + \left(\frac{1}{\alpha_{i,p}} - \frac{1}{\alpha_{j,q}} \right) \sum_{n_l^R \in cls_R(k)} w(n_l^R) \\ &\quad + \left(\frac{1}{\beta_{i,v}} - \frac{1}{\beta_{j,v}} \right) c(e_{y,z}^R) \\ &\geq \frac{1}{\beta_{max}} c_{min} > 0. \end{aligned} \quad (12)$$

Thus, in this case, $\varphi(cls_R(k))$ always takes the positive value.

- (i-II) The case of $\alpha_{i,p} \leq \alpha_{j,q}$, $\beta_{i,v} \geq \beta_{j,v}$:

In this case, we have

$$\begin{aligned} \Delta\varphi(cls_R(k)) &\geq \frac{1}{\beta_{max}} c_{min} \\ &\quad + \left(\frac{1}{\beta_{max}} - \frac{1}{\beta_{min}} \right) c_{max} \\ &= \frac{1}{\beta_{max}} (c_{min} + c_{max}) - \frac{c_{max}}{\beta_{min}} \end{aligned} \quad (13)$$

At eq. (13), the condition for satisfying $\varphi(cls_R(k)) \geq 0$ is as follow.

$$\begin{aligned} \frac{1}{\beta_{max}} (c_{min} + c_{max}) - \frac{c_{max}}{\beta_{min}} &\geq 0 \\ \Leftrightarrow \frac{\beta_{max}}{\beta_{min}} &\leq \frac{c_{min}}{c_{max}} + 1 \leq 2. \end{aligned} \quad (14)$$

From eq. (13), the lower bound becomes small if the heterogeneity (i.e., max to min ratio) in terms of communication bandwidth is also small. If eq. (13) is satisfied, $\varphi(cls_R(k))$ takes the positive value irrespective of processing speed.

- (i-III) The case of $\alpha_{i,p} \geq \alpha_{j,q}$, $\beta_{i,v} \leq \beta_{j,v}$:

In this case, the target PE has slower processing

speed than $P_{i,p}$. Then we have

$$\begin{aligned} \Delta\varphi(\text{cls}_R(k)) &\geq \frac{c(e_{r,s}^R)}{\beta_{u,i}} + \left(\frac{1}{\alpha_{i,p}} - \frac{1}{\alpha_{j,q}} \right) \sum_{n_l^R \in \text{cls}_R(k)} w(n_l^R) \\ &\geq \frac{c_{\min}}{\beta_{\max}} + \left(\frac{1}{\alpha_{\max}} - \frac{1}{\alpha_{\min}} \right) \sum_{n_l^R \in \text{cls}_R(k)} w(n_l^R). \end{aligned} \quad (15)$$

The condition for satisfying $\varphi(\text{cls}_R(k)) \geq 0$ is as follow.

$$\begin{aligned} \frac{\alpha_{\max}}{\beta_{\max}} c_{\min} &\geq \left(\frac{\alpha_{\max}}{\alpha_{\min}} - 1 \right) \sum_{n_l^R \in \text{cls}_R(k)} w(n_l^R) \\ \Leftrightarrow \frac{\alpha_{\max}}{\beta_{\max}} &\geq \left(\frac{\alpha_{\max}}{\alpha_{\min}} - 1 \right) \frac{\sum_{n_l^R \in \text{cls}_R(k)} w(n_l^R)}{c_{\min}} \end{aligned} \quad (16)$$

In eq. (15), if α_{\max} is much larger than β_{\max} and heterogeneity in terms of processing speed is small, $\varphi(\text{cls}_R(k))$ has possibility of taking the positive value.

(i-IV) The case of $\alpha_{i,p} \geq \alpha_{j,q}$, $\beta_{i,v} \geq \beta_{j,v}$:

In this case, we have

$$\begin{aligned} \Delta\varphi(\text{cls}_R(k)) &\geq \frac{c(e_{r,s}^R)}{\beta_{u,i}} + \left(\frac{1}{\alpha_{i,p}} - \frac{1}{\alpha_{j,q}} \right) \sum_{n_l^R \in \text{cls}_R(k)} w(n_l^R) \\ &\quad + \left(\frac{1}{\beta_{i,v}} - \frac{1}{\beta_{j,v}} \right) c(e_{y,z}^R) \\ &\geq \frac{c_{\min}}{\beta_{\max}} + \left(\frac{1}{\alpha_{\max}} - \frac{1}{\alpha_{\min}} \right) \sum_{n_l^R \in \text{cls}_R(k)} w(n_l^R) \\ &\quad + \left(\frac{1}{\beta_{\max}} - \frac{1}{\beta_{\min}} \right) c_{\max}. \end{aligned} \quad (17)$$

The condition for satisfying $\varphi(\text{cls}_R(k)) \geq 0$ is as follows.

$$\begin{aligned} \frac{c_{\min} + c_{\max}}{\beta_{\max}} &\geq \left(\frac{1}{\alpha_{\min}} - \frac{1}{\alpha_{\max}} \right) \sum_{n_l^R \in \text{cls}_R(k)} w(n_l^R) \\ &\quad + \frac{c_{\max}}{\beta_{\min}}. \end{aligned} \quad (18)$$

From this result, at least heterogeneity in terms of processing speed and communication bandwidth should be small in order to satisfy $\varphi(\text{cls}_R(k)) \geq 0$.

(ii) Nor $\text{com}_{in}(\text{cls}_R(k))$ and $\text{com}_{out}(\text{cls}_R(k))$ are localized: Since the algorithm tries to trace incoming edges and outgoing edges to find the target PE, the edge which corresponding to $\text{com}_{in}(\text{cls}_R(k))$ or $\text{com}_{out}(\text{cls}_R(k))$ is not always localized by the proposed cluster remapping. This case assumes that some edges which are not parts of $LV_R(k)$ are localized. In this case, the new WSL is derived by tracing every edges and tasks after cluster remapping. This fact means that the path of WSL can be changed. Thus, the lower bound of $\varphi(\text{cls}_R(k))$ can

TABLE II

COMPARISON RESULTS IN TERMS OF THE SCHEDULE LENGTH

No.	α	β	CCR	$ V_{cls}^R $	Schedule Length		
					A	B	C
1	5	5	0.1	156	1.000	1.002	1.002
2			1.0	58	1.000	1.011	1.008
3			5.0	42	1.000	1.031	1.048
4			10.0	16	1.000	1.109	1.144
5	5	10	0.1	165	1.000	1.001	1.044
6			1.0	55	1.000	1.076	1.071
7			5.0	32	1.000	1.103	1.142
8			10.0	14	1.000	1.107	1.281
9	10	5	0.1	139	1.000	1.001	1.003
10			1.0	48	1.000	1.068	1.042
11			5.0	37	1.000	1.103	1.009
12			10.0	27	1.000	1.198	1.201
13	10	10	0.1	188	1.000	1.004	1.002
14			1.0	67	1.000	1.143	1.107
15			5.0	40	1.000	1.170	1.140
16			10.0	29	1.000	1.179	1.151

not be estimated.

From results of the theoretical analysis a cluster to be selected at line 7 in fig. 4 should be the case of (i-I). However, the algorithm can not always select by (i-I) because WSL after each cluster remapping may be changed due to the variation of communication time and processing time for each task. This means that a strategy to use (i-I) in every cluster remapping step has possibility to increase WSL by the change of the path dominating WSL. Thus, at eq. (7) the algorithm tries to find the target PE by summing up all communication times involved by the cluster selected at line 2 in fig. 4 in order to localize communication as many as possible.

VI. EXPERIMENTS

We conducted the experiments by a simulation to confirm advantages of our proposal, i.e., how the cluster remapping can reduce the schedule length. We compared with the method proposed in [11] in terms of the following points.

- 1) Effect on the cluster remapping with compared to the case of “non remapping”.
- 2) Effect on the proposed remapping policy and algorithm.

Thus, comparison targets are, (A) the proposed cluster remapping, (B) each cluster is randomly remapped. (C) non remapping[11].

A. Experimental Environment

In the simulation, a random DAG is generated. In each DAG, each task size and each data size are decided randomly. Also CCR (Communication to Computation Ratio)[13], [14] is changed from 0.1 to 10. The max to min ratio in terms of data size and task size is set to 100. Also we decided the Parallelism Factor (PF) is defined as ρ , taking values of 0.5, 1.0, and 2.0 [15]. By using PF, the depth of the DAG is defined as $\frac{\sqrt{|V_0|}}{\rho}$. Since we assume a heterogeneous distributed system by multicore computers, each PE's performance and network bandwidth are varied by parameters. The simulation environment was developed by JRE1.6.0.0, the operating system is Windows XP SP3, the CPU architecture is Intel Core 2 Duo 2.66GHz, and the memory size is 2.0GB.

TABLE III
COMPARISON RESULTS IN TERMS OF THE SCHEDULE LENGTH AND SELECTED PE TYPES

No.	α	β	CCR	$ V_{cls}^R $	Schedule Length Ratio to (A)			Ratio of of (i-I) (%)			Ratio of (i-IV) (%)		
					A	B	C	A	B	C	A	B	C
1	5	5	0.1	143	1.000	1.003	1.011	24.0	40.0	9.3	6.7	16.0	46.7
2			1.0	67	1.000	1.010	1.013	27.9	44.2	11.6	4.7	14.0	51.2
3			5.0	41	1.000	1.044	1.089	29.2	58.3	8.3	8.3	16.7	45.8
4			10.0	14	1.000	1.072	1.182	33.3	50.0	0.0	0.0	33.3	83.3
5	5	10	0.1	166	1.000	1.002	1.009	27.0	39.2	5.4	4.1	14.9	39.2
6			1.0	73	1.000	1.013	1.023	34.1	53.7	4.9	7.3	17.1	39.0
7			5.0	38	1.000	1.041	1.099	36.4	72.7	4.5	9.1	22.7	45.5
8			10.0	18	1.000	1.102	1.183	57.1	71.4	0.0	11.7	14.3	42.9
9	10	5	0.1	145	1.000	1.000	1.009	22.9	47.1	7.1	8.6	15.2	41.4
10			1.0	55	1.000	1.018	1.026	22.4	53.1	6.1	10.2	16.3	22.4
11			5.0	39	1.000	1.039	1.088	43.5	82.6	8.7	13.0	8.7	21.7
12			10.0	13	1.000	1.121	1.282	33.3	50.0	0.0	0.0	16.7	66.7
13	10	10	0.1	173	1.000	1.006	1.087	28.6	48.6	8.6	7.1	15.7	34.3
14			1.0	66	1.000	1.149	1.181	34.2	50.0	7.9	10.5	15.8	39.5
15			5.0	40	1.000	1.166	1.159	27.3	54.5	4.5	4.5	9.1	45.5
16			10.0	26	1.000	1.133	1.198	37.5	50.0	0.0	0.0	12.5	37.5

B. Effect on Cluster Remapping

One comparison is done by executing 100 random DAGs and averaging the schedule length for each approach (A)-(C). Since (C) does not require cluster remapping, at first the simulation output the schedule length by (C). Then each remapping procedures is performed in (A) and (B), respectively. Then both approaches output each schedule length for the same DAG as (C). Table II shows comparison results by the experiment. In the table, α and β are ratios of maximum to minimum processing speed and maximum to minimum communication bandwidth, respectively. In the 6th column, values mean the schedule length ratio when the schedule length obtained by (A) is set to 1. Thus, a value over 1 is worse than (A). In every cases, it is observed that the proposed method (A) outperforms other approaches. If β is small such as No. 1-5 and No. 9-12, we can not observe noticeable characteristics among three approaches, except that the schedule length obtained by (A) is the smallest. On the other hand, β is large such as No. 5-8, the schedule length obtained by (C) is considerably large with increasing CCR. From this result, it is conceivable that data localization is necessary irrespective of cluster remapping methods if each data size is large. As for No. 13-16, the schedule length obtained by (B) is the largest with increasing CCR. From this result, the cluster remapping method has large effect on the schedule length if the heterogeneity of the network is large.

From these results, it is concluded that the proposed cluster remapping method has good effect on the schedule length by effectively localizing data communications among PEs.

C. Relationship between PE Selection Policies and the Schedule Length

According to the results obtained in sec. V, selecting the target PE having faster processing speed and larger communication bandwidth (type of (i-I)) in sec. V than the original PE can lead to the reduction of WSL after one cluster remapping procedure has finished. Nonetheless, the proposed algorithm tries to find the target PE by summing up all communication times involved by the moving target cluster rather than finding a cluster of (i-I) in sec. V. This is because not always a cluster

of type (i-I) can be found and WSL path may be changed by a cluster remapping procedure, thereby

In this experiment, we compared the schedule length and distribution of the selected PE type ((i-I) to (ii) at sec. V) in (A) proposed algorithm, (B) trying to find a cluster of type (i-I), (C) trying to find a cluster of type (i-IV). This comparison is conducted by averaging the schedule length of DAGs having 1000 tasks by 100 tries for all three approaches. In the method (B), if a cluster of type (i-I) is not found, the method selects a PE randomly from the set of PEs by which at least one communication involved by a cluster selected at line 2 in fig. 4 is localized. In the method (C), if a cluster of type (i-IV) is not found, the target PE is selected as the same policy as (B). Table. III shows the comparison results. "Ratio of (i-I)" means the percentile of the number of that a PE of type (i-I) is selected as the target PE to the number of all cluster remapping, while "Ratio of (i-IV)" means the percentile of the number of that a PE of type (i-IV) is selected as the target PE to the number of all cluster remapping. From this table, it is observed that in every cases (No. 1 - 16), the proposed algorithm has the smallest schedule length, while (B) has the largest ratios of (i-I) and (C) has the largest ratios of (i-IV) in every cases. From this result, it can be conceived that selecting a PE of type (i-IV) has bad effects on both WSL and the schedule length. Furthermore, Even if a PE of type (i-I) is selected as the moving target, the schedule length can be made larger by the facts that WSL path may be changed. This is because an communication time dominating $com_{in}(cls_R(i))$ or $com_{out}(cls_R(i))$ is made smaller by a cluster remapping, while other edges may dominates $com_{in}(cls_R(i))$ or $com_{out}(cls_R(i))$.

From this result, it is concluded that the PE selection criteria by the proposed cluster remapping have good effect on the schedule length.

VII. CONCLUSION AND FUTURE WORKS

In this paper, we presented a cluster remapping method in a multicore distributed system for processor utilization. The method tries to move clusters for data localization with taking into account both data dependencies which can have good effect on the schedule length. This procedure is performed by

calculate the difference between time taken to execute every task in the cluster in the new PE and the time taken to execution and data communication in the previously decided PE decided by the method of [11]. From preliminary experiments, the proposed method was proved to have good effect on the schedule length.

As a future work, we develop more efficient method which does not use remapping in multicore distributed systems for processor utilization.

REFERENCES

[1] I. Foster, "The Grid: A new infrastructure for 21st century science," *Physics Today*, Vol.55(2), pp. 42-47, 2002.

[2] G. DeCandia et al, "Dynamo: amazon's highly available key-value store," *Proc. of ACM SIGOPS symposium on Operating systems principles (SOSP'12)*, pp. 205 - 220, 2007.

[3] S. Di and C.L. Wang, "Dynamic Optimization of Multiattribute Resource Allocation in Self-Organizing Clouds," *IEEE Trans. on Parallel and Distributed Systems*, Vol. 24, No. 3, pp. 464-478, 2013.

[4] M. Xu, L. Cui, H. Wang, and Y Bi, "A Multiple QoS Constrained Scheduling Strategy of Multiple Workflows for Cloud Computing," *Proc. of 2009 IEEE International Symposium on Parallel and Distributed Processing with Applications*, pp. 629-634, 2009.

[5] H. Mohammadi Fard, R. Prodan, J. J. D. Barrionuevo, and T. Fahringer, "A Multi-Objective Approach for Workflow Scheduling in Heterogeneous Environments," *Proc. of 2012 12th IEEE/ACM International Symposium on Cluster, Cloud and Grid Computing*, pp. 300-309, 2012.

[6] J.S. Kim et al., " Using Content-Addressable Networks for Load Balancing in Desktop Grids, " *Proc. of 16th ACM International Symposium on High Performance Distributed Computing (HPDC '07)*, pp. 189- 198, 2007.

[7] A. Leite, H. Mendes, L. Weigang, A. de Melo, and A. Boukerche, "An Architecture for P2P Bag-of-Tasks Execution with Multiple Task Allocation Policies in Desktop Grids, " *Proc. of IEEE International Conference on Cluster Computing*, pp. 1-11, 2011.

[8] A. Gerasoulis and T. Yang, "A Comparison of Clustering Heuristics for Scheduling Directed Acyclic Graphs on Multiprocessors," *Journal of Parallel and Distributed Computing*, Vol. 16, pp. 276-291, 1992.

[9] T. Yang and A. Gerasoulis, "DSC: Scheduling Parallel Tasks on an Unbounded Number of Processors," *IEEE Trans. on Parallel and Distributed Systems*, Vol. 5, No. 9 pp. 951-967, 1994.

[10] J. C. Liou, M. A. Palis, "An Efficient Task Clustering Heuristic for Scheduling DAGs on Multiprocessors," *Proc. of the 8th Symposium on Parallel and Distributed Processing*, October, 1996.

[11] Hidehiro Kanemitsu, Gilhyon Lee, Hidenori Nakazato, Takashige Hoshiai, and Yoshiyori Urano, "A Processor Mapping Strategy for Processor Utilization in a Heterogeneous Distributed System," *Journal of Computing*, Vol. 3, Issue 11, pp. 1 - 8, November 2011.

[12] Hidehiro Kanemitsu, Gilhyon Lee, Hidenori Nakazato, Takashige Hoshiai, and Yoshiyori Urano, "On the Effect of Applying the Task Clustering for Identical Processor Utilization to Heterogeneous Systems," *Grid Computing - Technology and Applications, Widespread Coverage and New Horizons*, InTech(ISBN: 978-953-51-0604-3), pp. 29 - 46, March, 2012.

[13] O. Sinnen and L. A. Sousa, "Communication Contention in Task Scheduling," *IEEE Trans. on Parallel and Distributed Systems*, Vol. 16, No. 6., pp. 503-515, 2005.

[14] O. Sinnen, "Task Scheduling for Parallel Systems," Wiley, 2007.

[15] H. Topcuoglu, S. Hariri, M. Y. Wu, "Performance-Effective and Low-Complexity Task Scheduling for Heterogeneous Computing," *IEEE Trans. on Parallel and Distributed Systems*, Vol. 13, No. 3 pp. 260-274, 2002.



Hidehiro Kanemitsu received the B.S. degree from Waseda University, Japan in Science, and the M.S. and D.S. degrees from Waseda University, Japan in Global Information and Telecommunication Studies (GITS). His research interests are in areas of parallel and distributed computing, grid, peer-to-peer computing, and web service technology. He is currently an assistant professor at Media Network Center, Waseda University, Japan.



Masaki Hanada received the B.E. degree in Resources Engineering from Waseda University in 1996, and the M.S. and D.S. degrees in Global Information and Telecommunication Studies from Waseda University in 2003 and 2007, respectively. He has been an assistant professor at the Department of Information Systems, Tokyo University of Information Sciences. His research interests include QoS/traffic control and resource management in communication networks.



Takashige Hoshiai has been a Professor at Sojo University since 2012. He was a senior research scientist supervisor at NTT Network Service Systems Laboratories from 1986 to 2012. He received his Ph.D. degree in Communications and Systems from The University of Electro-Communications, Japan. His research areas are distributed object technologies, real-time systems, agent systems and P2P. Since he proposed a new business model called " Brokerless Model " in 1998, especially, he has studied SIONet architecture that is a solution of P2P

platforms.



Hidenori Nakazato received his B. Engineering degree in Electronics and Telecommunications from Waseda University in 1982, and his MS and Ph.D. degrees in Computer Science from University of Illinois in 1989 and 1993, respectively. He was with Oki Electric from 1982 to 2000 where he developed equipment for public telephony switches, distributed environment for telecommunications systems, and communications quality control mechanisms. He has been a Professor at Graduate School of Global Information and Telecommunications Studies, Waseda

University since 2000. His research interests include performance issues in distributed systems and networks, cooperation mechanisms of distributed programs, distributed real-time systems, and network QoS control.

A Stereo-Vision Approach for a Natural 3D Hand Interaction with an AR Object

Seonho Lee*, Junchul Chun*

*Department of Computer Science, Kyonggi University, San 94-6 Yiui-Dong, Yeongtong-Gu, Suwon, S. Korea

sunho36@naver.com, jcchun@kgu.ac.kr

Abstract—Providing natural hand interaction between a virtual object and a user on Augmented Reality is a major issue to manipulate a rendered object in a convenient way. Conventional 2D image-based recognition and interaction technique in AR has a limitation to perform a natural interaction between the user and the virtual object. In this paper, we present a stereo-vision based natural 3D hand interaction with the augmented object. In the proposed 3D hand interaction approach, 3D hand location and finger direction can be easily obtained by using stereo-vision technique while user hand is approaching to the virtual object. Two types of hand manipulation for the augmented object such as the hand pointing and hand pinching are defined. The collision detection between user hand and the virtual object is determined by using a simple ray casting emitted from the user's finger-point against the virtual object in the case of hand pointing. In the hand pinching, the collision is occurred when the thumb and the index finger are approaching to the object and the degree of angle between two fingers becomes a predetermined value. From the experiments, the proposed 3D hand interaction method can control the virtual object in a natural way rather than using a vision-based 2D hand interaction since the stereo-vision technique can obtain the depth information from the AR environments.

Keyword—Stereo-vision, Haptic interface, Augmented Reality, Collision detection, Hand detection

I. INTRODUCTION

Recently one of the main issues in Augmented Reality (AR) is how to interact the overlaid virtual objects in a convenient fashion by users. Newly introduced tracking and interaction methods in AR allow users to work with and examine the real physical world, while controlling augmented objects in the system more feasible fashion. In general AR can be classified into two categories such as marker-based AR and marker-less AR. In marker-based AR a specific marker is used

for overlaying an object in the scene. Meanwhile, marker-less AR does not require the forethought of adding markers to a scene in order to render a virtual object. It uses a detected feature from the scene as a marker instead of using a predetermined specific marker. Regardless of their types of AR system, most of AR systems need various interactions between users and augmented object in many AR applications. Therefore, the major issue in AR is how to interact with a virtual model in dynamic or convenient way. Conventional vision-based interaction techniques in AR are based on 2D image analysis and recognition methods and have a limitation to obtain three dimensional information of the virtual object and user who participates in the interaction.

In this paper, we present a vision-based 3D hand interaction with a virtual object in AR system with a natural way. To develop the 3D hand interaction we adopt stereo-vision technique which can expand the dimension of the AR interaction from 2D to 3D and provide more intuitive interactions between the virtual object and users. In the proposed 3D hand interaction, a user can directly contact with a virtual object by simply detecting the collision between user's hand and the virtual object while the interaction is being processed.

The rest of the paper includes related work, the description of the proposed vision-based 3D interaction method, the experimental results and the conclusion and future works.

II. RELATED WORKS

Both marker-based and marker-less AR systems require some indication of where exactly the virtual objects should be augmented. This has been conventionally accomplished by AR markers such as ARTag[1] or ARToolkit[2] in marker-based AR. In mobile AR system ARToolkitPlus[3] is well-adopted because it provides an efficient management of the memory and fixed point unit computing by optimizing the libraries of ARToolkit.

In order to register a virtual object to a detected marker on the scene, we can use the vision-based tracking technologies such as feature-based and model based approach. The main idea underlying feature-based methods is to find a correspondence between 2D image features and their 3D world coordinate system. The camera pose can be found from projecting the 3D coordinates of the features into the 2D image coordinate along with minimizing the difference between their corresponding 2D features. The ARToolKit library utilizes the four corners of a

Manuscript received July 29, 2013. This work was supported by Basic Science Research program through the National Research Foundation of Korea(NRF) funded by the Ministry of Education, Science and Technology(No. 2012006018).

Seonho Lee is a graduate student in the department of computer science at Kyonggi University, South Korea. (Tel: +82-31-249-8947; e-mail: sunho36@naver.com).

Junchul Chun is currently a professor in the department of computer science and a principal investigator of GIP(Graphics and Image Processing Lab) at Kyonggi University, South Korea. (Tel: +82-31-249-9668; Fax: +82-31-249-8949; e-mail: jcchun@kgu.ac.kr).

square marker to the positions of the 3D object rendered. Tracking algorithms for non-square visual markers such as ring shaped and circular shaped markers were also used[4]. Model-based methods tracking explicitly use a model of features of tracked objects such as 2D template object or CAD model.

Once a virtual object is registered on the marker, the users usually want to manipulate or interact with the augmented object. The most of introduced interaction techniques for AR applications allow end users to contact with virtual objects in an intuitive way. Tangible interface and tangible interaction metaphor have become one of the most frequently used AR interaction methods[5]. Tangible AR interactions leads to combining real object input with human gesture interaction and hand gesture interaction methods have been widely studied from the perspective of computer vision and AR[6].

In vision-based interaction, hand and fingertip tracking along with hand gesture recognition method are widely used to provide an easy way to interact with virtual object in AR. The approaches to use bare stretched human hand as a distinctive pattern instead of a marker for marker-less AR system are introduced[7]-[9]. In their work, 6-DOF camera pose was estimated by tracking fingertips and virtual objects are augmented on hand coordinate system. However, the limitation of these approaches is the inspection of the object is hindered when the fingertips are occluded by themselves when the hand is flipping or moving. Chun and Lee[10][11] presents a real-time vision-based approach to manipulate the overlaid virtual objects dynamically in a marker-less AR system using bare hand with a single camera. In their approach, the left bare hand is considered as a virtual marker in the marker-less AR and the right hand is used as a hand mouse. Thus the manipulation of the virtual objects on the marker-less AR system can be dynamically obtained and a vision-based hand control interface which exploits the fingertip tracking for the movement of the objects and pattern matching for the hand command initiation is developed. However, all of these interactions are based on vision-based 2D interaction with the augmented object in AR. Simple 3D interaction in AR[15] was presented however in this work we provide various scenarios of 3D interaction with more feasible fashion in actual AR applications.

III. PROPOSED APPROACH

A. Manipulation of a Virtual Object in AR

The interaction between a human and an augmented object in AR is by manipulating the virtual object by actual human hand illustrated in Fig 1. In this work, we introduce the two types of hand interaction by hand pointing and hand pinching.

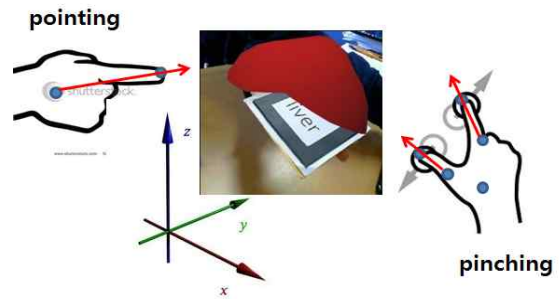


Fig. 1 Manipulating a virtual object in AR by hand pointing and pinching interaction

Fig 2 shows the overall steps of the proposed 3D hand interaction method, which consists of three major phase. In the first phase, the human hand is detected from input video image using the skin color model and image segmentation. In the second phase, the 3D locations of fingertip, the center of the palm and the center of the marker are evaluated using the disparity map of the stereo-vision. In the final stage, the user can interact with an augmented object by detecting collision between the human hand and the object.

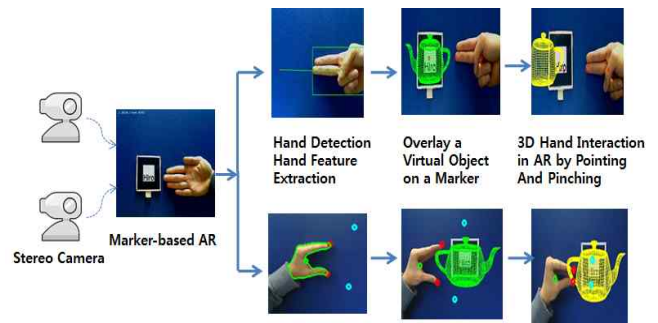


Fig. 2 Steps for stereo-vision based 3D hand interaction in AR

B. Hand Detection Method

For hand region detection like in our previous works, we use $YCbCr$ skin color model which is proven to detect skin region effectively to segmenting hand region[10][11]. Skin color model has been widely used for hand and face detection because the use of color information can simplify the task of hand localization in complex environments. Mostly the primary components of RGB are used for skin segmentation. Other models such as HSI , normalized RGB , and $YCbCr$ etc. are used for the segmentation of skin-like region[12]. Even though, color information is an efficient tool for identifying skin region if the skin tone color can be properly adapted for different lighting conditions, it has some limitation since the skin color model is sensitive to the light source varies significantly or complex background.

As a skin color model we adopt the $YCbCr$ since it is perceptually uniform and it is similar to the TSL space in terms of the separation of luminance and chrominance. It is known that the chrominance components of the skin color are independent of the luminance component. Thus, the normalized

RGB color model is transformed to YC_bC_r model by using following equation (1).

$$\begin{bmatrix} Y \\ C_b \\ C_r \end{bmatrix} = \begin{bmatrix} 0.299 & 0.587 & 0.114 \\ -0.16874 & -0.3313 & 0.500 \\ 0.500 & -0.4187 & -0.0813 \end{bmatrix} \begin{bmatrix} R \\ G \\ B \end{bmatrix} + \begin{bmatrix} 0 \\ 128 \\ 128 \end{bmatrix} \quad (1)$$

By disregarding the luminance component (Y), robustness of skin detection can be obtained in the case of variations lighting conditions. Thus, in this work we only utilize C_b , C_r values from samples of skin color pixels. For the hand region detection, the threshold values of each chrominance components are derived from the set of hand images. The average values of C_b and C_r for hand region obtained through the experiments are as follow

$$(128 \leq C_b \leq 170) \cap (73 \leq C_r \leq 158) \quad (2)$$

With carefully selected threshold range values, a pixel value is assigned to the hand region if its value meets the range. Fig 2 shows the hand region with C_b , C_r values from the RGB based input hand image. In order to enhance the segmented hand region by removing noise a morphological operator are applied to the segmentation result. The center of the hand can be extracted from the medial axis of the segmented hand region $I(p)$. The distance transform which is used to compute the medial axis of the segmented hand [13] is used to obtain the single connected hand. The distance transform (DT) is the transformation that generates a map D whose value in each pixel p of the segmented region O is the smallest distance from this pixel to the background O^c . The distance map D can be defined as follow

$$D(p) = \min \{d(p, q) | q \in O^c\} = \min \{d(p, q) | I(q) = 0\} \quad (3)$$

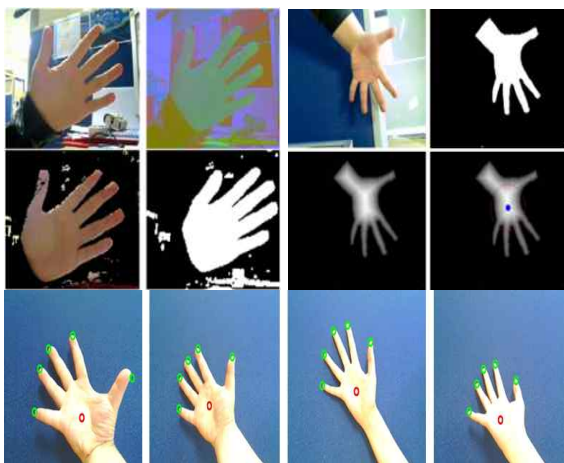


Fig 3. Steps for hand segmentation: (a) $C_b C_r$ converted input image and segmentation of hand(left) (b) distance transform of the hand segmentation and the center of the hand(right) (c) Finger tip detection (bottom)

C. Stereo Vision Technique

In this work, we use stereo camera to get the 3D coordinates of the hand and the marker itself for detecting any possible collision between the user and the virtual object while manipulating the augmented object. Using two different views from the same scene then we can estimate the 3D coordinates of any point in the scene by finding the position of that point in the left image and in the right image and then apply some trigonometry. To get the accurate 3D coordinates of the points such as fingertip or the center of the marker, we calibrate the stereo camera. The calibration can make that the match of a point in the left image will appear in the exact same line on the right image and it can also fix the possible distortion caused by the lenses.

An offline camera calibration is performed by use of a simple planar grid pattern of known size in the field of view. Fig 4 illustrates two grid patterns for left and right un-calibrated images and their rectified images after calibrating those images. We can see each correspondent point of the left and right images are same epipolar line after calibrating the stereo images.

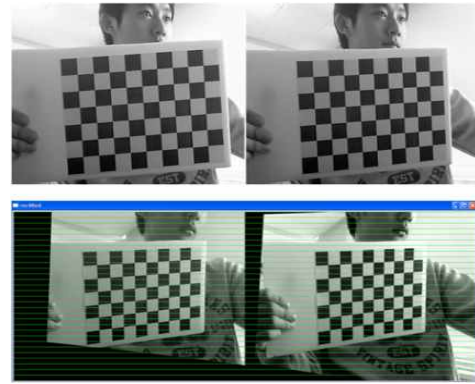
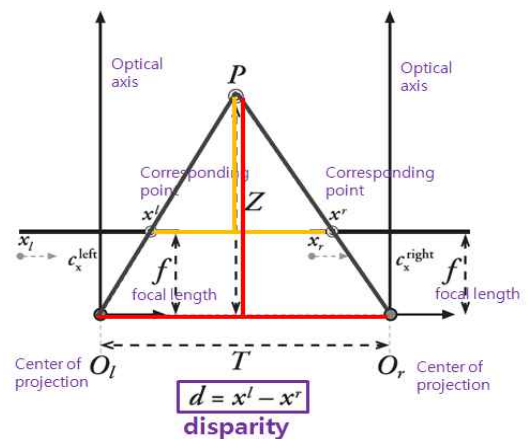


Fig 4. The rectified images from two images after calibration

Using the calibrated images, we can calculate the dense disparity map which provides the distance between the camera and the object. Fig 5 shows the geometry of the stereo vision and the relationship between disparity and camera distance.



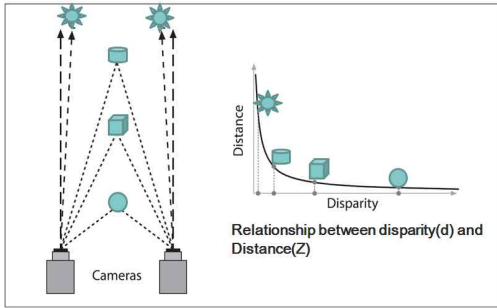


Fig 5. The geometry of stereo vision (top) and the relationship between disparity and camera distance (bottom)

Once the disparity (d) between x^l and x^r is calculated, the depth value (z) can be obtained by using T and the focal length f as follows:

$$z = f \frac{T}{d} \tag{4}$$

The calculated (z) value will be used for the (z) coordinate value of the objects such as the center of the hand or the marker in the marker-based AR system. Fig 6 shows a dense disparity map from two images taken from a left and right camera.

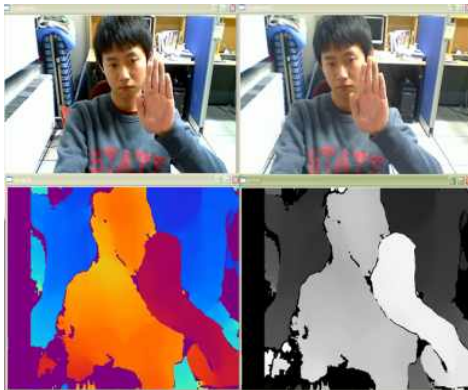


Fig 6. Dense disparity map from two input images

D. Collision Detection Using Ray Casting

It is natural that the collision between the human hand and the augmented object can be occurred during manipulating the virtual 3D object. In AR, however, the collision is occurred between a virtual and a real object thus the collision detection method may be different comparing with the ways in the real world. In this work, since we already have 3D information of the hand and the marker for the AR using stereo-vision technique, the 3D direction of the finger tip can be obtainable like Lee's work[14]. When both the calculated finger direction is aligned with the central position of the marker or the positions of augmented object and the hand is approaching to the object in the some distances, we can assume the collision between two objects.

Since the manipulation of an object can be done by two types of hand interaction i.e. pointing and pinching, the collision detection between the hand and a virtual object is also defined by two different approaches, respectively. Fig 7 illustrates the

direction of the finger when we use two feature points (P_0, P_1) of the hand in the hand pointing.

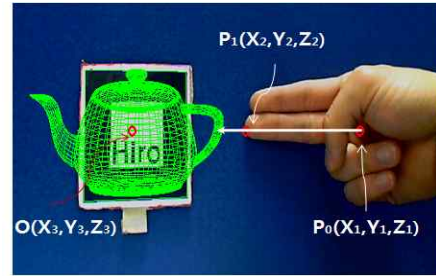


Fig 7. The direction of the finger pointing by simple ray casting

The direction of the finger can be easily calculated as a linear parametric function $f(t)$ between the centre of the hand $P_0(x_1, y_1, z_1)$ and the location of the fingertip $P_1(x_2, y_2, z_2)$ as follows:

$$\begin{aligned} f_x(t) &= x_1 + (x_2 - x_1)t \\ f_y(t) &= y_1 + (y_2 - y_1)t \\ f_z(t) &= z_1 + (z_2 - z_1)t \end{aligned} \tag{5}$$

The linear function $f(t)$ can be used for evaluating where the user is pointing at and the parameter t can control the magnitude of the function. For the collision detection, we can use finger ray casting which is known to be a fast for pointing at and selecting a distant object. The collision between the hand and the virtual object is detected when the ray touch the virtual object. In this work, we assume that two objects are collided in a certain range of distance (D) for example the parameter t of $f(t)$ is less than equal to 2 or the distance between the locations of the hand and marker is less than a predefined distance (ϵ). Three different reactions from the virtual object: pushing, pulling and changing the color of the virtual object are obtained when the collision between the user and the virtual object is detected.

Meanwhile, when the pinching is used the collision between the object and finger is determined by the angle between the thumb and the index finger as illustrated in Fig 8.

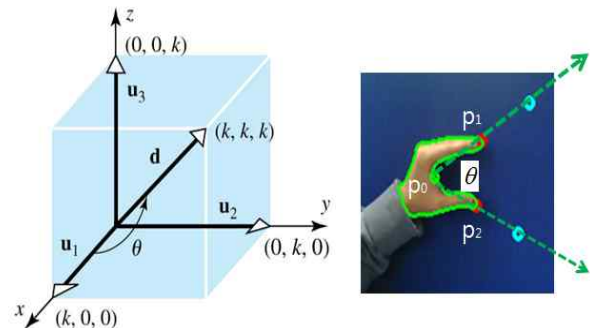
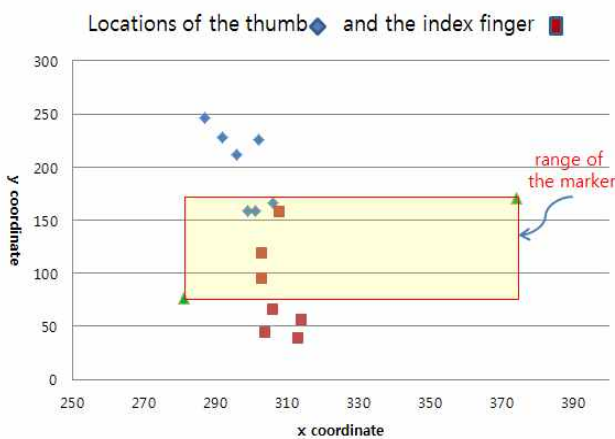


Fig 8. The angle of the thumb and a finger in pinching interaction

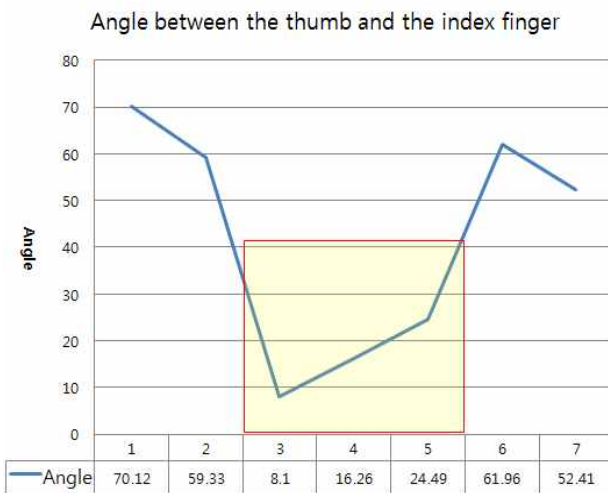
The degree of angle θ between $\vec{u} = (P_0, P_1)$ and $\vec{v} = (P_0, P_2)$ becomes as follow:

$$\cos \theta = \frac{\vec{u} \cdot \vec{v}}{\|\vec{u}\| \|\vec{v}\|} \quad (6)$$

Fig 9 (a) illustrates the locations of the thumb and the index fingers during pinching interaction in a sequences of image frames between the user and a virtual object when the z-coordinates of the fingers and the augmented object are same locations. The collisions between the fingers and the object are detected in the range of the marker. In this work, it is assumed that the collision between the finger and the virtual object is occurred when the thumb and the index finger are approaching to object and the degree of angle between two fingers is located in the range of 0° 0 to 42° during pinching the virtual 3D object as illustrated in Fig 9 (b).



(a) Locations of the thumb and the index finger in a sequence of image frames during pinching interaction



(b) Angle between the thumb and the index finger during pinching interaction

Fig 9. Collision detection in pinching interaction.

IV. EXPERIMENTAL RESULTS

The proposed 3D hand interaction supports four different manipulations of the augmented object in AR. In this experiment, we use ARTokit to register the virtual object on a real scene. One of the difficulties in developing AR applications is the tracking the users viewpoint however ARToolkit can solve this problem using vision algorithm. In the experiment we use two Logitech Quick Cameras to obtain stereo images.

Fig 10 illustrates the sequence of hand images and detected 3D locations of the centre of hand, fingertips and finger ray using stereo-vision technique and our proposed method.

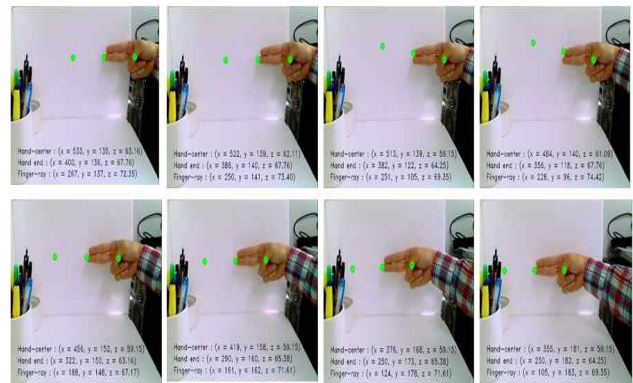
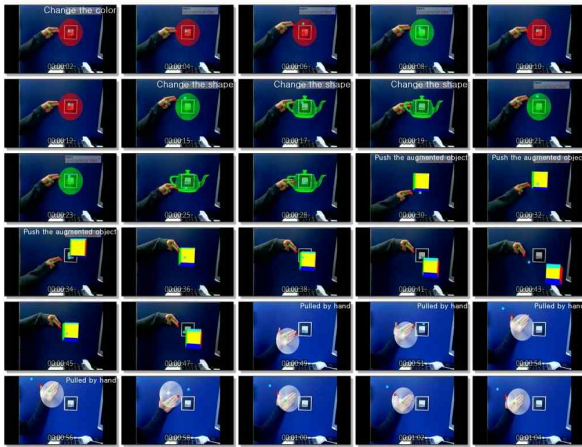


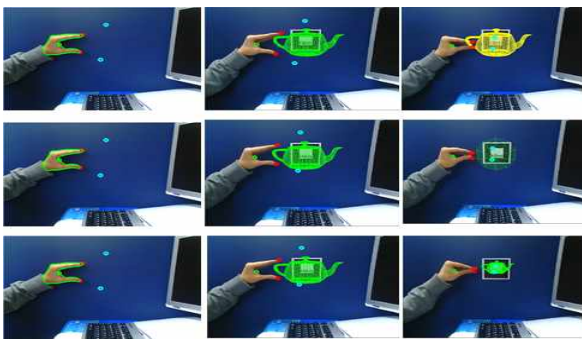
Fig 10. 3D locations of the center of hand, fingertip and its ray.

Based on the hand pointing and the hand pinching interaction with a virtual object in AR, we can produce various 3D interaction results. In the hand pointing interaction, 4 different reactions are generated when the hand is collided with the augmented object as illustrated in Fig 11(a). The first interaction is to change the colour feature of the virtual object when a user touches the augmented object. The second interaction is changing the shape of the object. The third interaction is pushing the augmented object from the currently registered position on the marker. While applying this interaction, the rendered object is translated from the current location of the marker to the opposite direction and got back to its original position when user's hand is moved away from the current marker. Final interaction is pulling the augmented object and locating the object on the hand. Like pushing, the object can be relocated into original position when the human hand is disappeared from the scene.

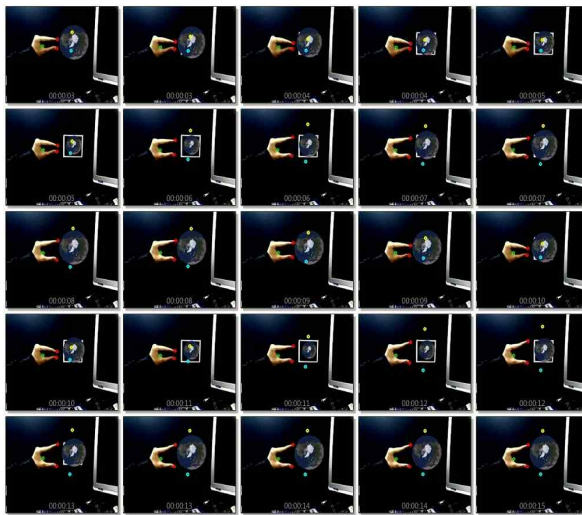
Meanwhile, in the hand pinching interaction, the color, shape and size of the virtual object is instantly changed when the object is touched by pinching as illustrated in Fig 11(b). The sequence of the image in Fig 11(c) is the size variation of the virtual 3D object when a user manipulates the object during pinching interaction.



(a) The hand pointing interaction



(b) Three different reaction with the hand pinching interaction



(c) The size variation of the object by pinching interaction

Fig 10. Manipulation of virtual object using the hand pointing and pinching interaction

CONCLUSION

In this paper we present a stereo vision-based natural 3D hand interaction with an augmented object in Augmented Reality System. In traditional AR interaction using 2D input image, it have been limitations to provide a natural interaction between the user and the augmented object because of the lack of Z information of the user and the virtual object. The proposed stereo-vision technique can overcome this

disadvantage of 2D image and support more feasible manipulation of the virtual object in AR. In the proposed 3D hand interaction, the 3D information of the hand and the virtual object was utilized to detect the 3D collision between two models when the hand was approaching to the virtual object. The user interaction can change the features of the object such as color and shape. In addition, the user can change the geometric locations of the object by pushing or pulling the object from the current 3D locations of the object. This simple collision detection can make the 3D hand interaction come true in AR applications.

As for the future work, we will study to combine the proposed stereo-vision technique with actual haptic device for manipulating a virtual object in AR.

REFERENCES

- [1] M Fiala. ARTag, a fiducial marker system using digital techniques, In CVPR 05, (2005), Vol 2., pp. 590-596.
- [2] H. Kato and M. Billinghurst, Marker tracking and HMD calibration for a video-based augmented reality conferencing system, In IWAR '99(1999), pp. 85-94.
- [3] D. Wagner and D. Schmalstieg ARToolkitPlus for Pose Tracking on Mobile Devices, In Proceedings of 12th Computer Vision Winter Workshop'07 (2007), pp. 139-146.
- [4] Cho, Y; Lee, J. & Neumann, U. A multi-ring fiducial system and an intensity-invariant detection method for scalable augment reality, In *IWAR '98*, (1998). pp. 147-156..
- [5] H. Kato, M. Billinghurst, I. Poupyrev, K. Imamoto and K. Tachibana, Virtual object manipulation on a table-top AR environments, In *ISAR '00*, (2000), pp. 111-119.
- [6] Lee, W. & Park, J. Augmented foam: A tangible augmented reality for product design. In *ISMAR '05*, (2005), pp. 106-109.
- [7] T. Lee and T. Hollerer, Hand AR: Markerless Inspection of Augmented Reality Objects Using Fingertip Tracking, In Proc. IEEE ISWC '07,(2007), pp. 83-90.
- [8] T. Lee and T. Hollerer, "Initializing Markerless Tracking Using a Simple Hand Gesture," In Proc. ACM/IEEE ISMAR '07, (2007), pp. 1-2.
- [9] T. Lee and T. Hollerer, "Hybrid Feature Tracking and User Interaction for Markerless Augment Reality," In IEEE Int'l Conference on Virtual Reality'08 (2008), pp. 145-152.
- [10] Lee, BS and Chun, JC, Interactive manipulation of augmented objects in marker-less AR using vision-based hand mouse, In Int'l Conference on Information Technology(ITNG), (2010), pp. 398-403.
- [11] Chun, J.C and Lee, B.S, Dynamic Manipulation of a Virtual Object in Marker-less AR system Based on Both Human Hands, Transactions on Internet and Information Systems, (2010), Vol. 4, No.4, pp. 618-632.
- [12] K. Min and J. Chun, A nonparametric skin color model for face detection from color images, PDCAT '04, pp. 115-119 , 2004
- [13] G. Borgefors, Distance transformations in digital images, Computer Vision, Graphics and Image Processing,(1986), Vol. 34, pp. 344-371.
- [14] M. Lee, R. Green, and M. Billinghurst, 3D Natural hand interaction for AR application, Image and Vision Computing New Zealand 2008,(2008), pp.1-6.
- [15] JC Chun, SH Lee, A Vision-based 3D Hand Interaction for marker-based AR, International Journal of Multimedia and Ubiquitous Eng., Vol. 7, No. 3, (2012), pp. 51-57.



Seonho Lee is currently a graduate student in the department of computer science at Kyonggi University, South Korea. He received BS degree from Kyonggi University majoring computer science in 2012. His major research interests are augmented reality and haptic interaction in AR



Junchul Chun is currently a professor in the department of computer science and a principal investigator of GIP(Graphics and Image Processing Lab) at Kyonggi University, South Korea. He has been served as a chief research director at Contents Convergence Software Research Center supported by Geyonggi Regional Government in South Korea. He received BS from Chung-Ang University majoring computer science. He also received Ph.D and MS degrees of computer science and engineering from the University of Connecticut, U.S. respectively. His major research areas are vision-based interaction, augmented reality and computer graphics.

The Optimum Ring Ratio of 16-APSK in LTE Uplink over Nonlinear System

Pornpimon Chayratsami*, Sorapong Thuaykaew**

**Department of Engineering Education, Faculty of Industrial Education,
King Mongkut Institute of Technology Ladkrabang, Bangkok 10520, Thailand*

***Celestica Inc., Leamchabang, Sriracha, Chon Buri, 20230, Thailand*
kcpormpi@gmail.com, siamcreative@gmail.com

Abstract— Single Carrier Frequency Division Multiple Access (SC-FDMA) has been selected for use in the Long Term Evolution (LTE) uplink due to its lower Peak-to-Average Power Ratio (PAPR) relative to OFDMA. The resultant lower PAPR results in fewer excursions into the amplifier's nonlinear region, where signal distortion can occur and results in degraded bit error rate (BER). The SC-FDMA scheme normally applies 16-ary Quadrature Amplitude Modulation (16-QAM), but amplitude phase shift keying (APSK) modulation has a lower PAPR than does 16-QAM, resulting in improved BER. This paper investigates the constellation ring ratio of the 16-APSK modulation scheme and its effects on BER through its effects on the PAPR. Simulation results are used to conclude that a ring ratio that ranges from 2.5 to 3.5 delivers the best results and provides BER and PAPR improvement.

Keyword—16-APSK, SC-FDMA, LTE, Nonlinear system, PAPR

I. INTRODUCTION

THE 3GPP Long Term Evolution or LTE is a standard that has been developed by the 3rd Generation Partnership Project (3GPP), to become a truly global mobile standard and to apply to high-speed wireless data transmission for mobile phone and data terminal [1], [2]. It is the next step in progression from GSM / EDGE and UMTS / HSPA technologies with higher capacity and faster speed.

In order to reduce the interference signals and to improve the channel capacity of the LTE system, orthogonal frequency division multiple access (OFDMA) and single carrier frequency multiple access (SC-FDMA) are employed for the downlink and uplink, respectively. The SC-FDMA is the multiplexing technique for the LTE uplink because its PAPR is lower than that of other transmission techniques, especially, OFDMA [1], [3], [4].

The high PAPR is a principal weakness of OFDM. It brings on the signal distortion in the nonlinear region of high power amplifier (HPA) [3]. The closer the HPA is operated to the saturation region, the more frequent are excursions into the

nonlinear region and the more pronounced is the signal distortion. The signal distortion induces the degradation of bit error rate (BER). Therefore, it is desirable to have low PAPR to improve the BER performance.

To reduce the PAPR of OFDM, there are mainly two categories, which are signal scrambling techniques and signal distortion techniques [5]. The practical solutions of the signal scrambling techniques include block coding, Selective Level Mapping (SLM), and Partial Transmit Sequences (PTS). The signal distortion techniques include clipping, peak windowing, peak cancellation, peak power suppression, weighted multicarrier transmission, companding, etc.

Previously, there have been many researches on the PAPR reduction techniques. For examples, the signal scrambling techniques of the Partial Transmit Sequences and the block coding are proposed in [6] and [11]. The signal distortion techniques of clipping, suppression, peak windowing, peak cancellation, and companding are proposed in [7], [8], [9], [10], and [12], respectively. However, the disadvantage of all these techniques is the complexity increase of the system.

Other than the PAPR reduction techniques stated above, J. Gazda, D. Dupak and D. Kocur in [4] proposed to apply the M-ary APSK modulation to reduce the PAPR in the LTE uplink. They show that 16-APSK outperforms the standardized 16-QAM, which is generally used in the LTE uplink. The BER performance of the 16-APSK system improves for two reasons, the low PAPR of the APSK modulation causes fewer excursions into the nonlinear region and the 16-APSK signal is more robust to the distortions caused by the amplifier nonlinearities than is 16-QAM. Also, W. Sung, S. Kang, P. Kim and D. Chang in [13] give the preliminary analysis on the PAPR of the 16-APSK modulation in the digital video broadcasting for satellites (DVB-S2). They show that the PAPR of the 16-APSK depends on a ratio of the radius of each ring.

However, according to the authors' knowledge, the effects of the constellation ring ratio of the 16-APSK (4+12 APSK) modulation scheme are not yet evaluated in the LTE uplink system. Therefore, this paper will present the investigation on the constellation ring ratio of the 16-APSK modulation used in the LTE uplink system with the nonlinear distortion due to a HPA. The optimal value of the ring ratio is also proposed.

Manuscript received July 31, 2013.

Pornpimon Chayratsami is with King Mongkut Institute of Technology Ladkrabang, Ladkrabang, Bangkok, 10520, Thailand (corresponding author phone: 66-8-5119-0510; fax: 66-2-738-7055; e-mail: kcpormpi@gmail.com).

Sorapong Thuaykaew is with Celestica Inc., Leamchabang, Sriracha, Chon Buri, 20230, Thailand. (e-mail: siamcreative@gmail.com).

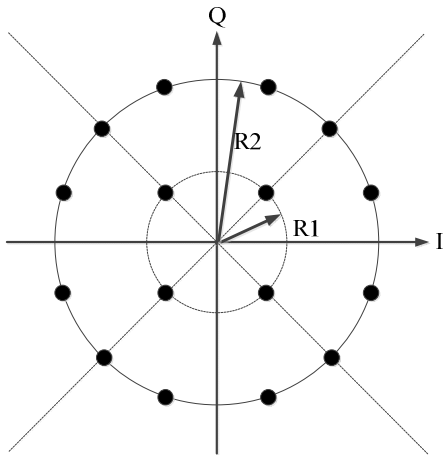


Fig. 1. 16-APSK (4+12 APSK) Constellation

The paper is organized as follows. First, the effects of the constellation ring ratio of the 16-APSK modulation, on both the PAPR and the BER, are presented in Section II. Section III shows the description of the system model adopted for the analysis and the simulation. Then, the simulation results are shown in section IV. Finally, section V provides conclusions.

II. EFFECTS OF THE APSK CONSTELLATION RING RATIO

Amplitude phase shift keying (APSK) is a digital modulation scheme that conveys data by changing or modulating both the amplitude and the phase. It is a combination of Amplitude shift keying (ASK) and Phase shift keying (PSK) applied to more effectively populate the signal space. Its constellation is composed of concentric rings, each with uniformly spaced PSK points [14]. Fig. 1 shows an example of 16-APSK constellation which has 2 concentric rings, with 4 PSK points in the inner and 12 PSK points in the outer. The effects of its constellation ring ratio on PAPR and BER could be analyzed as following.

A. The Effects on PAPR

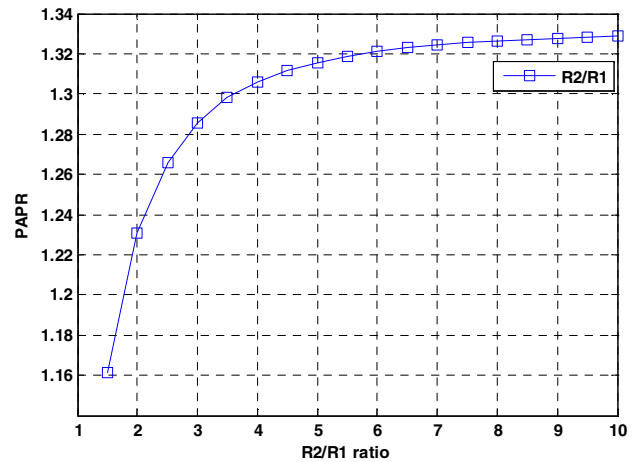
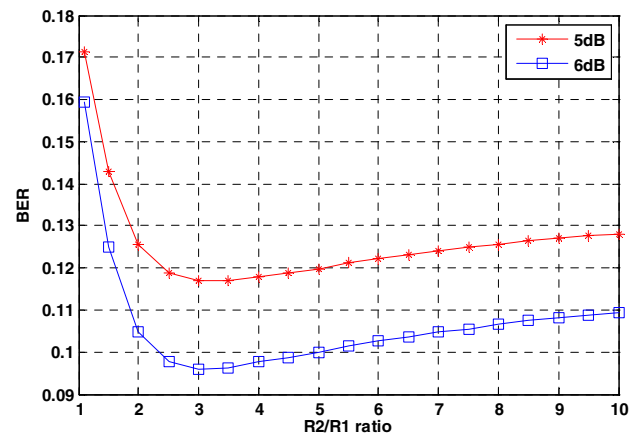
Peak to Average Power Ratio (PAPR) is the ratio between the maximum power and the average power of the transmitted signal. The PAPR is defined as [3]

$$PAPR = \frac{\max_{n=0,1,\dots,N-1} |\tilde{x}_n|^2}{\frac{1}{N} \sum_{n=0}^{N-1} |\tilde{x}_n|^2} \quad (1)$$

where \tilde{x}_n is the transmitted signal.

For 16-APSK modulation, there are many types of constellation patterns, such as 4+12 ASPK, 5+11 ASPK, and 6+10 APSK. Each type assigns a different number of points to each ring, with the total number of points summing to 16. Here, the 4+12 APSK is used in the investigation, since it delivers the best performance under the nonlinear conditions imposed by the saturation region of a power amplifier and is adopted in DVB-S2 [15].

The average power level of the 4+12 APSK, which has the constellation mapping shown in Fig. 1, can be defined as [13]


 Fig. 2. The relationship between the ratio (R_2/R_1) of 4+12 APSK and PAPR

 Fig. 3. R_2/R_1 ratio vs. BER of 16-APSK for the linear transmission over AWGN channel

$$E_s = \frac{R_1^2 + 3R_2^2}{4} = \frac{(1 + 3\beta_0^2)R_1^2}{4} \quad (2)$$

where R_1 is the radius of the inner ring,

R_2 is the radius of the outer ring,

and $\beta_0 = R_2 / R_1$ is the ratio between the outer and the inner ring radius.

From eq. (1) and (2), we can plot the relationship between the ratio (R_2/R_1) of the 4+12 APSK and the PAPR as shown in Fig. 2. This shows that the PAPR increases when the ratio (R_2/R_1) increases.

B. The Effects on BER

Considering the 16-APSK modulation for linear transmitter over an additive white Gaussian noise (AWGN) channel operating at energy per bit to noise power spectral density ratio (E_b/N_0) of 5 dB and 6 dB, the simulation results in Fig. 3 show the effects of the ratio (R_2/R_1) on the performance of the system. From Fig. 3, it is seen that the ratio in the range from 2.5 to 5 gives the lowest BER for both E_b/N_0 values.

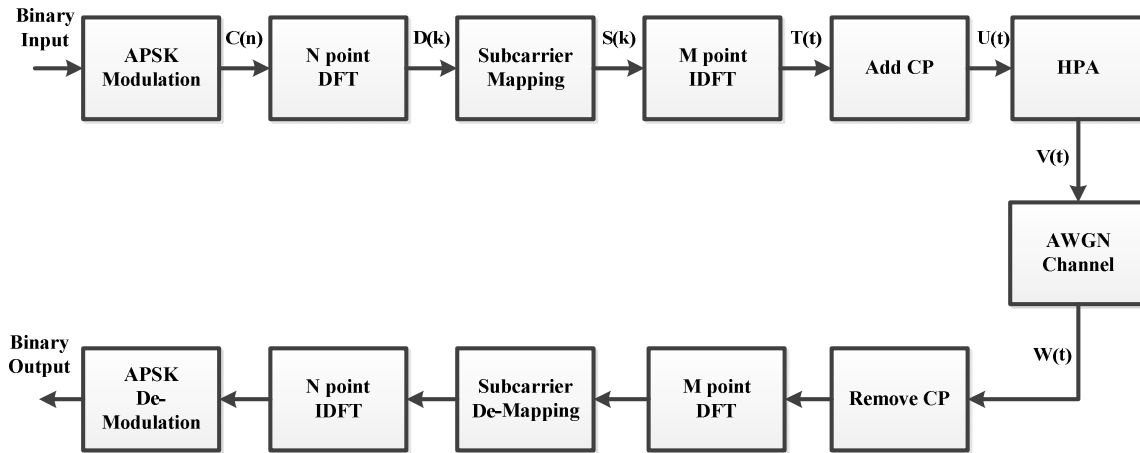


Fig. 4. Block diagram of the SC-FDMA system with APSK modulation

From the effects of the constellation ring ratio of 16-APSK modulation on the PAPR and BER, the appropriate value of the ratio can be determined by selecting the ratio that minimizes both the PAPR and the BER.

The previous analysis shows the effects of the constellation ring ratio of 16-APSK modulation on the PAPR in general and the BER for the linear channel only. This clearly shows that the constellation ring ratio can play a significant role in the nonlinear channel as well.

Next, the optimal ratio values providing a low BER and PAPR in the presence of nonlinearities will be addressed.

III. SYSTEM MODEL

Fig. 4 shows the block diagram of the general SC-FDMA system [3] with the APSK modulation. The binary sequence is modulated into data symbols, $C(n)$, by using the 4+12 APSK modulation scheme. Then, a block of N modulated symbols is applied to the N -point Discrete Fourier Transform (DFT) to produce a frequency domain representation, $D(k)$.

$$D(k) = \frac{1}{\sqrt{N}} \sum_{n=0}^{N-1} C(n) e^{-j2\pi nk/N} \quad (3)$$

This output is fed to the Localized FDMA (LFDMA) subcarrier mapping block, which is the subcarrier mapping used in the LTE standard. At this point, each of the N -DFT outputs is mapped to one of M orthogonal subcarriers ($M > N$) as

$$S(k) = \begin{cases} D(k) & ; 0 \leq k \leq M-1 \\ 0 & ; \text{Otherwise} \end{cases} \quad (4)$$

Then, the M -point inverse DFT (IDFT) transforms these data symbols into the time-domain samples, $T(t)$, of these subcarriers.

$$T(t) = \frac{1}{\sqrt{M}} \sum_{k=0}^{M-1} S(k) e^{+j2\pi kt/M}$$

Similar to OFDM, the cyclic prefix is added to the symbols. Before entering the AWGN channel, the transmitted signal is amplified by the high power amplifier (HPA), which makes the overall channel nonlinear. The signal at this point can be expressed as

$$V(t) = A[r(t)] e^{j[\Phi(r(t)+\theta(t))]} \quad (5)$$

where $r(t)$ and $\theta(t)$ are the amplitude and phase of the input signal to the HPA.

At the receiver, the received signal is processed by removing the cyclic prefix, first. Then, the signals are demodulated by using M -point DFT, subcarrier De-mapping, N -point IDFT and the APSK demodulator.

For this investigation, the nonlinear HPA uses the Soft Limiter (SL) model, which defines the Amplitude Modulation to Amplitude Modulation (AM/AM) and the Amplitude Modulation to Phase Modulation (AM/PM) characteristics as following [8]

$$F[\rho] = \begin{cases} -A, & \text{if } \rho < -A \\ \rho, & \text{if } -A \leq \rho \leq A \\ A, & \text{if } \rho > A \end{cases} \quad (6)$$

and

$$\Phi[\rho] = 0 \quad (7)$$

where A is the saturating level of the amplifier,

ρ is the amplitude of the input signals,

$F[\rho]$ is the amplitude of the output signals of the Soft Limiter,

and $\Phi[\rho]$ is the phase of the output signals of the Soft Limiter.

There is only amplitude distortion and no phase distortion in the SL model. The severity of the distortion can be measured by the Input-Back-Off (IBO) of the PA, which can be calculated as following [16]

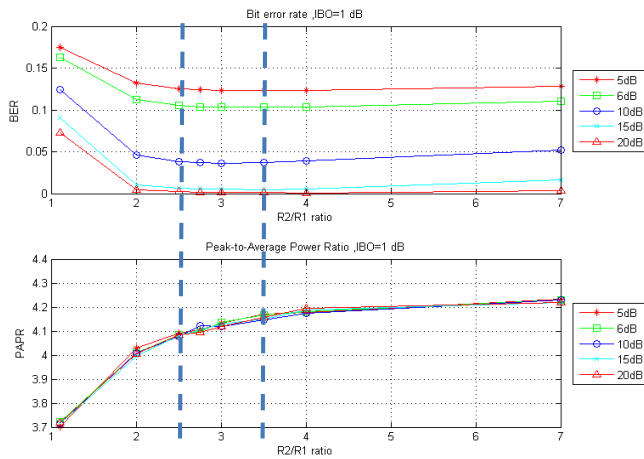


Fig. 5. BER and PAPR under nonlinear PA when IBO = 1 dB

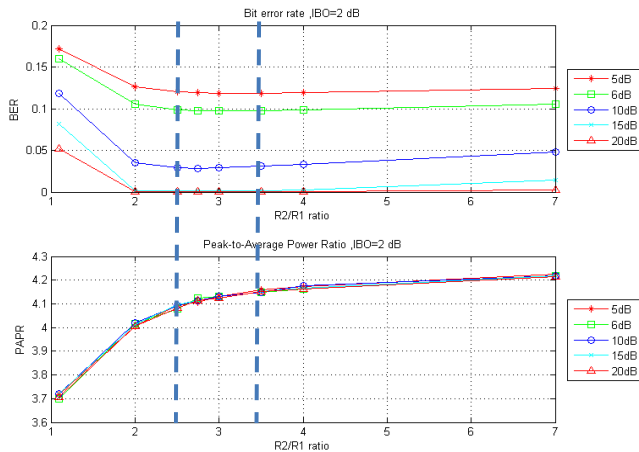


Fig. 6. BER and PAPR under nonlinear PA when IBO = 2 dB

$$IBO = 10 \log_{10} \frac{A_s^2}{P_{in}} \quad (8)$$

where A_s is the saturation level of the amplifier input and P_{in} is the average input power of the amplifier.

The investigation on the constellation ring ratio of the 16-APSK (4+12 APSK) modulation scheme, used in the LTE uplink system with the nonlinear distortion due to a PA, is based on the computer simulations. The results are shown in the next section.

IV. SIMULATION RESULTS

The simulation of a general SC-FDMA transmission is set up to meet the LTE standard for 5 MHz bandwidth: the IDFT size (M) of 512, DFT size (N) of 300, and a cyclic prefix (CP) of 144 [3], [17]. The 16-APSK modulation scheme, with various constellation ring ratios, is used instead of the 16-QAM modulation that is normally used in the LTE standard.

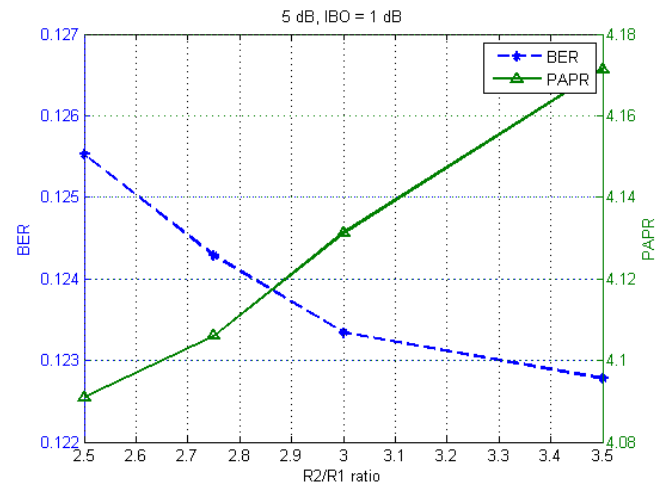


Fig. 7. The superimposed plot of BER and PAPR when SNR = 5 dB and IBO = 1 dB

 TABLE I
THE OPTIMUM RING RATIOS FOR VARIOUS SNRS AND IBO = 1 AND 2 dB.

SNR	IBO	
	1 dB	2 dB
5 dB	2.86	2.81
6 dB	2.75	2.65
10 dB	2.62	2.60
15 dB	2.85	-
20 dB	2.93	2.73

The simulation results include the optimum ring ratio analysis, the Bit Error Rate (BER) analysis, the 16-QAM and 16-APSK performance comparison, the Peak-to-Average Power Ratio (PAPR) analysis, and the 16-QAM and 16-APSK PAPR comparison. The description of the results is shown below.

A. Optimum Ring Ratio Analysis

To determine the appropriate range of ratio ($R2/R1$) for the 16-APSK modulation scheme in the nonlinear channel, the BER and PAPR performances are shown in Fig. 5 and Fig. 6, with the distortion measured by the IBO of 1 dB and 2 dB, respectively. The BER and PAPR are measured with various SNR. These results show that the ring ratio in the range of 2.5 to 3.5 gives the lowest BER range, but not the highest PAPR values.

Consider more carefully in the above resultant range of 2.5-3.5, the optimum ring ratio for each E_b/N_0 may be estimated by superimposing the BER and PAPR performance curves on the dual-scale data chart. Here, the superimposed chart is chosen because it is commonly used when two data sets have only one axis in common [18].

For example, the superimposed plot of BER and PAPR when SNR = 5 dB and IBO = 1 dB, created by the “plotyy()” function in MATLAB, is shown in Fig. 7. The plot indicates that the optimum ring ratio is at $R2/R1 = 2.86$ because the BER and the PAPR are optimized (low BER and low PAPR) at their intersection.

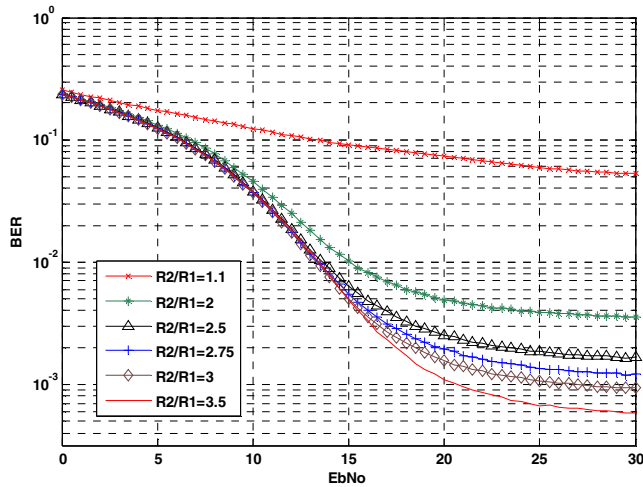


Fig. 8. BER performance when IBO = 1 dB with various R2/R1

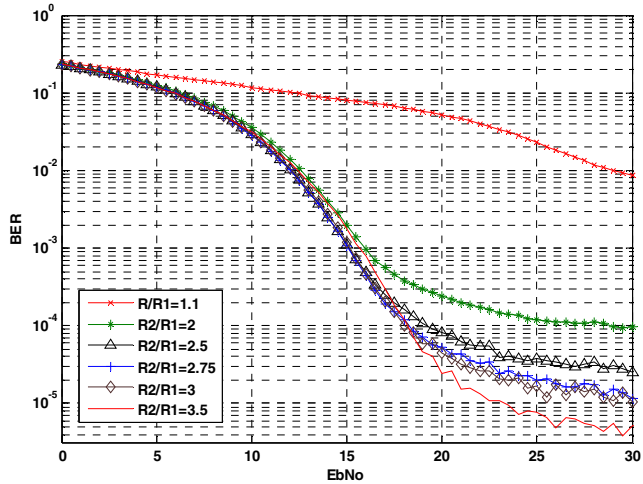


Fig. 9. BER performance when IBO = 2 dB with various R2/R1

By doing the same to the results getting from the simulation for various SNRs and IBO = 1 dB and 2 dB, the optimum ring ratios are found for each value of SNR as shown in Table I. However, these ratios just give the idea of what the optimum ring ratios should be for the specific values of SNR and IBO. The superimposed plot might provide the optimum ratios differently if the scale of the y-axis is changed. This is the trade-off of the dual-scale chart.

Notice that there is no optimum ratio when SNR = 15 dB and IBO = 2 dB (no intersection of BER and PAPR curves). This might be the scale problem of this plot. Also, in practical implementation, the SNR values could be changed constantly due to the channel condition variation. Therefore, it is impossible to determine the optimum ring ratio specifically and it is more appropriate to state it in range.

B. Bit Error Rate Analysis

From Fig. 5 and Fig. 6, the ratio R2/R1 gives low PAPR but high BER when the ratio R2/R1 is lower than 2.5. Fig. 8 and Fig. 9 show the simulation results of the system with the IBO of

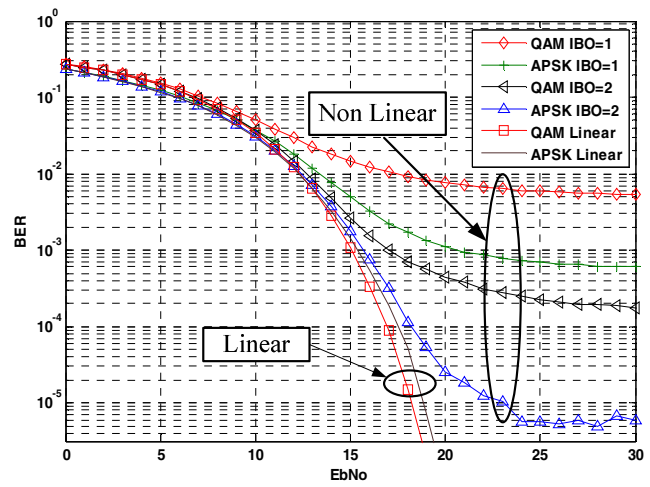


Fig. 10. BER performance when the ratio = 3.5 with various IBO

1 dB and 2 dB, and various values of ring ratios (1.1, 2, 2.5, 2.75, 3, and 3.5), respectively.

In this analysis, we consider at SNR = 20 dB, which gives the highest throughput for the LTE system with four bits per symbol modulation [3]. The BERs from Fig. 8 are 7.5×10^{-2} , 5×10^{-3} , 2.5×10^{-3} , 2×10^{-3} , 1.6×10^{-3} , and 1.1×10^{-3} for each ring ratio. At the same SNR of 20 dB, the BERs for each ratio of the system with IBO = 2 dB shown in Fig. 9 are 5×10^{-2} , 2.5×10^{-4} , 8×10^{-5} , 5×10^{-5} , 4.5×10^{-5} , and 2.5×10^{-5} . The results in both figures show that the ratio range of 2.5-3.5 gives better BER performance than that of 1.1 and 2. Also, These results agree that the best BER performance occurs when the ratio R2/R1 is equal to 3.5 at high Eb/No.

In addition, the error floor occurs at high SNR and it is caused by the channel nonlinearity based upon the simulation results.

C. 16-QAM and 16-APSK Performance Comparison

Fig. 10 shows the BER performance comparison of the standard 16-QAM and the 16-APSK with the ring ratio R2/R1 of 3.5. To make a fair comparison, both modulation schemes are set to have the same average energy per symbol.

The 16-QAM modulation scheme gives better BER performance than the 16-APSK in the linear channel. But, the 16-APSK modulation scheme performs better than the 16-QAM in the nonlinear channel for LTE system. These outcomes confirm the results in [4]. The error floors associated with the average bit error probability shift down from 5×10^{-3} to 6×10^{-4} and from 2×10^{-4} to 6×10^{-5} for the IBO of 1 dB and 2dB, respectively.

D. Peak-to-Average Power Ratio (PAPR) Analysis

The Peak-to-Average Power Ratio (PAPR) is analyzed by using Complementary Cumulative Distribution Function (CCDF). The CCDF of PAPR, which is the probability that PAPR is higher than a certain PAPR value $PAPR_0$ ($\Pr(PAPR > PAPR_0)$), for N subcarriers of an OFDM multi-carrier signal can be calculated by [3]

$$\Pr(PAPR > PAPR_0) = 1 - (1 - e^{-PAPR_0})^N \quad (9)$$

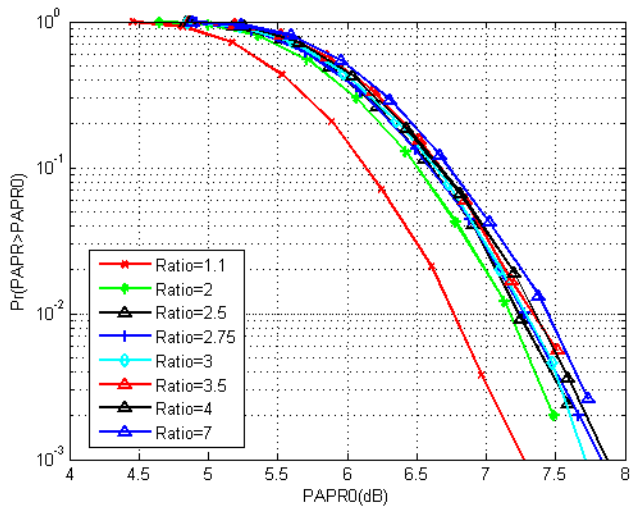


Fig. 11. CCDF of PAPR for the nonlinear system with IBO of 1 dB and various ring ratios

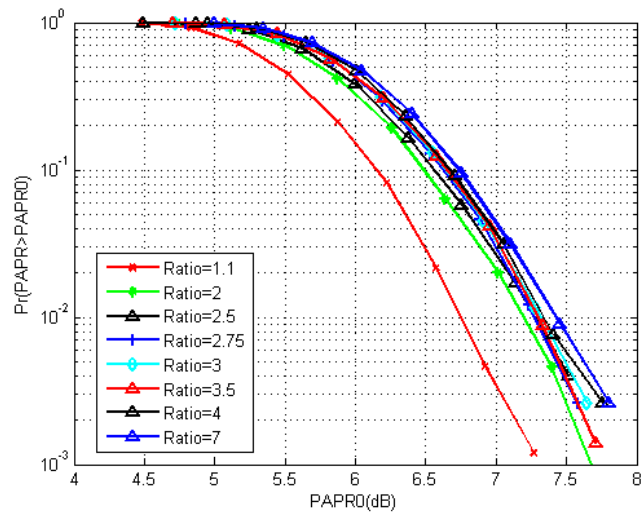


Fig. 12. CCDF of PAPR for the nonlinear system with IBO of 2 dB and various ring ratios

where N is the number of subcarriers
 $PAPR_0$ is the clipping level in the nonlinear system.

The CCDF is measured by using the Monte Carlo simulation for the system applying the 16-APSK (4+12 APSK) modulation with various values of ring ratios in the nonlinear system with IBO of 1 dB and 2 dB. The comparison of the CCDF of PAPR for the ring ratios of 1.1, 2, 2.5, 2.75, 3, 3.5, 4, and 7 is shown in Fig. 11 and Fig. 12.

Consider at the 99 percentile that the $\Pr(PAPR > PAPR_0)$ is less than 10^{-2} , the ring ratio of 1.1 gives the smallest PAPR while the PAPRs of the others are similar.

To choose the optimum ratio for the 16-APSK, one should consider both the BER and PAPR performances. Then, the ratio of 1.1 is not the appropriate choice for the system even if it has the smallest PAPR because it gives the poorest BER to the system as shown in Subsection B.

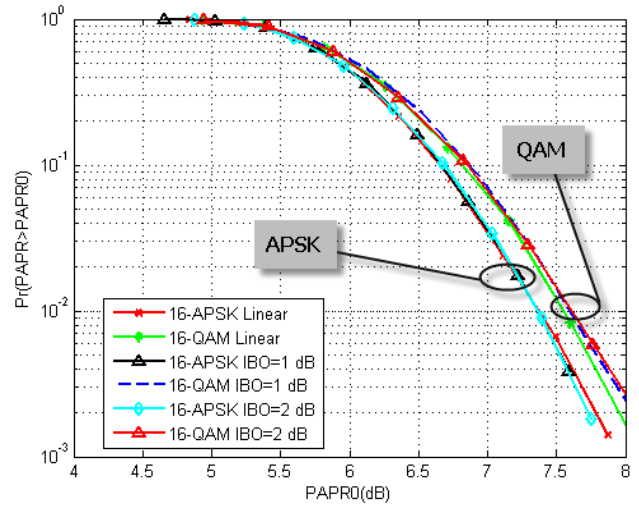


Fig. 13. Comparison of CCDF of PAPR for the 16-QAM and 16-APSK modulations in the nonlinear system

E. 16-QAM and 16-APSK PAPR Comparison

To make a comparison of the system applying the standard 16-QAM and 16-APSK with constellation pattern of 4+12 and ring ratio of 3.5, the average energy per symbol is set to be the same for both modulation schemes. Fig. 13 shows the PAPR performance comparison in terms of CCDF measurement. The system that applies the 16-QAM modulation scheme has a higher PAPR than the 16-APSK in both linear and nonlinear channels for LTE system.

Consider at the 99 percentile that the $\Pr(PAPR > PAPR_0)$ is less than 10^{-2} , the $PAPR_0$ of the 16-QAM system is equal to 7.6 dB while it is 7.4 dB for the 16-APSK system. This means that the system with 16-APSK outperforms the one with 16-QAM for 0.2 dB or 2.63 percent.

V. CONCLUSION

LTE technology is attractive in the telecommunications industry due to the high speed data transfer rate it offers. Therefore, the modulation techniques must be selected properly as an important consideration because it can push the system to its fullest potential. The APSK modulation works better in terms of both BER and PAPR performances than QAM in the nonlinear system. So, the APSK modulation is an appropriate modulation scheme to be adopted, as studies have noted in [4], and the ratio of R2/R1 is an important factor affecting the PAPR and BER of the APSK. The PAPR increases as the ratio of R2/R1 increases. While BER changes differently to the R2/R1 ratio and is shown to have one range with a low BER. In this paper, it is shown that the optimal R2/R1 ratio of the 4+12 APSK is more suitable to state in range, which is between 2.5 to 3.5. This optimal ratio range gives the best results in terms of the low BER and PAPR to the nonlinear LTE uplink system. Also, the 16-APSK with the proposed ring ratio provides better BER and PAPR performances compared with the standard system with 16-QAM in the nonlinear system. The authors hope that this paper will help to drive the performance of the LTE system that makes the implementation widespread in the future.

REFERENCES

- [1] H. Holma and A. Toskala, *LTE for UMTS –OFDMA and SC-FDMA Based Radio Access*, John Wiley & Sons, 2009.
- [2] F. Khan, *LTE for 4G Mobile Broadband Air Interface Technologies and Performance*, Cambridge University Press, 2009.
- [3] H. G. Myung, *Single carrier FDMA a new air interface for long term evolution*, John Wiley & Sons, 2008.
- [4] J. Gazda, D. Dupak and D. Kocur, "M-APSK modulation for SC-FDMA communication systems," *Radioelektronika (RADIOELEKTRONIKA), 2011 21st International Conference*, 2011, pp. 1-4.
- [5] V. Vijayarangan and R. Sukanesh, "An Overview of Techniques for Reducing Peak to Average Power Ratio and Its Selection Criteria for Orthogonal Frequency Division Multiplexing Radio Systems," *Journal of Theoretical and Applied Information Technology*, Vol. 5, No. 1, pp. 25-36, 2009.
- [6] S. K. Yusof and N. Faisal, "Reducing PAPR of OFDM signals using partial transmit sequences," *9th Asia-Pacific Conference on Communications (IEEE Cat. No. 03EX732)*, 2003, pp. 411-414.
- [7] R. AliHemmati, P. Azmi, and F. Marvasti, "OFDM clipping distortion compensation using an iterative method," *VTC-2005-Fall. 2005 IEEE 62nd Vehicular Technology Conference*, 2005, vol. 1, no. 1, pp. 444-447.
- [8] S. Pagadarai, A. M. Wyglinski, and R. Rajbanshi, "A Sub-optimal Sidelobe Suppression Technique for OFDM-based Cognitive Radios," *Military Communications Conference*, Nov. 2008, pp. 1-6, 16-19.
- [9] G. Chen, R. Ansari, and Y. Yao, "Improved Peak Windowing for PAPR Reduction in OFDM," *VTC Spring 2009 - IEEE 69th Vehicular Technology Conference*, Apr. 2009, pp. 1-5.
- [10] Y. Huang and Z. Zeng, "A Simplified Peak Cancellation Method for OFDM Signals," *2012 International Conference on Computer Science and Electronics Engineering*, Mar. 2012, pp. 336-339.
- [11] K. Bani, R. Bansode, and B.K. Mishra, "Novel Technique for PAPR Reduction in OFDM System Using n/4-shifted-DQPSK Modulation & Turbo Code," *Devices, Circuits and Systems (ICDCS), 2012 International Conference*, 15-16 Mar. 2012, pp. 627-633.
- [12] Y. Wang, J. Ge, L. Wang, J. Li, B. Ai, and S. Member, "Nonlinear Companding Transform for Reduction of Peak-to-Average Power Ratio in OFDM Systems," *IEEE Transactions on Broadcasting*, pp. 1-7, 2012.
- [13] W. Sung, S. Kang, P. Kim and D. Chang, "Performance analysis of APSK modulation for DVB-S2 transmission over nonlinear channels," *International Journal of Satellite Communications*, pp. 295-311, 2009.
- [14] Z. Liu, Q. Xie, K. Peng, and Z. Yang, "APSK Constellation with Gray Mapping," *IEEE Communications Letters*, Vol. 15, No. 12, pp. 1271-1273, December 2011.
- [15] J. Sebesta, "Efficient Method for APSK Demodulation," *Proceedings of the 3rd International Conference on Circuits Systems and Signals (CSS'09)*, 2009, pp. 187-190.
- [16] G. Hill, "Peak Power Reduction in Orthogonal Frequency Division Multiplexing Transmitters," PhD. thesis, Victoria University of Technology, Melbourne, Australia, March 2011.
- [17] Technical Specification Group Radio Access, "Evolved Universal Terrestrial Radio Access (E-UTRA); Physical Channels and Modulation (Release 10)," 3rd Generation Partnership Project (3GPP), Tech. Rep. TS 36.211 Version 10.5.0, June 2012.
- [18] P. Isenberg, A. Bezerianos, P. Dragicevic, and J. D. Fekete, "A Study on Dual-Scale Data Charts," *IEEE Transactions on Visualization and Computer Graphics*, Vol. 17, no. 12, pp. 2469-2478, Dec. 2011.



Pornpimon Chayratsami received the BS degree in Electrical Engineering from King Mongkut Institute of Technology Ladkrabang, Thailand, in 1994 and the MS and PhD degrees in Electrical Engineering from University of Colorado, USA, in 1999 and 2004, respectively. Since 2004, she has been an instructor at King Mongkut Institute of Technology Ladkrabang, Thailand. Her research interests include digital communications, wireless communications, signal processing, and engineering education.



Sorapong Thuaykaew was born in Chiang Mai, Thailand, on Apr 2, 1984. He received the B.S. in Telecommunication engineering and M.S. in Industrial Education from King Mongkut Institute of Technology Ladkrabang, Thailand in year 2006 and 2013, respectively. He is currently a test engineer at Celestica, Inc., Leamchabang, Chon Buri. His main research interests include design and analysis of physical layer algorithms, multiple access schemes, and mobile communication.

Volume 2 Issue 5, Sep 2013, ISSN: 2288-0003

**ICACT-TACT
JOURNAL**



**Global IT
Research Institute**

1713 Obelisk, 216 Seohyunno, Bundang-gu, Sungnam Kyunggi-do, Republic of Korea 463-824
Business Licence Number : 220-82-07506, Contact: secretariat@icact.org Tel: +82-70-4146-4991